University of Alberta

Solvent Microextraction with Simultaneous Back Extraction and the Effect of Tetra-*n*-butylammonium Ion on ODS Bonded Phase.

by

Minhui Ma

A thesis submitted to the Faculty of Graduate Studies and Research
in partial fulfillment of the requirements for
the degree of Doctor of Philosophy

Department of Chemistry

Edmonton, Alberta
Fall 1998

National Library of Canada
Acquisitions and Bibliographic Services
395 Wellington Street
Ottawa ON K1A 0N4
Canada

Bibliothèque nationale du Canada
Acquisitions et services bibliographiques
395, rue Wellington
Ottawa ON K1A 0N4
Canada

Your file Votre référence

Our file Notre référence

The author has granted a non-exclusive licence allowing the National Library of Canada to reproduce, loan, distribute or sell copies of this thesis in microform, paper or electronic formats.

L'auteur a accordé une licence non exclusive permettant à la Bibliothèque nationale du Canada de reproduire, prêter, distribuer ou vendre des copies de cette thèse sous la forme de microfiche/film, de reproduction sur papier ou sur format électronique.

The author retains ownership of the copyright in this thesis. Neither the thesis nor substantial extracts from it may be printed or otherwise reproduced without the author's permission.

L'auteur conserve la propriété du droit d'auteur qui protège cette thèse. Ni la thèse ni des extraits substantiels de celle-ci ne doivent être imprimés ou autrement reproduits sans son autorisation.

0-612-34805-9

Canada

University of Alberta

Library Release Form

Name of Author: Minhui Ma

Title of Thesis: Solvent Microextraction with Simultaneous Back Extraction and the Effect of Tetra-*n*-butylammonium Ion on ODS Bonded Phase.

Degree: Doctor of Philosophy

Year This Degree Granted: 1998

Permission is hereby granted to the University of Alberta Library to reproduce single copies of this thesis and to lend or sell such copies for private, scholarly, or scientific research purposes only.

The author reserves all other publication and other rights in association with copyright in the thesis, and except as hereinbefore provided, neither the thesis nor any substantial portion thereof may be printed or otherwise reproduced in any material form whatever without the author's prior written permission.

Shang An Tian, Nanma
Dongyang, Zhejiang
P. R. China 322121

Date: September 29, 1998

University of Alberta

Faculty of Graduate Studies and Research

The undersigned certify that they have read, and recommend to the Faculty of Graduate Studies and Research for acceptance, a thesis entitled *Solvent Microextraction with Simultaneous Back Extraction and the Effect of Tetra-n-butylammonium Ion on ODS Bonded Phase* submitted by Minhui Ma in partial fulfillment of the requirements for the degree of Doctor of Philosophy.

Frederick J. Cantwell

Dr. F.F. Cantwell, supervisor

Gary Horlick

Dr. G. Horlick

B. Kratochvil

Dr. B. Kratochvil

W.A.G. Graham

Dr. W.A.G. Graham

Dr. F.M. Pasutto

Colin F Poole

Dr. C.F. Poole, external examiner

Date: September 21, 1998

Abstract

This thesis is in two parts. In Part I, a solvent microextraction technique is developed to perform simultaneous forward- and back-extraction across a microliter size organic liquid membrane. The organic liquid membrane phase, consisting of 30–80 μL of *n*-octane, is layered over 0.5–1.6 mL of stirred aqueous sample solution in a 1- or 2-mL micro-reaction vial, which is buffered at high pH for the extraction of basic drugs. The membrane phase is stabilized against mechanical disruption by a small Teflon ring, even when the sample solution is stirred at a speed of 2000 rpm. Two different versions of the apparatus are employed; one for quantitative extraction and the other for high preconcentration. For achieving quantitative extraction, the receiving phase is a 100- or 200-μL aqueous phase buffered at low pH, which is layered over the organic membrane phase. After extraction for a prescribed time, an aliquot of the receiving phase is injected directly into an HPLC for quantification. In 30 min, the basic drugs, mephentermine and 2-phenylethylamine, in a 0.5 or 1.0 mL of pH 13 aqueous sample solution are 100% and 90% extracted, respectively, into a 100 or 200 μL of pH 2.1 aqueous receiving phase. For achieving high preconcentration, the receiving phase is a 1.0- or 0.50-μL microdrop of a pH 2.1 aqueous phase, which is suspended in the organic membrane phase directly from the tip of a microsyringe needle. The source phase is a 1.6-mL sample solution buffered at pH 13. After extraction for a prescribed time, the complete microdrop is injected into an HPLC for quantification. In 15 min, the enrichment factors in the 1.0-μL receiving phase are about 500 for methamphetamine, mephentermine and methoxyphenamine, and about 160 for 2-phenylethylamine. Enrichment factors are approximately doubled for the same 15-min extraction time by using a 0.50-μL receiving drop. A quantitative kinetic model, based on the Whitman two-film theory, is been developed to describe the extraction process and is been verified experimentally.

In Part II of this thesis, the simultaneous sorption of tetra-*n*-butylammonium ion (TBA^+) and butanol on the bonded phase sorbent Partisil-10-ODS-3 from water (the mobile phase), at two different ionic strengths 0.50 and 0.050 mol/L, is studied by the column equilibration technique. When the TBA^+ concentration in the mobile phase is kept constant at 1×10^{-4} mol/L while the butanol concentration is varied from 0 to 0.03 mol/L, the plots of moles of TBA^+ sorbed versus moles of butanol sorbed from mobile phases decrease linearly for both ionic strengths. This indicates that butanol simply competes with TBA^+ for sorption space. In contrast, when the butanol concentration in the mobile phase is kept constant at 1×10^{-3} mol/L while the TBA^+ concentration is varied from 0 to 0.050 and 0.50 mol/L for the ionic strengths 0.050 and 0.50 mol/L, respectively, the plots of moles of butanol sorbed versus moles of TBA^+ sorbed from mobile phases decrease, but not linearly. This indicates that, in addition to competing with butanol for space, sorbed TBA^+ also has a second effect. The second effect of sorbed TBA^+ is that it causes an unfolding of the originally collapsed ODS chains. The unfolding of the ODS chains causes an increase in sorption space for butanol, a decrease in overlap between sorbed TBA^+ and butanol, and a decrease in the distribution coefficient of butanol. The last effect is due to reduced contact area between sorbed butanol and ODS chains. A quantitative model, developed on the basis of the above assumptions, fits well to the experimental data.

This work is dedicated to my wife Qiufei and my parents

for their love and support

Acknowledgments

I would like to thank my supervisor, Dr. Fred Cantwell, for his guidance, encouragement and dedication throughout the work presented in this thesis and for always managing to find the time to be available. I also gratefully acknowledge the financial assistance from the University of Alberta.

Table of Contents

Part I: Solvent Microextraction with Simultaneous Back Extraction (SME/BE) for Sample Clean-up and Preconcentration 1

Chapter 1 – Introduction 2

1.1 Liquid-Liquid Extraction 2

1.2 Solid Phase Extraction 3

1.3 Liquid-Liquid Extraction with Back Extraction 5

1.4 Purpose of This Study 6

Chapter 2 – Quantitative Extraction 7

2.1 Theory 7

2.1.1 Equilibration Considerations 7

2.1.2 Kinetic Considerations 10

2.2 Experimental Section 15

2.2.1 Chemicals 15

2.2.2 Apparatus and Procedures 15

2.3 Results and Discussions 20

2.3.1 Distribution Ratios 20

2.3.2 Diffusion Coefficients 23

2.3.3 Flow Pattern 31

2.3.4 Kinetics 31

2.3.5 Calibration Curves and Analytical Precision 36

Chapter 3 – Preconcentration into a Single Microdrop 39

3.1 Experimental Section 40

3.1.1 Chemicals 40

3.1.2 Apparatus 40

3.1.3 Procedures 42

3.2 Results and Discussions 44

3.2.1 Kinetics 44

3.2.2 Deviations at High C_{a2} 54

3.2.3 Calibration Curves and Analytical Significance 56

3.2.4 Other Tested Designs 58

Chapter 4 – Conclusions and Future Work 62

4.1 Conclusions 62

4.2 Future Work 63

4.2.1 Applications 64

4.2.2 Instrumentation 72

4.2.3 Theory 74

Bibliography 75

Part II: The Changes in Chain Conformation in the ODS Bonded Phase Caused by Sorbed Tetra-*n*-butylammonium Ion (TBA^+) and its Effect on the Sorption of *n*-Butanol 83

Chapter 5 – Introduction 84

5.1 Reversed-Phase Liquid Chromatography 84

5.2 Silica Support 85

5.3 Synthesis of Bonded Phases 87

5.4 Some Properties of Bonded Phases 92

5.4.1 Alkyl Chain Density of the Bonded Phases 92

5.4.2 Polymeric Phase vs. Monomeric Phase 93

5.4.3 Bonded Phase Thickness and Surface Area 96

5.4.4 Alkyl Chain Conformation 97

5.5 Retention Process 99

5.6 Scope of This Study 103

Chapter 6 – Experimental 105

6.1 Chemicals and Stock Solutions 105

6.2 Column Equilibration Technique 106

6.2.1 Column Equilibration Apparatus and Procedure 107

6.2.2 Holdup Volume Measurement 110

6.3 Solvent Extraction/Flow Injection Analysis for Determination of Eluted TBA^+ 111

6.4 Shake-flask Method for Measuring Partition Coefficient of Butanol 114

Chapter 7 – Results and Discussions 116

7.1 Determination of Loading Volumes for TBA^+ and Butanol 116

7.2 Sorption Isotherms 121

7.2.1 Langmuir Isotherm 123

7.2.2 Temkin Isotherm 125

7.2.3 Bilayer Isotherm 126

7.2.4 TBA^+ Sorption Isotherms 127

7.2.5 Butanol Sorption Isotherm 133

7.3 Effect of Butanol on TBA^+ Sorption 136

7.4 Effect of TBA^+ on Butanol Sorption 140

7.4.1 Non-linear relationship between $n_{s,BuOH}$ and $n_{s,TBA}$ 140

7.4.2 Possible Explanations 142

7.4.3 Theoretical Model 148

Chapter 8 – Conclusions and Future Work 163

8.1 Conclusions 163

8.2 Future Work 164

Bibliography 166

Appendix 173

List of Tables

Table — Page

2.1 Calibration of the tubing radii with caffeine $D = (6.3 \pm 0.4) \times 10^{-6}$ cm^2/s at 25.0°C.....27

2.2 Measurement of diffusion coefficients for mephentermine in water, 100 mM NaH_2PO_4 (pH 2.1), 0.10 M NaOH–0.10 M KCl, and *n*-octane at 25.0 °C.....29

2.3 Measurement of diffusion coefficients for 2-phenylethylamine in water, 100 mM NaH_2PO_4 (pH 2.1), 0.10 M NaOH–0.10 M KCl, and *n*-octane at 25.0 °C.....30

2.4 HPLC data for replicate extractions of mephentermine and 2-phenylethylamine from 1.00 mL of 1.00×10^{-4} mol/L sample solution into a 200-μL aqueous receiving phase.....38

3.1 Fitting parameters (k and t_{lag}) and constants for extraction rate curves of mephentermine and 2-phenylethylamine shown in Figures 3.4 and 3.5.....53

7.1 Minimum loading volumes required to reach equilibrium and loading volumes actually used in this study for the ionic strengths (IS) 0.50 and 0.050 mol/L.....120

7.2 Experimental data of TBA^+ sorption isotherms on Partisil ODS-3 at 25.0 °C.....129

7.3 Fitting parameters used to fit the TBA^+ isotherm to the extended Temkin equation.....132

7.4 Fitting parameters used in this study to fit the entire BuOH isotherm to the associative bilayer model and those obtained from double-reciprocal plot of $1/C_{s,BuOH}$ versus $1/C_{m,BuOH}$ for the concentration range 0 to 0.08 mol/L.....135

7.5 *n*-Hexadecane-aqueous distribution coefficients of butanol measured with the aqueous solutions containing 1.0×10^{-3} mol/L butanol and varying concentrations of TBA^+ and NaCl at the ionic strengths 0.50 mol/L and 0.050 mol/L at 25.0 °C.....144

7.6 The values of $n_{s,TBA,crit}$ tested and the fitting parameters obtained from the nonlinear least-square fitting of the model to the data obtained at 0.50 mol/L ionic strength.....155

List of Figures

Figure Page

2.1 Schematic diagram of the solvent microextraction with simultaneous back extraction (SME/BE) system for quantitative extraction.....8

2.2 Schematic Nernst diffusion films (a) and flow patterns (b) in the three-phase extraction system, showing how circulation is induced in the organic membrane phase and the aqueous receiving phase. Toroidal flow is illustrated conceptually with dotted lines and arrows in (b). The rotational component is omitted for clarity.....13

2.3 Flow injection system for the determination of diffusion coefficients. V1 is a 2-way slider valve, T1 is a tee-fitting, V2 is a sample injection valve, C1 is a stainless steel or Teflon coil, and C2 is a Teflon coil.....18

2.4 Plot of apparent distribution ratio K_I for 2-phenylethylamine versus time. The volumes of the aqueous phase and *n*-octane are both 2.00 mL. The initial concentration of 2-phenylethylamine in the aqueous phase (pH13) is 1.00×10^{-3} mol/L. The 5-mL vial is placed in a circulating water bath maintained at 25 °C. The aqueous phase is stirred at 1400 rpm 21

2.5 Plot of apparent distribution ratio K_I for mephentermine versus time. The volumes of the aqueous phase and *n*-octane are 2.00 mL and 50 μL, respectively. The initial concentration of mephentermine in the aqueous phase (pH 13) is 1.00×10^{-3} mol/L. The 2-mL vial is placed in a circulating water bath maintained at 25 °C. The aqueous phase is stirred at 1900 rpm.....22

2.6 Bandbroadening of a sharp solute plug in a laminar flow stream caused by non-uniform parabolic flow profile in a open tube (a) in the absence of radial diffusion of solute molecule, (b) with radial diffusion (finite D value), (c) with instantaneous radial diffusion ($D \rightarrow \infty$). Also shown are the distributions of solute concentration. Small vertical arrows represent radial diffusion.....24

2.7 Typical mephentermine peak from the Taylor dispersion method obtained using Teflon tubing with 0.10 M NaOH–0.10 M KCl as solvent. Also shown are manually drawn tangents to the inflection points and baseline construction. The *x*-axis is time, and the *y*-axis is absorbance.....28

2.8 Plots of observed concentrations of (•) mephentermine and (■) 2-phenylethylamine in the aqueous receiving phase versus stirring time at a stirring speed of 2050 rpm. Points indicate experimental data. Solid lines are fits to eq 2.19. The dashed line and the dotted line are the concentration profiles of mephentermine in the aqueous sample solution and the organic membrane phase, respectively, as calculated by eqs 2.17 and 2.18. The initial concentration of both compounds in the aqueous sample solution was 1.00×10^{-4} mol/L and the dotted horizontal line at 5.00×10^{-4} mol/L corresponds to quantitative extraction.....32

2.9 Calibration curves for (•) mephentermine and (■) 2-phenylethylamine plotted as HPLC peak area versus initial concentration in the aqueous sample solution. Points were obtained in duplicate. See text for details.....37

3.1 Schematic diagram of the SME/BE system for preconcentration into a single microdrop, with the magnetic stirrer on. A small vortex is evident at the bottom of the organic membrane phase. See text for description.....41

3.2 Plots of enrichment factor (EF) versus extraction time, showing the non-linear least-square fit (solid line) of the approximate first-order rate equation 3.7 to the five points (O), at 2, 5, 10, 15 and 20 min, generated from equation 2.19 using constants appropriate to the present 1-μl system (dashed line) for the extraction of mephentermine. See text for details.....47

3.3 Chromatograms of a mixture of 2-phenylethylamine (**1**), methamphetamine (**2**), mephentermine (**3**), and methoxyphenamine (**4**) in standard solutions, (a) 2.0×10^{-6} M **1**, 1.0×10^{-6} M **2**, **3** and **4**, (b) 2.0×10^{-5} M **1**, 1.0×10^{-5} M **2**, **3** and **4**, (c) 2.0×10^{-4} M **1**, 1.0×10^{-4} M **2**, **3** and **4**, prepared in 50 mM NaH_2PO_4 (pH2.5); and chromatograms of 1-μL back-extractants after (d) 5 min and (e) 15 min of extraction from a 1.6-mL sample solution of 2.0×10^{-6} M **1**, 1.0×10^{-6} M **2**, **3**, and **4** at pH 13, stirred at 1900 rpm. Chromatographic conditions: column, 15 cm long × 3.2 mm i.d., 5-μm ODS; detection, UV 220 nm; mobile phase, 25 mM NaH_2PO_4 (pH2.5)/methanol (70/30, v/v); flow rate, 0.5 mL/min; injection volume, 1.0 μL.....50

3.4 Plots of observed EFs of (•) mephentermine and (▪) 2-phenylethylamine in the 1.0_0-μL receiving phase versus extraction time at a stirring speed of 2050 rpm. Points indicate experimental data. Solid lines are fits to eq 3.7. The initial concentration of both compounds in the aqueous sample solution was 1.0×10^{-5} M. Other constants are given in Table 3.1.....51

3.5 Plots of observed EFs of (•) mephentermine and (▪) 2-phenylethylamine in the 0.50-μL receiving phase versus extraction time at a stirring speed

of 2050 rpm. Points indicate experimental data. Solid lines are fits to eq 3.7. The initial concentration of both compounds in the aqueous sample solution was 1.0×10^{-5} M. Other constants are given in Table 3.1.....52

3.6 Plots of observed EFs of (•) mephentermine and (▪) 2-phenylethylamine in the 0.50-μl receiving phase versus extraction time, showing deviations from the theoretical rate equations. The rest are the same as Figure 3.5.....55

3.7 Calibration curves for (•) mephentermine and (▪) 2-phenylethylamine plotted as HPLC peak area versus initial concentration in the aqueous sample solution. Points were obtained in duplicate. See text for details. The last data point corresponding to very high C_{a2} of mephentermine was not included in the linear regression for the reason discussed in section 3.2.2.....57

3.8 The Teflon rod probe system shown for the extraction from 5 mL of aqueous sample solution through a 10-μL *n*-octane organic phase into a 1-μL aqueous receiving drop.....59

3.9 Plots of observed EFs of mephentermine in the 1-μL receiving phase versus extraction time at a stirring speed of 1200 rpm. Experimental conditions: $C_{a1,initial} = 1.0 \times 10^{-5}$ M, $V_{a1} = 5$ mL, $V_o = 10$ μL, $V_{a2} = 1.0$ μL, 25.0 °C.....60

3.10 The drop-in-drop probe system shown for the extraction from 5 mL of aqueous sample solution through a 10-μL *n*-octane organic phase into a 1-μL aqueous receiving drop.....61

4.1 Schematic diagram of the extraction of ionic compounds using an ion-pairing reagent through an organic liquid membrane. The extraction of analyte anion A^- is shown as an example. Ion pairing can occur either in

the source phase or at the interface.....65

4.2 Schematic representation of the extraction of amino acids (a) from acidic source to basic receiving phases using a negatively charged pairing ion P^- and (b) from basic source to acidic receiving phases using a negatively charged pairing ion P^+.....67

4.3 Schematic illustration of the transport of metal ions through an organic liquid membrane using carriers: (a) C^- as complexing agent dissolved in the source phase, (b) C as complexing agent dissolved in membrane phase, and (c) $R_4N^+Cl^-$ as liquid anion exchanger dissolved in the membrane phase. Q^- and L^{3-} are complexing agents.....69

4.4 (a) BLM cell for measuring metal ion transport across a chloroform membrane. (b) Pb^{2+} concentrations in the source (•) and receiving (o) phases versus time. Initial conditions: source phase, 15 mL of 0.10 M Pb^{2+} in acetate buffer at pH 6.18; membrane phase, 30 mL of 5.0 mM acyclic polyether dicarboxylic acid in chloroform; receiving phase, 15 mL of 0.10 M nitric acid. From reference 101.....71

4.5 Schematic diagrams of (a) the tubing-in-tubing drophead and (b) the on-line microdrop extraction-HPLC system. V: LC injection valve.....73

5.1 Synthesis of octadecylsilyl (ODS) reversed phase bonded phase from mono- and di-functional silanes.....89

5.2 Synthesis of octadecylsilyl (ODS) reversed phase bonded phase from trifunctional silane.....90

5.3 Instantaneous ODS chain conformations shown in stereo view obtained by molecular dynamics simulations of an unit cell (32 Å per side) with an average chain density of 2.1 $\mu mol/m^2$ at 300 K. (a) Multiple ODS

chains with no solvent, (b) a single ODS chain with no solvent, and (c) multiple ODS chains with 20% water–80% methanol at 50 ps of molecular dynamics. Hydrogen atoms in (a) and (c) and solvents in (c) have been removed for easy viewing. These conformations can be viewed in three dimensions using either viewers or naked eyes. (From reference 68.).....98

6.1 Column equilibration apparatus.....108

6.2 Solvent extraction/flow injection analysis system for the determination of TBA^+. V1 is a 2-way slider valve, V2 is a 3-way slider valve, v3 is a sample injection valve, T1 and T2 are tee-fittings, EC is an extraction coil, and PS is a phase separator.....113

7.1 TBA^+ loading curves for 3.062×10^{-4} mol/L TBA^+ in pH 5.0 buffer at ionic strengths of 0.050 mol/L at flow rates 1 mL/min (●) and 3 mL/min (▲) and of 0.50 mol/L at flow rates 1 mL/min (○) and 3 mL/min (△).....117

7.2 Loading curves for 1.021×10^{-4} mol/L TBA^+ alone (●) and in the presence of 5.00×10^{-4} mol/L butanol (▲), and for 5.00×10^{-4} mol/L butanol alone (○) and in the presence of 1.021×10^{-4} mol/L TBA^+ (△). Sample solution is buffered at pH 5.0 with an ionic strength of 0.050 mol/L.....118

7.3 Loading curves for 1.021×10^{-4} mol/L TBA^+ alone (●) and in the presence of 5.00×10^{-4} mol/L butanol (▲), and for 5.00×10^{-4} mol/L butanol alone (○) and in the presence of 1.021×10^{-4} mol/L TBA^+ (△). Sample solution is buffered at pH 5.0 with an ionic strength of 0.50 mol/L.....119

7.4 A hypothetical sorption isotherm (solid line). The distribution coefficient, $K_{D,i}$, at any point of the isotherm is the ration of $C_{s,i}/C_{m,i}$.....122

7.5 TBA^+ sorption isotherms on Partisil-10 ODS-3 from pH 5 aqueous solutions at two ionic strengths: 0.50 M (○) and 0.050 M (●). Solid lines are fits to the extended Temkin equation with fitting parameters given in Table 7.3.....130

7.6 TBA^+ sorption isotherms expanded from Figure 7.5 to show the region with TBA^+ concentrations lower than 0.060 mol/L.....131

7.7 BuOH sorption isotherms on Partisil-10 ODS-3 from pH 2 aqueous solutions. Solid line is fit to the bilayer equation with fitting parameters given in Table 7.4. Data from reference 84.....134

7.8 Plot of the number of moles of TBA^+ sorbed versus the number of moles of BuOH sorbed in the ODS stationary phase at two ionic strengths: 0.50 mol/L (●) and 0.050 mol/L (○). The TBA^+ concentration in the mobile phase is kept constant at 1.0×10^{-4} mol/L and the butanol concentration is varied from 0 to 0.030 mol/L. Solid lines are the linear least-square fits.....137

7.9 Plot of moles of TBA^+ sorbed in the ODS stationary phase at two ionic strengths: 0.50 mol/L (●) and 0.050 mol/L (○). The butanol concentration in the mobile phase is kept constant at 1.0×10^{-3} mol/L and the TBA^+ concentration is varied from 0 to 0.50 or 0.050 mol/L for ionic strengths 0.50 and 0.050 mol/L, respectively.....141

7.10 Simultaneous sorption of 1-propanol and octane-1-sulphonate in ODS stationary phase from pH3.0 phosphate buffer containing 2 % 1-propanol and varying concentrations of octane-1-sulphonate (a) (From reference 130). The solid lines in (a) are digitized and replotted as $C_{s,propanol}$ versus $C_{s,octane\text{-}1\text{-}sulphonate}$ (b). Temperature: 40 °C.....146

7.11 Simultaneous sorption of 1-propanol and octane-1-sulphonate in ODS stationary phase from pH3.0 phosphate buffer containing 10 % 1-propanol and varying concentrations of dodecane-1-sulphonate (a) (From reference 130). The solid lines in (a) are digitized and replotted as $C_{s,propanol}$ versus $C_{s,dodecane\text{-}1\text{-}sulphonate}$ (b). Temperature: 40 °C.....147

7.12 Schematic diagrams of ODS bonded stationary phase sorbed with TBA^+ ( ) and butanol ( ) at (a) low and (b) high surface concentrations of sorbed TBA^+.....150

7.13 Nonlinear least-square fit of the model to the experimental data (O) obtained at the ionic strength 0.50 mol/L with a testing value of $n_{s,TBA,crit}$ = 1.6×10^{-5} mol. The last four data points (◇) are not included in the fitting because of the significant salting-in effect at high concentrations of TBA^+ in the mobile phase.....156

7.14 Nonlinear least-square fit of the model to the experimental data (O) obtained at the ionic strength 0.50 mol/L with a testing value of $n_{s,TBA,crit}$ = 2.2×10^{-5} mol. The last four data points (◇) are not included in the fitting because of the significant salting-in effect at high concentrations of TBA^+ in the mobile phase.....157

7.15 Nonlinear least-square fit of the model to the experimental data (O) obtained at the ionic strength 0.50 mol/L with a testing value of $n_{s,TBA,crit}$ = 3.8×10^{-5} mol. The last four data points (◇) are not included in the fitting because of the significant salting-in effect at high concentrations of TBA^+ in the mobile phase.....158

7.16 Plot of the number of moles of butanol sorbed versus the number of moles of TBA^+ sorbed in the ODS stationary phase at two ionic strengths:

0.50 mol/L (●) and 0.050 mol/L (○). The butanol concentration in the mobile phase is kept constant at 1.0×10^{-3} mol/L and the TBA^+ concentration is varied from 0 to 0.50 and 0.050 mol/L for ionic strengths 0.50 and 0.050 mol/L, respectively. Solid lines are the nonlinear least-square fits of the model to data with $n_{s,TBA,crit} = 2.2 \times 10^{-5}$ for both ionic strengths. The last four data points for ionic strength 0.50 mol/L as shown in Figure 7.9 are not included in the fitting because of the significant salting-in effect at high concentrations TBA^+ in the mobile phase.....160

List of Symbols

Part I:

a	tube radius (cm)
A_1	interfacial area for the a1-o interface (cm^2)
A_2	interfacial area for the o-a2 interface (cm^2)
$C_{a1,initial}$	initial concentration of analyte in the aqueous source phase (mol/L)
C_{a1}	concentration of analyte in the source phase at time t (mol/L)
C_o	concentration of analyte in the organic phase at time t (mol/L)
C_{a2}	concentration of analyte in the receiving phase at time t (mol/L)
$C_{a1,eq}$	equilibrium concentration of analyte in the source phase (mol/L)
$C_{o,eq}$	equilibrium concentration of analyte in the organic phase (mol/L)
$C_{a2,eq}$	equilibrium concentration of analyte in the receiving phase (mol/L)
D_{a1}	diffusion coefficient of analyte in the source phase (cm^2/s)
D_o	diffusion coefficient of analyte in the organic phase (cm^2/s)
D_{a2}	diffusion coefficient of analyte in the receiving phase (cm^2/s)
EF	enrichment factor
EF_{max}	maximum enrichment factor
k_1, k_2, k_3, k_4	first-order extraction rate constants (s^{-1})
k	first-order rate constant related to the individual rate constants k_1, k_2 and k_3 (s^{-1})
K_1	distribution ratio between the organic and the source phases (L/L)
K_2	distribution ratio between the organic and the receiving phases (L/L)
K_a	acid dissociation constant
K	Taylor dispersion coefficient (cm^2/s)

m	total mass of solute injected in Taylor dispersion apparatus (mol or g)
$n_{i,a1}$	amount of analyte in the aqueous source phase at time t (mol)
$n_{i,o}$	amount of analyte in the organic membrane phase at time t (mol)
$n_{i,a2}$	amount of analyte in the aqueous receiving phase at time t (mol)
V_{a1}	volume of the aqueous source phase (cm^3)
V_o	volume of the organic membrane phase (cm^3)
V_{a2}	volume of the aqueous receiving phase (cm^3)
t	time (s)
$\bar{t}$	dispersion time (s)
t_{lag}	lag-time (s)
$\bar{U}$	average linear velocity of flow (cm/s)
$\bar{\beta}_{o1}$	overall mass transfer coefficient with respect to the organic membrane phase through the a1-o interface (cm/s)
$\bar{\beta}_{a2}$	overall mass transfer coefficient with respect to the aqueous receiving phase through the o-a2 interface (cm/s)
β_{a1}	individual mass transfer coefficient for the aqueous source phase (cm/s)
β_{a2}	individual mass transfer coefficient for the aqueous receiving phase (cm/s)
β_{o1}, β_{o2}	individual mass transfer coefficient for the organic phase with respect to the a1-o and o-a2 interfaces, respectively (cm/s)
δ_{a1}	diffusion film thickness in the aqueous source phase (cm)
δ_{a2}	diffusion film thickness in the aqueous receiving phase (cm)
δ_{o1}, δ_{o2}	diffusion film thicknesses in the organic phase with respect to the a1-o and o-a2 interfaces, respectively (cm)
κ	distribution coefficient of neutral molecule (L/L)
σ^2	variance of the distribution (s^2)

Part II:

$A_{s,TBA}$	space available in the stationary phase for TBA^+ sorption (cm^2)
$A_{s,t,TBA}$	total space available for TBA^+ sorption in the absence of sorbed butanol (cm^2)
$A_{s,BuOH}$	space occupied by butanol (cm^2)
$\bar{A}_{BuOH}$	space in the TBA^+ sorption plane that is effectively occupied per mol of butanol sorbed (cm^2/mol of BuOH)
$A_{s,BuOH}$	space available in the stationary phase for butanol sorption (cm^2)
$A_{s,t,BuOH}$	total space available for butanol sorption in the absence of sorbed butanol (cm^2)
$A_{s,TBA}$	space occupied by TBA^+ (cm^2)
$\bar{A}_{TBA}$	space in the butanol sorption plane that is effectively occupied per mol of TBA^+ sorbed (cm^2/mol of TBA)
$A_{s,t,BuOH,init}$	total space initially available for the sorption of butanol in the absence of sorbed TBA^+ (cm^2)
$\bar{A}_{TBA,init}$	space occupied per mole of sorbed TBA^+ extrapolated to $n_{s,TBA} = 0$ (cm^2/mol of TBA)
$C_{m,i}$	concentration of solute *i* in the mobile phase (mol/L)
$C_{s,i}$	concentration of solute *i* in the stationary phase (mol/kg) or (mol/cm^2)
$C_{s,i,max}$	maximum concentration of solute *i* sorbed as a monolayer on the sorbent (mol/kg) or (mol/cm^2)
ΔG_{BuOH}	free energy of transfer of butanol from the mobile phase to the ODS stationary phase (J/mol)
$\Delta G_{BuOH,init}$	free energy of transfer of butanol in the absence of sorbed TBA^+ (J/mol)
$K_{D,i}$	distribution coefficient of solute *i* (L/kg) or (L/cm^2)

$K_{D,BuOH,init}$	distribution coefficient of butanol in the absence of TBA^+ (L/kg) or (L/cm^2)
K_i	sorption equilibrium constant for solute *i* (L/kg) or (L/cm^2)
$K_{1,i}$, $K_{2,i}$	sorption equilibrium constants for solute *i* sorbed in the first monolayer and the second layer, respectively (L/kg) or (L/cm^2)
n_i	moles of solute *i* sorbed at the ODS stationary phase (mol)
$n_{T,i}$	total moles of solute *i* eluted from the column (mol)
$n_{DL,TBA}$	moles of TBA^+ excluded from the diffuse layer (mol)
$n_{s,TBA}$	moles of TBA^+ sorbed in the ODS stationary phase (mol)
$n_{s,TBA,crit}$	critical number of moles of TBA^+ sorbed in the stationary phase (mol)
$n_{s,BuOH}$	moles of butanol sorbed in the ODS stationary phase (mol)
n_{ODS}	moles of ODS chains in the stationary phase (mol)
R	ideal gas constant (8.314 J/mol·K)
T	temperature (K)
V_m	void volume of the packed bed, the frits, and the connecting tubing (L)
θ	fraction of the sorbent surface covered with sorbed molecule

Part I

Solvent Microextraction with Simultaneous Back Extraction (SME/BE) for Sample Clean-up and Preconcentration

Chapter 1

Introduction

In spite of the great improvement in sensitivity and selectivity of modern analytical instrumentation, sample preparation techniques are still critically important in the determination of analytes in complex matrices such as biological and environmental samples. In many analytical procedures, sample preparation is the time and cost determining step. The goals of sample preparation are to isolate analytes from interferences (i.e. clean-up) and to provide a concentration appropriate for detection. The latter often means preconcentration. Liquid-liquid extraction (LLE) and solid phase extraction (SPE) are the most commonly used techniques for preconcentration and clean-up prior to high performance liquid chromatographic (HPLC) and capillary electrophoretic (CE) analysis.[1-5]

1.1 Liquid-Liquid Extraction

For many decades, liquid-liquid extraction (LLE) has been a widely used and accepted method for the preparation of aqueous samples. However, manual LLE, performed most frequently in separatory funnels, generates a large amount of organic solvent waste and is time- and labor-intensive and not suitable for automation. Also, emulsion formation is often a problem. In spite of these drawbacks, about 45% of the respondents, according to a recent survey,[5] are still using LLE for sample preparation. Among the advantages of LLE are straightforward method development, high reproducibility, and high sample capacity.

Numerous efforts have been made to improve upon the manual LLE technique. The use of solvent extraction-flow injection (SE-FI)[6,7] has solved some of the problems,

but it generally is less sensitive than batch extraction and requires more complex hardware. Laboratory workers generally do not use flow extraction systems in routine sample preparation.[8] To reduce solvent consumption, LLE has been performed in volumetric flasks[9-11] or in centrifuge tubes[12,13] with small phase ratios, e.g. 1 mL or 50 μL solvent with 100 mL or 2 mL aqueous sample. Miniaturized LLE procedures are more readily automated. They have been carried out automatically in vials by GC or LC autosamplers.[8,14-16]

Techniques recently have been developed to perform LLE using only one microdrop of organic solvent. Liu and Dasgupta[17] described an elegantly designed microdrop LLE system which was able to perform automatic drop-in-drop extraction and in situ optical detection. Jeannot and Cantwell introduced two extremely simple new techniques, in which a single drop of *n*-octane is contained either at the end of a Teflon rod[18] or directly on the tip of a GC microsyringe needle[19] in a stirred aqueous sample solution. After stirring for a prescribed time, part or all of the organic phase is injected into the GC for quantification. Due to the extremely small phase ratio, the latter system has been successfully applied to speciation studies.[20] More recently, microdrop LLE-GC using a microsyringe has also been reported by others.[21]

1.2 Solid Phase Extraction

Because of the above mentioned drawbacks of conventional LLE, solid phase extraction (SPE)[22-25] has become the technique most commonly used in sample preparation for HPLC. The extraction process involved in SPE is similar to the separation process in chromatography. Solid phase sorbent is contained either in a cartridge or in a membrane (extraction disk). Liquid sample and solvent are passed through cartridge or disk either by suction or by positive pressure. Octadecyl (C_{18}) and octyl (C_8) modified

silica phases are the most frequently used sorbents, although other sorbents such as polymer based phases or ion exchange resins are also used.

The advantages of SPE over conventional LLE include higher recovery, more efficient separation of interferences from analytes, reduced organic solvent consumption, easier collection of the total analyte fraction, more convenient manual procedures, and easier automation.[2] However, the current SPE techniques still have a number of problems. For example, batch-to-batch reproducibility continues to be the number one concern of chromatographers during the selection of SPE devices.[5] For samples with suspended particles, column clogging is a problem. The technique is still fairly labor-intensive for manual operation.[5] Solvent evaporation and re-dissolution are often required prior to injection into HPLC because the eluting solvents are often stronger than the mobile phase used and also because of the relatively large volume of solvent used for elution. These steps are tedious and also prone to loss of analytes by evaporation and adsorption. For trace enrichment, a large volume of sample is often required because the initial-to-final sample volume ratio determines the enrichment factor. However, handling a large volume of sample can be extremely time consuming. For example, it took about 6.5 hours to pass 500 mL of water sample through a SPE disk in order to achieve 1000–fold preconcentration into a 0.50-mL final solution.[26]

To eliminate the need for solvent evaporation and other tedious manual manipulations, SPE has been performed on-line using a short precolumn.[27-30] In this way, analytes in the whole sample can be transferred to the HPLC or CE system, resulting in a larger enrichment factor. However, for analytes with insufficient retention in the precolumn, this advantage can be lost due to sample breakthrough. Solid phase microextraction (SPME)[31-34] is another SPE technique which does not require solvent evaporation and which makes possible high preconcentration from a small volume of

sample. When combined with thermal desorption in GC, SPME is a totally solvent-free and extremely versatile sample preparation technique for volatile and semi-volatile compounds. However, when SPME is coupled to HPLC or CE, a solvent desorption step is still required[35] and sometimes a lengthy process is required to recover all sorbed analytes and to avoid carry-over.[36-38] Because the coatings available so far are non- or slightly polar, the current applications of SPME are limited to nonpolar compounds or compounds of medium polarity.[39,40]

1.3 Liquid-Liquid Extraction with Back Extraction

As mentioned earlier, the coupling of LLE to GC is also relatively easy by direct injection of the organic phase. However, this is not the case for reversed phase HPLC for which it is necessary to evaporate the organic phase to dryness and to re-dissolve the residue in an aqueous medium. If the analytes in the organic phase are ionizable, back extraction into a second aqueous phase is a viable alternative because it not only makes possible direct injection of the aqueous back-extractant into the HPLC but it also provides further purification. However, sequential forward- and back-extraction methods involve many tedious manipulations which may cause even more loss of analytes and more contamination than does solvent evaporation. No simple and reliable alternatives to a manual approach are currently available to perform LLE with back extraction, although some efforts have been made to simplify the process. Multiple SE-FI systems,[41,42] which involve the use of multiple phase segmentations and separations, are available but are complicated. In a recent development, in which the need for phase separation and segmentation was eliminated by coating a film of organic phase on a Teflon tube wall,[43] the sample capacity of the wetting film is very small.

One significant development in this area is the supported liquid membrane (SLM) technique[44-50] which employs a porous membrane, in the form of either a flat sheet or a hollow fiber, impregnated with an organic solvent to separate an aqueous source phase (i.e. sample solution) and aqueous receiving phase (i.e. back-extractant). In this technique, the aqueous source phase is continuously pumped, while the aqueous receiving phase is often stagnant. With this configuration, the consumption of organic solvent is minimal and on-line coupling to HPLC is very simple.[47,48] Because forward- and back-extraction are carried out simultaneously, SLM is capable of achieving much higher preconcentration than is the sequential forward- and back-extraction method. This is because of the "pumping" phenomenon that occurs during simultaneous forward- and back-extraction (e.g. driven by a pH difference between the two aqueous phases). However, memory effect and long-term instability of the supported organic membrane seem to be the current problems with the SLM technique.[49]

1.4 Purpose of This Study

The purpose of this study is to develop a new micro LLE technique which can perform simultaneous forward and back extractions. The goals are to make LLE with back extraction simpler for both manual operation and automation, to minimize the consumption of organic solvent, to achieve high recovery or high preconcentration in a relatively short time, and to build theoretical models to describe the mass transfer process involved in simultaneous forward and back extractions. The new technique developed is based on an unsupported liquid organic membrane. It has two different versions, one for quantitative extraction and the other for high preconcentration.

Chapter 2

Quantitative Extraction[a]

In this chapter, a micro LLE technique is introduced which can be used to perform forward and back extractions simultaneously and quantitatively, in a relatively short time. The system uses an unsupported liquid organic membrane (≤ 80 μL), held within a Teflon ring, to separate the aqueous sample and receiving phases (Figure 2.1). The aqueous sample solution is stirred by a magnetic stirrer to facilitate the mass transfer process. After extraction, an aliquot of the top aqueous receiving phase is injected directly into an HPLC for quantification. Quantitative extraction with an enrichment factor of 5 or higher can be achieved very simply. Another important objective of this work is to develop a theoretical model to describe the mass transfer kinetics involved in the system.

2.1 Theory

2.1.1 Equilibration Considerations

The system under consideration involves a series of two reversible extractions. The analyte in the aqueous sample solution is first extracted into the organic membrane phase and then back-extracted into the aqueous receiving phase. For analyte *i*, the extraction equations can be written as

$$i_{a1} \underset{k_2}{\overset{k_1}{\rightleftharpoons}} i_o \underset{k_4}{\overset{k_3}{\rightleftharpoons}} i_{a2} \qquad (2.1)$$

---

a. A version of this chapter has been published. Ma, M.; Cantwell, F.F. in press, *Anal. Chem.* 1998.

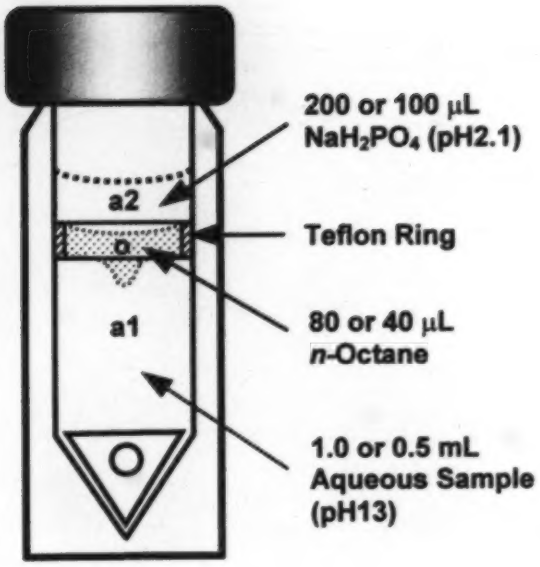

Figure 2.1. Schematic diagram of the solvent microextraction with simultaneous back extraction (SME/BE) system for quantitative extraction.

where the subscript a1 represents the aqueous source phase, i.e. the aqueous sample solution, o the organic membrane phase, and a2 the aqueous receiving phase. The constants, k_1, k_2, k_3, and k_4, are the first-order extraction rate constants. At equilibrium, the mass-balance relationship for i is given by

$$C_{a1,initial} = \frac{K_2 C_{a2,eq}}{K_1} + K_2 C_{a2,eq} \frac{V_o}{V_{a1}} + C_{a2,eq} \frac{V_{a2}}{V_{a1}} \qquad (2.2)$$

where $C_{a1,initial}$ and $C_{a2,eq}$ are the initial and equilibrium concentrations in the aqueous source and receiving phases, respectively, V_{a1}, V_o, and V_{a2} are the phase volumes for the respective phases, and K_1 and K_2 are the distribution ratios defined by

$$K_1 = C_{o,eq}/C_{a1,eq} \qquad (2.3)$$

and

$$K_2 = C_{o,eq}/C_{a2,eq} \qquad (2.4)$$

By rearranging eq 2.2, the analyte concentration at equilibrium in the aqueous receiving phase is given by

$$C_{a2,eq} = \frac{K_1 C_{a1,initial}}{K_2 + K_1 K_2 (V_o/V_{a1}) + K_1 (V_{a2}/V_{a1})} \qquad (2.5)$$

If $K_2 + K_1 K_2 (V_o/V_{a1}) \ll K_1 (V_{a2}/V_{a1})$, i.e. K_2 is very small and $V_o < V_{a2}$, eq 2.5 can be written as

$$C_{a2,eq} = \frac{V_{a1}}{V_{a2}} C_{a1,initial} \qquad (2.6)$$

This condition represents complete extraction (i.e. 100% recovery) of analyte from the sample to the aqueous receiving phase at equilibrium. In order to have a very small K_2, it is necessary to convert the back-extracted analyte by reactions (e.g. protonation, complexation) to a species in the receiving phase that has very slight affinity for the organic membrane phase. In this study, for example, the model compounds, mephentermine and 2-phenylethylamine, are protonated upon being back-extracted into the aqueous receiving phase to yield ammonium ions, which are insoluble in the organic membrane.

$$B_{a1} \rightleftharpoons B_o \rightleftharpoons BH_{a2}^+ \qquad (2.7)$$

The required experimental conditions include a high pH in the aqueous source phase and a low pH in the aqueous receiving phase so that almost only the neutral form of the analyte exists in the source phase and only the ionic form exists in the receiving phase.

2.1.2 Kinetic Considerations.

For a two-phase extraction system, the equation for the mass transfer across an interface can be written as[51-53]

$$\frac{dn_{i,o}}{dt} = -\frac{dn_{i,aq}}{dt} = A\,\bar{\beta}_o\,(K_i\,C_{i,aq} - C_{i,o}) = A\,\bar{\beta}_{aq}\,(C_{i,aq} - C_{i,o}/K_i) \qquad (2.8)$$

where $C_{i,aq}$ and $C_{i,o}$ are the concentrations of analyte in the aqueous and the organic phases, respectively, at time t, A is the interfacial area, $\overline{\beta}_o$ and $\overline{\beta}_{aq}$ are the overall mass transfer coefficients with respect to the organic and the aqueous phases, and K is the distribution ratio. The amount of analyte extracted into the organic phase per unit time is equal to the amount of analyte lost from the aqueous phase. The above equation can be rewritten as

$$\frac{dn_{i,o}}{dt} = -\frac{dn_{i,aq}}{dt} = \frac{A\,\overline{\beta}_o\,K_i}{V_{aq}}\,n_{i,aq} - \frac{A\,\overline{\beta}_o}{V_o}\,n_{i,o} = k_1\,n_{i,aq} - k_2\,n_{i,o} \qquad (2.9)$$

For the three-phase extraction system as defined by eq 2.1, the rate equations with respect to the analyte in each phase can be derived by analogy with two consecutive reversible homogeneous first-order chemical reactions:

$$\frac{dn_{i,a1}}{dt} = \frac{A_1\,\overline{\beta}_{o1}}{V_o}\,n_{i,o} - \frac{A_1\,\overline{\beta}_{o1}\,K_1}{V_{a1}}\,n_{i,a1} = k_2\,n_{i,o} - k_1\,n_{i,a1} \qquad (2.10)$$

$$\frac{dn_{i,o}}{dt} = \frac{A_1\,\overline{\beta}_{o1}\,K_1}{V_{a1}}\,n_{i,a1} - \frac{A_1\,\overline{\beta}_{o1}}{V_o}\,n_{i,o} + \frac{A_2\,\overline{\beta}_{a2}}{V_{a2}}\,n_{i,a2} - \frac{A_2\,\overline{\beta}_{a2}}{V_o\,K_2}\,n_{i,o} \qquad (2.11)$$

$$\frac{dn_{i,a2}}{dt} = \frac{A_2\,\overline{\beta}_{a2}}{V_o\,K_2}\,n_{i,o} - \frac{A_2\,\overline{\beta}_{a2}}{V_{a2}}\,n_{i,a2} = k_3\,n_{i,o} - k_4\,n_{i,a2} \qquad (2.12)$$

where $n_{i,a1}$, $n_{i,o}$, and $n_{i,a2}$ are the amount of analyte in the aqueous source phase, the organic membrane phase, and the aqueous receiving phase at time t, respectively, A_1 and A_2 are the interfacial areas for the a1-o and the o-a2 interfaces, and $\overline{\beta}_{o1}$ and $\overline{\beta}_{a2}$ are the overall mass transfer coefficients with respect to the organic membrane phase and the aqueous receiving phase through the a1-o and the o-a2 interfaces, respectively. The

overall mass transfer coefficients are related to the individual mass transfer coefficient by the following expressions:

$$\frac{1}{\bar{\beta}_{o1}} = \frac{1}{\beta_{o1}} + \frac{K_1}{\beta_{a1}} \tag{2.13}$$

$$\frac{1}{\bar{\beta}_{a2}} = \frac{1}{\beta_{a2}} + \frac{1}{K_2\,\beta_{o2}} \tag{2.14}$$

where β_{a1}, β_{a2}, β_{o1}, and β_{o2} are the individual mass transfer coefficients for the respective phases.

According to the Whitman two-film theory,[51,53] in the interfacial region there exist two stagnant layers of solution, the Nernst diffusion films, one on either side of the interface which extend into the solution for distances δ. Farther away from the interface than the distances δ are the bulk solutions, which are considered to be so rapidly mixed that each bulk solution is entirely homogeneous at any time. These films vary from 10^{-2} cm thick with slow stirring to 10^{-4} cm thick with intensive stirring,[54] and can be crossed only by diffusion. The film thickness is inversely related to the stirring speed[19] and is also affected by viscosity and density of the liquids and the equipment geometry. At steady state of diffusion across the stagnant films adjacent to the interface, $\beta = D/\delta$, where D is the diffusion coefficient of the analyte and δ is the film thickness in the appropriate phase. There are four Nernst diffusion films in this three-phase extraction system, two for each interface (see Figure 2.2a). Therefore, eqs 2.13 and 2.14 can be written as

$$\frac{1}{\bar{\beta}_{o1}} = \frac{\delta_{o1}}{D_o} + \frac{K_1\,\delta_{a1}}{D_{a1}} \tag{2.15}$$

$$\frac{1}{\bar{\beta}_{a2}} = \frac{\delta_{a2}}{D_{a2}} + \frac{\delta_{o2}}{K_2\,D_o} \tag{2.16}$$

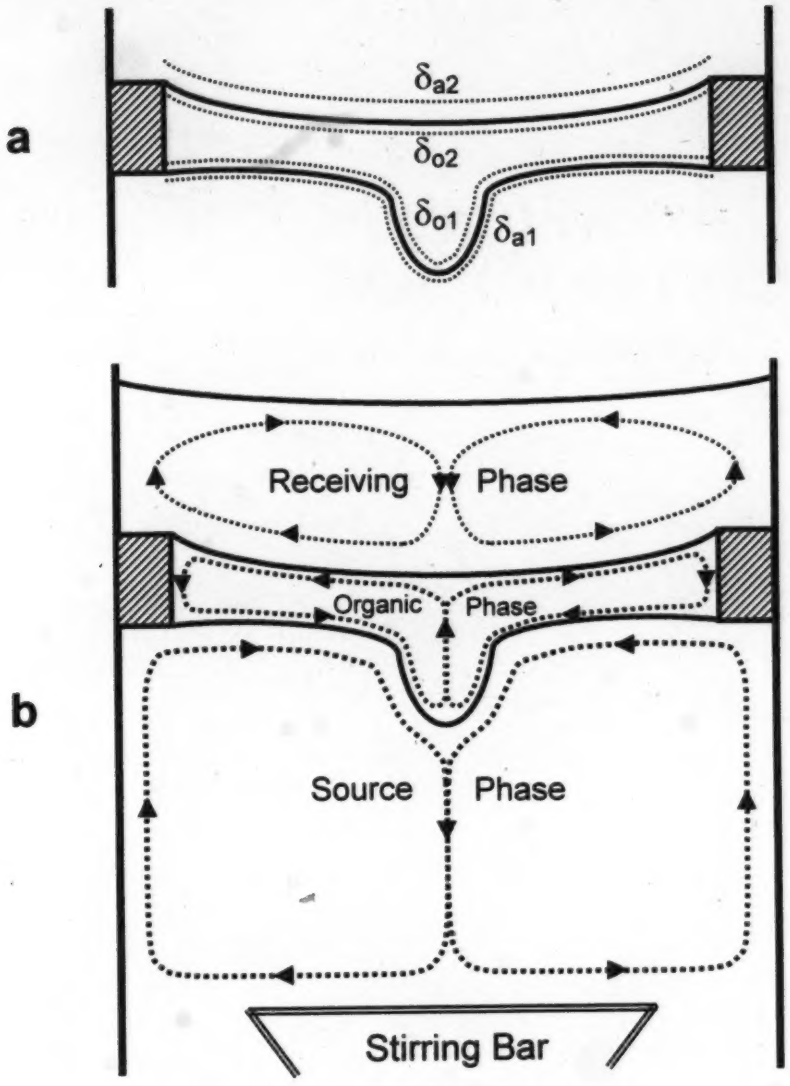

Figure 2.2. Schematic Nernst diffusion films (a) and flow patterns (b) in the three-phase extraction system, showing how circulation is induced in the organic membrane phase and the aqueous receiving phase. Toroidal flow is illustrated conceptually with dotted lines and arrows in (b). The rotational component is omitted for clarity.

The set of differential equations 2.10, 2.11, and 2.12 can be solved mathematically to obtain three expressions, which describe the change in the amount of analyte, or in the analyte concentration in each phase, with extraction time. There are different mathematical methods[55-57] that can be used to solve the set of differential equations. The following solutions are obtained using the method outlined by Frost and Pearson:[55]

$$C_{a1} = C_{a1,initial}\left\{\frac{k_2 k_4}{\lambda_2 \lambda_3} + \frac{k_1 (\lambda_2 - k_3 - k_4)}{\lambda_2 (\lambda_2 - \lambda_3)} e^{-\lambda_2 t} + \frac{k_1 (k_3 + k_4 - \lambda_3)}{\lambda_3 (\lambda_2 - \lambda_3)} e^{-\lambda_3 t}\right\} \quad (2.17)$$

$$C_o = C_{a1,initial}\frac{V_{a1}}{V_o}\left\{\frac{k_1 k_4}{\lambda_2 \lambda_3} + \frac{k_1 (k_4 - \lambda_2)}{\lambda_2 (\lambda_2 - \lambda_3)} e^{-\lambda_2 t} + \frac{k_1 (\lambda_3 - k_4)}{\lambda_3 (\lambda_2 - \lambda_3)} e^{-\lambda_3 t}\right\} \quad (2.18)$$

$$C_{a2} = C_{a1,initial}\frac{V_{a1}}{V_{a2}}\left\{\frac{k_1 k_3}{\lambda_2 \lambda_3} + \frac{k_1 k_3}{\lambda_2 (\lambda_2 - \lambda_3)} e^{-\lambda_2 t} + \frac{k_1 k_3}{\lambda_3 (\lambda_2 - \lambda_3)} e^{-\lambda_3 t}\right\} \quad (2.19)$$

The extraction rate constants k_1, k_2, k_3, and k_4 are defined by eqs 2.1, 2.10, and 2.12, while λ_2 and λ_3 are given by:

$$\lambda_2 = \frac{1}{2}(p + q) \quad (2.20)$$

$$\lambda_3 = \frac{1}{2}(p - q) \quad (2.21)$$

where

$$p = (k_1 + k_2 + k_3 + k_4) \quad (2.22)$$

$$q = [p^2 - 4(k_1k_3 + k_2k_4 + k_1k_4)]^{1/2} \quad (2.23)$$

2.2 Experimental Section

2.2.1 Chemicals

Mephentermine sulfate (John Wyeth & Brother, Walkerville, ON, Canada), 2-phenylethylamine hydrochloride (Sigma, St. Louis, MO) were reagent grade and were used as received. *n*-Octane (≥ 99.5%) was obtained from Fluka (Buchs, Switzerland). Water was purified by the Nanopure system (Barnstead, Dubuque, IA). The mobile phase for HPLC was 60% 25 mM phosphate buffer (pH 2.5) and 40% methanol.

2.2.2 Apparatus and Procedures

2.2.2.1 Extraction

The solvent microextraction apparatus is shown diagrammatically in Figure 2.1. The 1.0-mL micro reaction vials and the Teflon coated stirring bars were obtained from Alltech Associates (Deerfield, IL). The 2.0-mL vials were made by Wheaton (Millville, NJ) and purchased from Supelco (Bellefonte, PA). The threaded neck of the 2-mL vial has been cut off because the inner diameter of the neck is smaller than that of the vial body. The Teflon FEP rings, 8.0 mm o.d. x 6.4 mm i.d. x 2 mm H for the 1.0-mL vial and 9.6 mm o.d. x 8.0 mm i.d. x 2 mm H for the 2.0-mL vial, were manually cut off from tubing obtained from Cole-Parmer (Vernon, IL). The vial was placed in a jacketed water bath and the temperature was maintained at 25.0 ± 0.1 °C by a circulating water bath, either a Lauda K-4/RD (Brinkmann, Rexdale, ON, Canada) or a Haake K15 with control module DC1 (Paramus, NJ). The aqueous sample solution was stirred at a constant speed with a Series H heavy-duty laboratory stirrer and motor controller from G.K. Heller,

Corp. (Floral Park, NY). The modification to the rotating magnet assembly has been described elsewhere.[19]

The aqueous sample solution used in the kinetic studies contained 1.0×10^{-4} mol/L of both mephentermine and 2-phenylethylamine in 0.10 M NaOH-0.10 M KCl (pH 13). For the calibration curve, several aqueous solutions of mephentermine and 2-phenylethylamine in the concentration range 1.0×10^{-5} M to 1.0×10^{-4} M were prepared in 0.10 M NaOH-0.10 M KCl (pH 13). An aqueous phosphate buffer solution (50 mM, pH 2.1) was used as the aqueous receiving phase.

To do the extraction, 1.0 mL (or 0.5 mL) of aqueous sample solution was pipetted into a dry 2-mL (or 1-mL) micro reaction vial. The Teflon ring was positioned such that the bottom of the ring was at the same level as the surface of the aqueous sample solution. Once the position of the ring was fixed, no further adjustment was needed for future extractions. The organic membrane phase, 80 μL (or 40 μL) of *n*-octane, was delivered on top of the aqueous sample solution and inside of the Teflon ring via a 100-μL Hamilton syringe. The aqueous receiving phase, 200 μL (or 100 μL) of the aqueous phosphate buffer (pH 2.1), was then added carefully along the inner wall of the glass vial to form an aqueous layer on top of the organic liquid membrane. Once they were formed, the organic membrane and the top aqueous layer were so stable that it was safe to employ the highest stirring speed (2050 rpm) attainable with the stirrer. After a prescribed extraction time, about 170 μL (or 70 μL) out of 200 μL (or 100 μL) of the receiving phase was pipetted with an Eppendorf micropipette into a 1-mL autosampler vial (Kimble Glass, Vineland, NJ) and the extract was manually injected into the HPLC injection valve.

The HPLC system consisted of a Waters 6000A pump (Milford, MA), a Rheodyne 8125 injection valve (Cotati, CA) with either a 10 μL or a 5 μL sample loop, a

150 × 3.2 mm Phenomenex Prodigy 5μm C_{18} column with a 30 x 3.2 mm guard column (Torrance, CA), a Waters Lamda-Max Model 481 UV detector monitoring at 220 nm, a Fisher Series 5000 recorder, and a Hewlett-Packard 3390A integrator. The flow rate was 0.50 mL/min.

2.2.2.2 Determination of Diffusion Coefficients

Diffusion coefficients of mephentermine and 2-phenylethylamine were measured at 25.0 ± 0.1 °C by the Taylor dispersion method[18,58] in four solvents: pH 13 aqueous solution, *n*-octane, 100 mM phosphate buffer (pH 2.5), and water. A flow injection system was used (see Figure 2.3), which consisted of a constant-pressure pump (He gas cylinder with sealed aluminum containers), 400 cm of loosely coiled (9-cm coil diameter) stainless steel tubing C1 (0.02 in nominal ID) or 430 cm of similarly coiled Teflon tubing C1 (0.03 cm nominal ID), a six-port stainless steel injection valve V2 (Valco HP series, Houston, TX) with a 10-μl stainless steel loop or a six-port Cheminert low pressure injection valve V2 (Model C22-3186, Valco) with a 10-μL Teflon loop, a Waters Lamda-Max Model 481 UV detector at 220 nm, and a Fisher Series 5000 recorder. The coiled stainless steel or Teflon tubing C1 was maintained at 25.0 ± 0.1 °C with the Haake K15 water bath. The solvent, ethanol, and water were contained in reagent bottles which were placed inside sealed aluminum containers. Ethanol was used to flush the system before switching solvent from organic to aqueous and vise versa. Constant pressure (about 5 to 10 psi) from a nitrogen cylinder (Linde) was applied to the aluminum container to produce solvent flow which can be started or stopped by using 2-way slider valves V1 (Laboratory Data Control, Riviera Beach, FL).

The concentrations of the model compounds in the solvents were adjusted so that a 10-μL sample plug would give a peak with an absorbance smaller than 0.2 AU (about 5 × 10^{-4} mol/L). The solutions of the compounds in *n*-octane were prepared by extracting

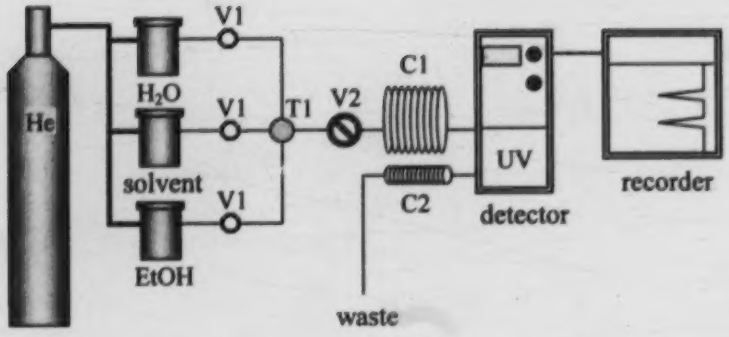

Figure 2.3 Flow injection system for the determination of diffusion coefficients. V1 is a 2-way slider valve, T1 is a tee-fitting, V2 is a sample injection valve, C1 is a stainless steel or Teflon coil, and C2 is a Teflon coil.

the neutral compounds in a pH 13 aqueous solution into *n*-octane. The flow rates were controlled by the pressure pump and a piece of Teflon tubing (0.01 in i.d.) with a length of 100 cm to 700 cm connected to the detector outlet. The solvents were degassed with helium before use. Caffeine in water, with $D = (6.3 \pm 0.4) \times 10^{-6}$ cm^2/s,[59] was used to calibrate the radii of the stainless steel and Teflon tubing. Peak width was measured by the "tangent" method.

2.2.2.3 Determination of Distribution Ratios

Distribution ratios of mephentermine and 2-phenylethylamine between aqueous solution (pH 13) and *n*-octane were determined at 25.0 ± 0.1 °C by measuring the amount of the compounds left in the aqueous phase after extraction. 2-mL or 5-mL micro reaction vials were used to perform the two-phase extraction. The phase ratios were 2.00 mL of aqueous phase to 50.0 μL of *n*-octane for mephentermine and 2.00 mL of aqueous phase to 2.00 mL of *n*-octane for 2-phenylethylamine. The aqueous phase was stirred by a triangular stirring bar with the G.K. Heller stirrer at a speed at which a vortex of several millimeters in depth was created at the aqueous-organic interface. After the extraction reached equilibrium, the organic phase was discarded, and a 1.00-mL aliquot of the aqueous phase was pipetted into a clean 5-mL vial and its pH adjusted to about 2.5 by adding 0.50 mL of 0.20 mol/L HCl and 0.50 mL of 0.10 mol/L NaH_2PO_4 (pH2.1) buffer. The solution was then injected into the HPLC to determine the amount of compound left in the aqueous phase.

2.3 Results and Discussions

2.3.1 Distribution Ratios

Although it is not necessary to measure the distribution ratios and diffusion coefficients of the analyte compounds in an analytical application where simple calibration suffices, they are required in the theoretical treatment of extraction kinetics. Distribution ratio, K (either K_1 or K_2), is related to distribution coefficient of the neutral molecule, κ, by

$$K \equiv \frac{C_o}{C_{aq}} = \frac{\kappa K_a}{K_a + [H^+]_a} \tag{2.24}$$

where

$$\kappa \equiv \frac{[B]_o}{[B]_{aq}} \tag{2.25}$$

C_o and C_{aq} are the total analyte concentrations in the organic phase and aqueous phase (either a1 or a2), respectively, K_a is the acid dissociation constant, and $[H^+]_a$ is the hydronium ion concentration in aqueous phase (either a1 or a2). The pK_a values for 2-phenylethylamine and mephentermine are 9.88 and 10.25, respectively.[60]

At pH_{a1} = 13, the measured K_1 values are 1.08 ± 0.01 L/L (n = 4) and 44.9 ± 0.4 L/L (n = 3) for 2-phenylethylamine and mephentermine, respectively, at 25 °C. Figures 2.4 and 2.5 show the rate curves of the apparent distribution ratios K_1 measured for 2-phenylethylamine and mephentermine, respectively. It can be seen from the Figures that the distribution equilibrium was established in less than 10 min for 2-phenylethylamine and in about 50 min for mephentermine. Because $K_1 \approx \kappa$, K_2 can be calculated by eq 2.24. At pH_{a2} = 2.1, the values are 1.8×10^{-8} L/L and 3.2×10^{-7} L/L for 2-phenylethylamine and mephentermine, respectively.

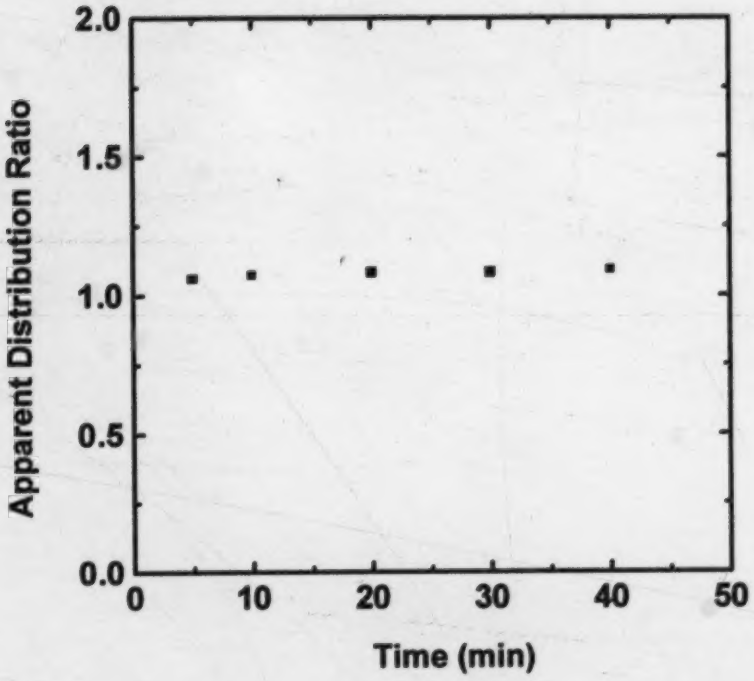

Figure 2.4 Plot of apparent distribution ratio K_1 for 2-phenylethylamine versus time. The volumes of the aqueous phase and *n*-octane are both 2.00 mL. The initial concentration of 2-phenylethylamine in the aqueous phase (pH 13) is 1.00×10^{-3} mol/L. The 5-mL vial is placed in a circulating water bath maintained at 25 °C. The aqueous phase is stirred at 1400 rpm.

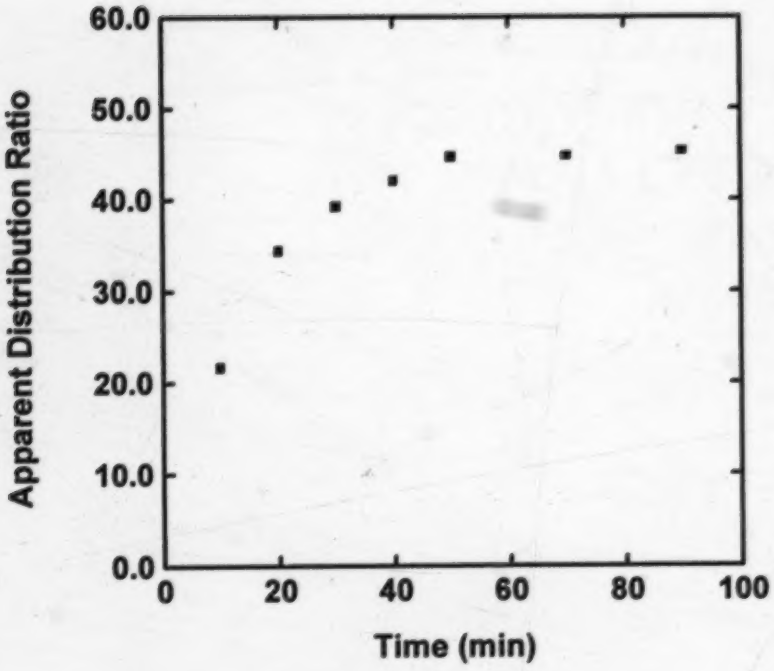

Figure 2.5 Plot of apparent distribution ratio K_1 for mephentermine versus time. The volumes of the aqueous phase and *n*-octane are 2.00 mL and 50 μL, respectively. The initial concentration of mephentermine in the aqueous phase (pH 13) is 1.00×10^{-3} mol/L. The 2-mL vial is placed in a circulating water bath maintained at 25 °C. The aqueous phase is stirred at 1900 rpm.

2.3.2 Diffusion Coefficients

The Taylor dispersion method is used to determine diffusion coefficients for 2-phenylethylamine and mephentermine in various solvents. This method is rapid and relatively inexpensive. It is based on the dispersion of solute in a liquid undergoing laminar tube flow. Laminar flow in a relatively long open tube of circular cross section gives rise to a non-uniform parabolic flow profile of velocities across the tube. When a sharp plug of solute is introduced into the laminar flow stream, it will spread out over the tube because of the non-uniform parabolic flow profile[61] (Figure 2.6a). However, because of the radial diffusion of solute molecules (as indicated by the vertical arrows in Figure 2.6a), the bandbroading will be less than that from the parabolic flow profile (see Figure 2.6b). The extent of such "relaxation" of the distribution of solute concentration from the parabolic shape is dependent upon the magnitude of the diffusion coefficient of the solute molecule. This is the basis of the Taylor dispersion method, i.e., the distribution of solute concentration is a result of the combined action of radial molecular diffusion and the variation of flow velocity over the cross-section.[61,62] If radial molecular diffusion were instantaneous (complete relaxation), there would be no bandbroadening because in that case solute molecules would be able to experience all the velocities (Figure 2.6c).

The theory was first discussed by Taylor[61,62] and later by Aris,[63] and was applied by Ouano[64] who demonstrated that the solute diffusion coefficient can be determined from the mean and variance of the solute concentration profile as it exits a tube. Taylor has shown that the distribution of solute concentration at a time t after a plug injection of fluid into a laminarly flowing stream can be expressed as[65-68]

$$C(t) = \frac{m}{\pi(2\pi)^{1/2} a^2 \bar{U}(2Kt/\bar{U}^2)^{1/2}} \exp\left[-\frac{(t-\bar{t})^2}{2(2Kt/\bar{U}^2)}\right] \qquad (2.26)$$

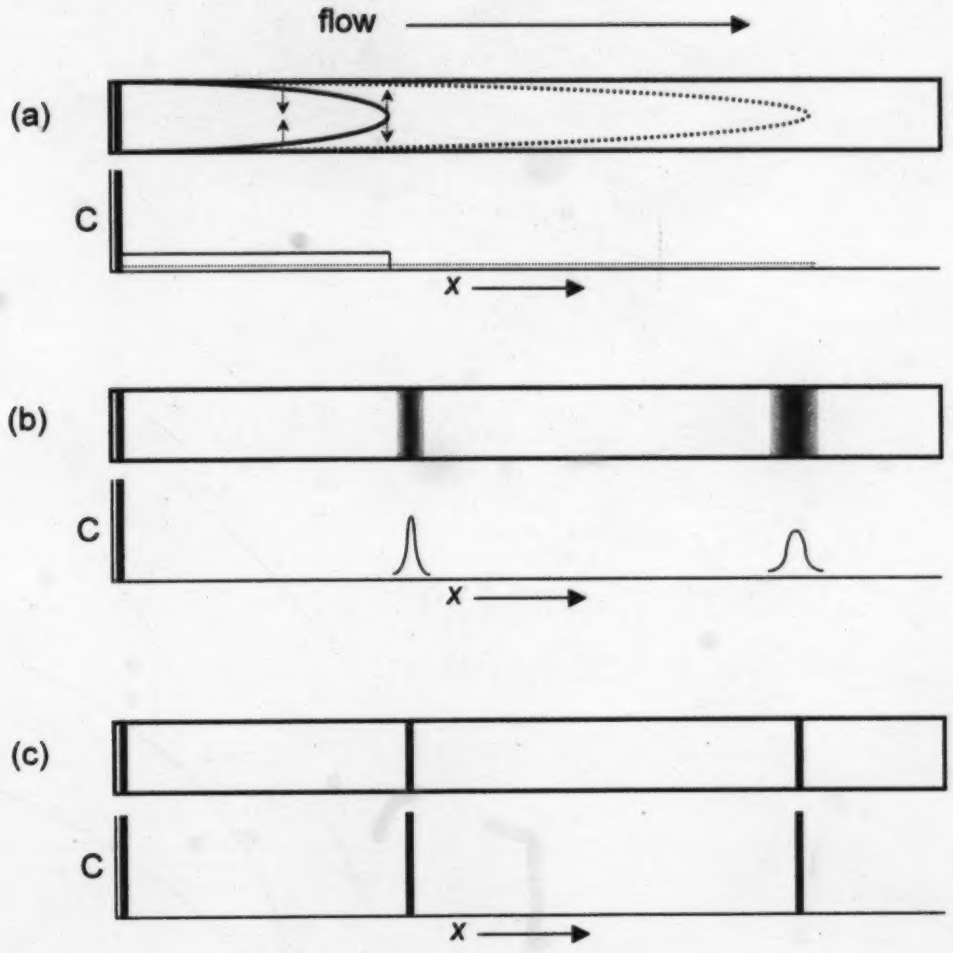

Figure 2.6 Bandbroadening of a sharp solute plug in a laminar flow stream caused by non-uniform parabolic flow profile in a open tube (a) in the absence of radial diffusion of solute molecule, (b) with radial diffusion (finite D value), (c) with instantaneous radial diffusion ($D \rightarrow \infty$). Also shown are the distributions of solute concentration. Small vertical arrows represent radial diffusion.

where m is the total mass of the solute injected, $\bar{t}$ is the dispersion time or the retention time of the solute peak, $\bar{U}$ is the average linear velocity of flow, a is the tube radius, and K is the Taylor dispersion coefficient. Eq 2.26 describes a Gaussian curve with mean $\bar{t}$ and variance

$$\sigma^2 = (2Kt/\bar{U}^2) \tag{2.27}$$

If radial differences in concentration are small compared to longitudinal differences, i.e., if the time necessary for a radial variation in concentration to die down through radial diffusion is shorter than the time necessary for an appreciable change in concentration to occure due to parabolic flow profile,[62] the Taylor's condition[61,65]

$$\bar{t} >> \frac{a^2}{3.8^2\, D} \tag{2.28}$$

is satisfied, where D is the diffusion coefficient (cm^2/s). This condition can be achieved by using narrow tubing and either slow flow or long tubing. Under this condition, the Taylor dispersion coefficient, K, can then be expressed as[65]

$$K = D + \frac{a^2 \bar{U}^2}{48\, D} \tag{2.29}$$

In liquid systems where diffusion coefficients are small, the first term D in eq 2.28 is negligible.[64] It means that for most experimental conditions the diffusion coefficient, D, is much smaller than the Taylor dispersion coefficient, K. In other words, logitudinal diffusion is negligible compared with dispersion caused by the parabolic flow profile. By combining with eq 2.27, eq 2.29 can be reduced to the final working equation

$$D = \frac{a^2 \bar{t}}{24 \sigma^2} \qquad (2.30)$$

The radii of the stainless steel tubing and the Teflon tubing were calibrated using caffeine in water, which has a diffusion coefficient of $(6.3 \pm 0.4) \times 10^{-6}$ cm^2/s at 25.0 °C.[59] The measured radii were 0.0257 ± 0.0002 cm for the stainless steel tubing and 0.0218 ± 0.0003 cm for the Teflon tubing (see Table 2.1). The variance of the solute peak was calculated from peak width at baseline, $w = 4\sigma$, measured by the "tangent" method.

With stainless steel tubing, the observed peaks for both compounds were nearly symmetrical in water and in 100 mM NaH_2PO_4 (pH 2.1). In *n*-octane, however, the peaks were found to be severely tailed, which was probably caused by adsorption of the basic neutral molecules to the active sites (oxide) on the stainless steel tubing because toluene peaks were still very symmetrical. Therefore, the diffusion coefficients of the model compounds in *n*-octane and in 0.10 M NaOH-0.10 M KCl were determined using Teflon tubing, which gave nearly symmetrical peaks with an asymmetry factor of 1.1 at 10% of peak height (see Figure 2.7). The determined diffusion coefficients are presented in Table 2.2 and 2.3 for mephentermine and 2-phenylethylamine, respectively.

Table 2.1 Calibration of the tubing radii with caffeine $D = (6.3 \pm 0.4) \times 10^{-6}$ cm^2/s at 25.0 °C.

Trial	Dispersion time $\bar{t}$ (s)	Peak width w (s)	Variance σ^2 (s^2)	Tubing radius a (cm)
Stainless Steel:				
1	1170	283	5013	0.0255
2	1152	286	5098	0.0259
3	1157	286	5098	0.0258
			Average:	0.0257 ± 0.0002
Teflon:				
1	1092	235	3451	0.0219
2	1092	238	3540	0.0221
3	1111	233	3393	0.0215
			Average:	0.0218 ± 0.0003

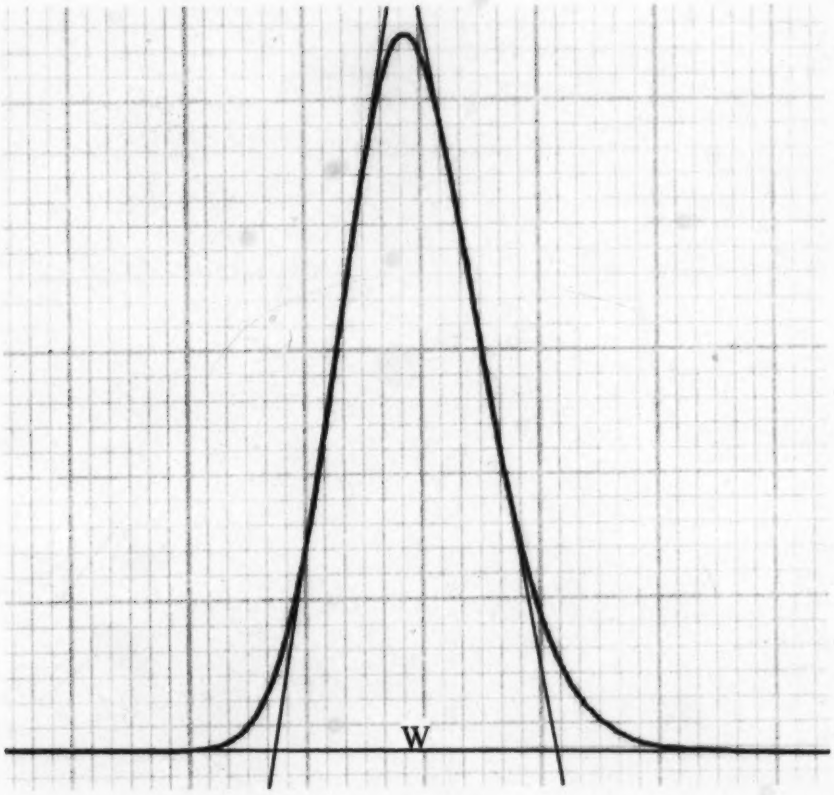

Figure 2.7 Typical mephentermine peak from the Taylor dispersion method obtained using Teflon tubing with 0.10 M NaOH–0.10 M KCl as solvent. Also shown are manually drawn tangents to the inflection points and baseline construction. The *x*-axis is time, and the *y*-axis is absorbance.

Table 2.2 Measurement of diffusion coefficients for mephentermine in water, 100 mM NaH_2PO_4 (pH 2.1), 0.10 M NaOH–0.10 M KCl, and *n*-octane at 25.0 °C.

(Solvent) Trial	Dispersion time $\bar{t}$ (s)	Peak width w (s)	Variance σ^2 (s^2)	Diffusion Coeff. D (cm^2/s) × 10^6
(water):[a]				
1	1162	324	6561	4.87
2	1170	326	6658	4.84
3	1169	329	6757	4.76
			Average:	4.8 ± 0.1
(100 mM NaH_2PO_4):[a]				
1	1258	331	6856	5.05
2	1294	341	7259	4.90
3	1272	331	6856	5.10
4	1294	338	7157	4.97
			Average:	5.0 ± 0.1
(0.10 M NaOH–0.10 M NaCl):[b]				
1	1243	290	5271	4.67
2	1255	286	5098	4.87
3	1234	283	5013	4.87
			Average:	4.8 ± 0.1
(*n*-octane):[b]				
1	530	98	605	17.3
2	533	101	635	16.6
3	530	101	635	16.5
			Average:	17 ± 1

a. with stainless steel tubing. b. with Teflon tubing.

Table 2.3 Measurement of diffusion coefficients for 2-phenylethylamine in water, 100 mM NaH_2PO_4 (pH 2.1), 0.10 M NaOH–0.10 M KCl, and *n*-octane at 25.0 °C.

(Solvent) Trial	Dispersion time $\bar{t}$ (s)	Peak width w (s)	Variance σ^2 (s^2)	Diffusion Coeff. D (cm^2/s) × 10^6
(water):[a]				
1	1138	281	4935	6.35
2	1138	290	5256	5.94
3	1145	293	5365	5.88
			Average:	6.0 ± 0.3
(100 mM NaH_2PO_4):[a]				
1	1178	288	5184	6.25
2	1188	286	5112	6.41
3	1188	290	5256	6.20
			Average:	6.3 ± 0.1
(0.10 M NaOH–0.10 M NaCl):[b]				
1	1194	247	3813	6.19
2	1193	250	3906	6.07
3	1200	246	3782	6.28
			Average:	6.2 ± 0.1
(*n*-octane):[b]				
1	535	91	518	20.4
2	533	94	552	19.3
3	533	91	518	20.3
4	530	96	576	18.2
5	535	96	576	18.4
6	533	96	576	18.3
			Average:	19 ± 1

a. with stainless steel tubing. b. with Teflon tubing.

2.3.3 Flow Pattern

For a two-phase extraction system, flow patterns in both the aqueous and the organic phases can be visualized by suspending charcoal powder in each phase.[18] The flow patterns for the presently employed three-phase system can be shown in a similar way. Parallel motion is induced in the organic membrane phase by the stirring in the aqueous source phase, and it, in turn, induces parallel motion in the aqueous receiving phase. The circulatory flow in each phase consists of both a horizontal-rotational component and a vertical-toroidal component. The toroidal components of flow in each phase are shown diagramatically in Figure 2.2b. Although it is difficult visually to quantify the toroidal circulation rates in any phase, it is relatively easy to quantify the horizontal-rotational components of circulation in the a1 and a2 phases. These rotational components were observed to decrease from the stirred aqueous source phase (2000 rpm) to the organic membrane phase to the aqueous receiving phase (about 60 rpm). It will be shown in the next section that circulation in the organic membrane phase is essential to reduce the film thickness (δ_{o2}) and facilitate mass transfer. Although circulation in the aqueous receiving phase is much less important in terms of mass transfer rate, some circulation is desirable to bring the needed hydronium ions to the interface and to homogenize the phase prior to HPLC analysis.

2.3.4 Kinetics

Shown in Figure 2.8 are typical extraction rate curves, plotted as concentration vs. time, for the extraction of mephentermine and 2-phenylethylamine from 1.00 mL of a 1.00×10^{-4} mol/L stirred aqueous sample solution into a 200 μL aqueous receiving phase. The solid lines represent fits of the data points to eq 2.19, based on nonlinear least-squares fitting performed with the aid of Solver in Microsoft Excel. The two interfacial

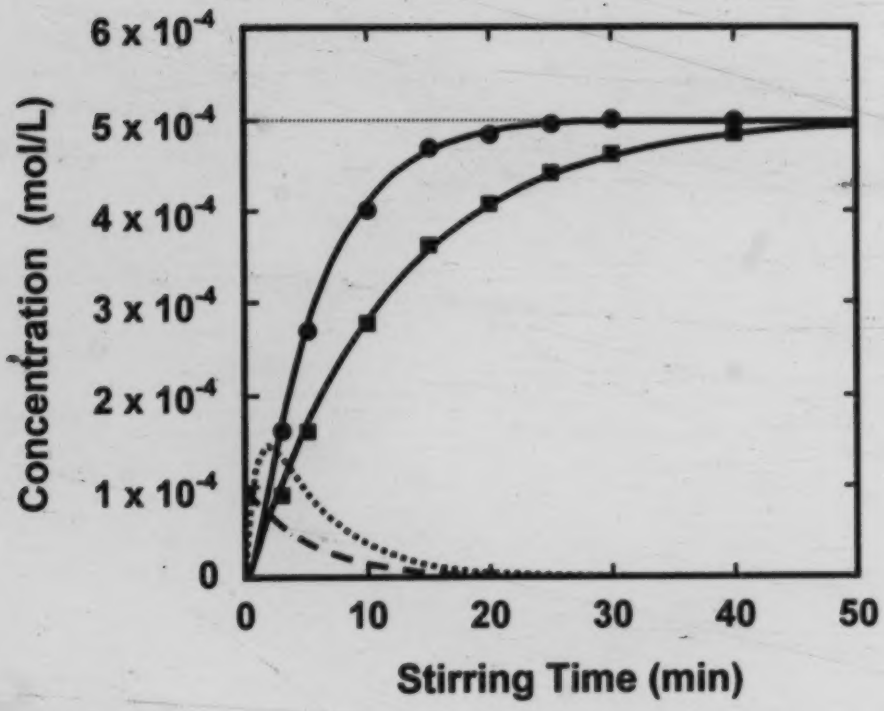

Figure 2.8 Plots of observed concentrations of (•) mephentermine and (■) 2-phenylethylamine in the aqueous receiving phase versus stirring time at a stirring speed of 2050 rpm. Points indicate experimental data. Solid lines are fits to eq 2.19. The dashed line and the dotted line are the concentration profiles of mephentermine in the aqueous sample solution and the organic membrane phase, respectively, as calculated by eqs 2.17 and 2.18. The initial concentration of both compounds in the aqueous sample solution was 1.00×10^{-4} mol/L and the dotted horizontal line at 5.00×10^{-4} mol/L corresponds to quantitative extraction.

areas, A_1 and A_2, were estimated to be 0.8_0 cm^2 and 0.5_2 cm^2, respectively, based on the inner diameter (0.80 cm) of the Teflon ring and the actual shapes of the interfaces during the solvent extraction (see Figure 2.2). At a stirring speed of 2050 rpm, the vortex at the a1-o interface was found to be approximately 0.5 cm deep and 0.2 cm wide on average.

Figure 2.8 shows that the fits of the experimental data to the theoretical kinetic model are excellent. In the model, the diffusion film thicknesses, δ_{a1}, δ_{o1}, δ_{o2}, and δ_{a2}, are the only unknown parameters whose values must be obtained from the nonlinear least-squares fitting. Depending upon the values of other constants in eqs 2.15 and 2.16, diffusion across some films may not contribute to the overall rate of extraction. For example, under current experimental conditions, only the first three film thicknesses, δ_{a1}, δ_{o1}, and δ_{o2}, are actually obtainable from the fitting to the extraction rate curve for 2-phenylethylamine because the value of K_2 is extremely small. Hence the first term, δ_{a2}/D_{a2}, in eq 2.16 is negligible and not included in the fitting. For mephentermine, not only is δ_{a2}/D_{a2} negligible but also δ_{o1}/D_o is negligible because K_1 is large (see eq 2.15). Therefore, only two fitting parameters, δ_{a1} and δ_{o2}, are used to fit the extraction rate curve of mephentermine. The values of the film thicknesses were found to be 12 μm (δ_{a1}) and 58 μm (δ_{o2}) for mephentermine and 12 μm (δ_{a1}), 20 μm (δ_{o1}), and 36 μm (δ_{o2}) for 2-phenylethylamine.

Since diffusion-film thicknesses are determined by the hydrodynamics of the system, the δ_{a1}, δ_{o1}, δ_{o2}, and δ_{a2} should have values that are independent of the compound being extracted. For δ_{a1}, this is found to be the case. A value of δ_{a1} = 12 μm was found for the extraction of both compounds. For the film thickness δ_{o2} which could also be observed for both compounds, the values were 58 μm for mephentermine and 36 μm for 2-phenylethylamine. This discrepancy may be within experimental error, which however is not readily estimated for the values of δ_{o2}.

Implicit in the kinetic model are the following assumptions: (1) the mixing in each bulk phase is very rapid so that they are homogeneous at any time, (2) the ionization of analyte at the o-a2 interface is a significantly faster process than mass transfer through the diffusion films, (3) sufficient ionizing agent is always present on the a2 side of the o-a2 interface, and (4) there exist no other complications, such as adsorption at interfaces, which may slow down the overall mass transfer rate. The first three assumptions are valid under current experimental conditions. Protonation is an extremely fast process. At pH 2.1, about half of the 50 mM phosphate buffer exist in the acidic form so that the protonation agent concentration is about 25 times higher than the combined analyte concentration (1.0×10^{-3} mol/L) in the aqueous receiving phase, assuming quantitative extraction for both compounds. The induced 60-rpm horizontal-rotational component of circulation in the aqueous receiving phase suggests that circulation may be fast enough to transport sufficient amount of protonation agent to the interface. This was confirmed experimentally by reducing the initial phosphate buffer concentration from 50 mM to 25 mM. The same extraction rate was observed.

The fourth assumption is true for extraction into a 100–200 μL of a2 phase, but, as discussed in Chapter 3, it may not be true at high analyte concentrations in a2. It has been demonstrated by many studies[69-71] that when adsorption of surface-active species occurs at the liquid-liquid interface it can produce an interfacial resistance which reduces the mass-transfer rates of both the adsorbed compounds and other extractable compounds across the interface.

With the presently proposed model it is possible to calculate the concentration profiles of the analytes in the aqueous sample solution and in the organic membrane phase over the whole extraction process. Such concentration profiles for mephentermine are given in Figure 2.8. The model is also useful in optimizing extraction experiments

because it can predict how various parameters affect the extraction system. If the distribution coefficient (κ) of an analyte is too small (<< 1), it would be impossible to extract the compound quantitatively. According to the model, only 25% is extracted in 25 min for a compound with a distribution coefficient κ = 0.1. Higher κ values can be achieved by choosing a better organic solvent as the liquid membrane phase. This will lead to both a fast and more quantitative extraction. On the other hand, increasing κ above about 5 produces only a slight further increase in both extraction rate and completion of extraction. Therefore, large distribution coefficients are not required in order to achieve quantitative extraction in about 30 min with the current extraction system. Whether quantitative extraction is attainable is ultimately determined by the equilibrium of the extraction system. According to eq 2.5, a very small value of K_2 or a large value of ($pK_a - pH_{a2}$) is desirable. To achieve 99.5% extraction, the required minimum values of ($pK_a - pH_{a2}$) are 3.7 and 3.0 for mephentermine and 2-phenylethylamine, respectively.

Since the phase ratio (V_{a1}/V_{a2}) is five, quantitative extraction should produce an analyte concentration of 5.0×10^{-4} mol/L in the aqueous receiving phase (the light dotted horizontal line in Figure 2.8). It can be seen that mephentermine was extracted quantitatively in about 25–30 min. Even for 2-phenylethylamine, which has a much smaller distribution coefficient, 88% was extracted in 25 min and 97% extracted in 40 min. This technique provided the convenience and extraction efficiency which was impossible with the two-phase solvent extraction method. If 2-phenylethylamine were extracted by using a two-phase solvent extraction system with the same phase ratio (1.0 ml aqueous and 80 μL organic), 46 sequential extractions would be needed in order to have 97% recovery. Also, tedious steps, such as phase separation, solvent evaporation and residual re-dissolution, would be required prior to injection into HPLC.

2.3.5 Calibration Curves and Analytical Precision

Because the aqueous receiving phase was injected directly into an HPLC, the chromatographic peak area is proportional to C_{a2}, which in turn is proportional to $C_{a1,initial}$, the initial concentration of analyte in the aqueous sample solution (refer to eq 2.19). Under the same experimental conditions, a plot of peak area vs. $C_{a1,initial}$ for a series of standard concentrations yields a linear calibration curve, as shown in Figure 2.9.

To obtain the calibration curves, the aqueous sample solutions of different initial analyte concentrations were stirred at 1900 rpm for 30 min, by which time the extraction was quantitative (>99.5%) for mephentermine and about 90% complete for 2-phenylethylamine. V_{a1}, V_o, and V_{a2} were 1.0 mL, 80 μL, and 200 μL, respectively. After extraction, 10 μL of the 200-μL receiving phase was injected into HPLC for quantification. Duplicate extraction was performed for each sample solution. The calibration curves in Figure 2.9 are linear, with slopes of $(9.03 \pm 0.23) \times 10^{10}$ L/mol and $(5.00 \pm 0.18) \times 10^{10}$ L/mol, zero intercepts of $(1.05 \pm 1.38) \times 10^5$ and $(0.66 \pm 1.05) \times 10^5$, and correlation coefficients (R) of 0.9998 and 0.9997 for mephentermine and 2-phenylethylamine, respectively.

Analytical precision was slightly better for nearly quantitative extractions. However, even for 5-min or 10-min extractions the typical relative standard deviation was only about 2.0% (n = 3) (see Table 2.4), which is quite acceptable for routine application.

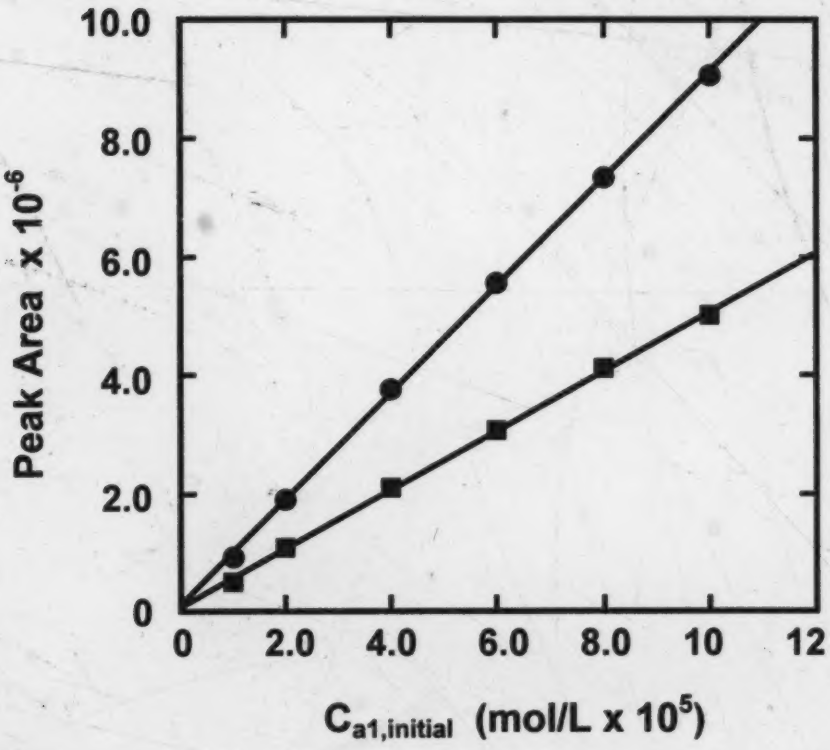

Figure 2.9 Calibration curves for 30-min extractions of (•) mephentermine and (■) 2-phenylethylamine, plotted as HPLC peak area versus initial concentration in the aqueous sample solution. Points were obtained in duplicate (two 30-min extractions). See text for details.

Table 2.4 HPLC data for replicate extractions of mephentermine and 2-phenylethylamine from 1.00 mL of 1.00×10^{-4} mol/L sample solution into a 200-μL aqueous receiving phase.

Extraction Time	Peak Area			% rsd
	trial #1	trial #2	trial #3	
3 min:				
mephentermine	1663530	1619500	1683530	2.0
2-phenylethylamine	629820	616050	628710	1.2
5 min:				
mephentermine	2677270	2728570	2636130	1.7
2-phenylethylamine	1034530	1024170	1014630	1.0
10 min:				
mephentermine	4003770	3855670	3893770	2.0
2-phenylethylamine	1733830	1680330	1707270	1.6
15 min:				
mephentermine	4604370	4564833	4537530	0.7
2-phenylethylamine	2181870	2216900	2191930	0.8
20 min:				
mephentermine	4776170	4691030	4672970	1.2
2-phenylethylamine	2486970	2430200	2445330	1.2
25 min:				
mephentermine	4823100	4726970	4741400	1.1
2-phenylethylamine	2640133	2662700	2574370	1.7
30 min:				
mephentermine	4809470	4882670	4908630	1.0
2-phenylethylamine	2742500	2745900	2812570	1.4
40 min:				
mephentermine	4833670	4814580	4898030	0.9
2-phenylethylamine	2910200	2911780	2861050	1.0

Chapter 3

Preconcentration into a Single Microdrop

The solvent microextraction apparatus described in chapter 2 is designed for quantitative extraction. With a sample volume of 1.00 mL and a receiving phase volume of 200 μL, the enrichment factor is 5. The maximum attainable enrichment factor with that design is about 15 if a sample volume of 1.50 mL and a receiving phase volume of 100 μL are employed. In the case of very low concentrations of analyte, high preconcentration might be required. To achieve higher preconcentration or larger enrichment factors, the phase ratio of the source to the receiving phase (V_{a1}/V_{a2}) has to be increased by increasing the sample volume and/or decreasing the receiving phase volume.

In this part of the study, the previously described solvent microextraction apparatus is modified to increase the source-to-receiving phase ratio. The goal is to achieve much higher preconcentration in a relatively short time, at the sacrifice of quantitative extraction/back-extraction. The volume of the aqueous receiving phase is reduced to the microliter and sub-microliter range in the form of a single microdrop suspended in the organic membrane phase from the tip of a microsyringe needle. In this way, enrichment factors as high as 1000 are attainable in an extraction time of about 15 minutes.

---

a. A version of this chapter has been published. Ma, M.; Cantwell, F.F. in press, *Anal. Chem.* **1998**.

3.1 Experimental Section

3.1.1 Chemicals

Mephentermine sulfate obtained from John Wyeth & Brother (Walkerville, ON, Canada), and 2-phenylethylamine hydrochloride, methoxyphenamine hydrochloride, and methamphetamine hydrochloride (1.25 mg/mL in methanol) obtained from Sigma (St. Louis, MO) were reagent grade and used as received. *n*-Octane (≥ 99.5%) was obtained from Fluka (Buchs, Switzerland). Water was purified by the Nanopure system (Barnstead, Dubuque, IA). The mobile phase used for HPLC was either 60:40 (v/v) or 70:30 (v/v) 25 mM phosphate buffer (pH 2.5)/methanol.

3.1.2 Apparatus

The solvent microextraction apparatus is shown diagrammatically in Figure 3.1. The 2.0-mL vials were made by Wheaton (Millville, NJ) and purchased from Supelco (Bellefonte, PA). The threaded neck of the 2-mL vial has been cut off because the inner diameter of the neck is smaller than that of the vial body. The Teflon FEP ring, 9.6 mm o.d. x 6.4 mm i.d. x 3 mm H (manually cut off from tubing obtained from Cole-Parmer (Vernon, IL)), was positioned in the vial such that the surface of a 1.60-mL aqueous sample solution would just touch the bottom of the ring. Once the position of the ring was set, it stayed in place indefinitely, over many extractions. A 1-μL plunger-in-needle syringe with a utility stop (cat. No. 1001 and 2310, Unimetrics, Shorewood, IL) was used for suspending the microdrop of receiving phase during extraction and also for injection into the HPLC valve after extraction. The 22-gauge syringe needle had a 90° cut, suitable for use on HPLC valves. The utility stop was used to set the desired volume (i.e. 1.0_0-μL or 0.50-μL). A small Teflon sleeve, 1/16" o.d. x 0.5 mm i.d. x 1.5 mm H (manually cut off from Teflon tubing), was pushed onto the microsyringe needle until the tip of the

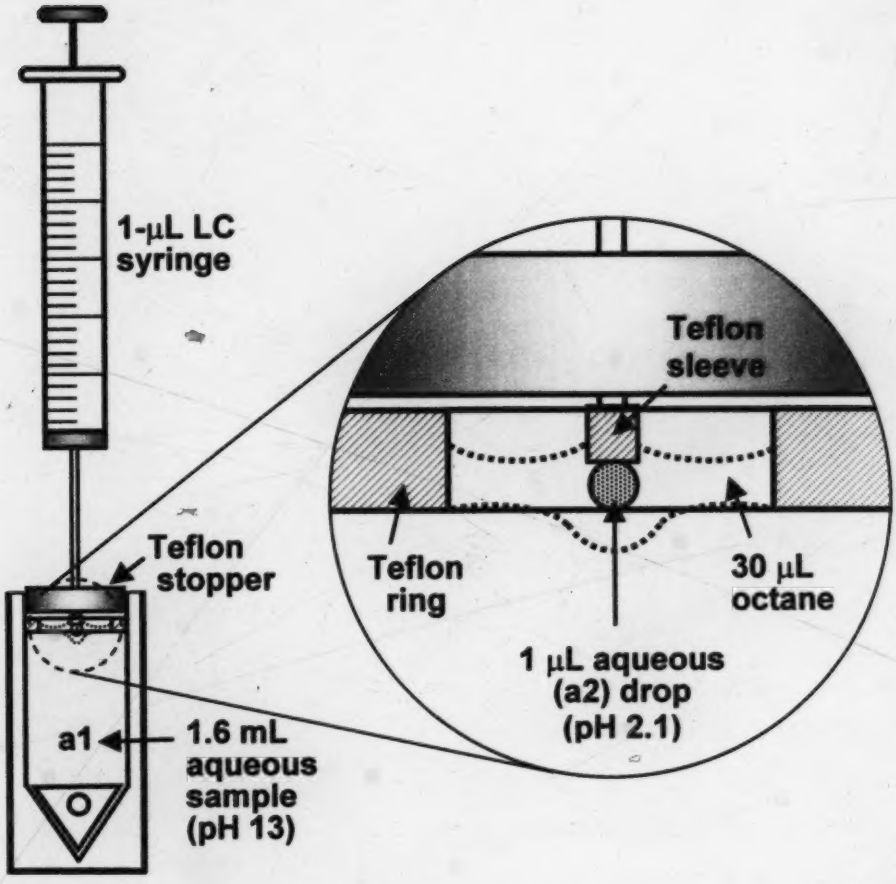

Figure 3.1 Schematic diagram of the SME/BE system for preconcentration into a single microdrop, with the magnetic stirrer on. A small vortex is evident at the bottom of the organic membrane phase. See text for description.

needle was even with the end of the sleeve. A Teflon stopper, 9.5 mm diameter × 4.5 mm high, with a slightly larger than 22 gauge (> 0.7 mm) hole in the center served both as a needle position guide and as a vial cover. The temperature of the vial was controlled by using a circulating water bath (Haake K15 with control module DC1, Paramus, NJ). A Series H heavy-duty laboratory stirrer and motor controller (G.K. Heller Corp., Floral Park, NY) was used to stir the aqueous sample solution.[30] The modification to the rotating magnet assembly has been described elsewhere.[19]

The HPLC system consisted of a Waters 6000A pump (Milford, MA), a Rheodyne 8125 injection valve (Cotati, CA) with a 5 μL sample loop, a 150 × 3.2 mm Phenomenex Prodigy 5μm C18 column with a 30 x 3.2 mm guard column (Torrance, CA), a Waters Lamda-Max Model 481 UV detector set at 220 nm, a Fisher Series 5000 recorder, and a Hewlett-Packard 3390A integrator. The mobile phase flow rate was 0.50 ml/min.

3.1.3 Procedures

Three standard solutions containing all four compounds, methamphetamine, mephentermine, 2-phenylethylamine and methoxyphenamine, at concentrations ranging from 1.0×10^{-4} M to 1.0×10^{-6} M were prepared in 25 mM NaH_2PO_4 (pH 2.5). For both the kinetic studies and the extraction calibration curves, the 1.60-mL aqueous sample solutions (a1) were prepared in the dry 2-mL vial by adding 16 μL of the appropriate stock solutions to 1.58 mL of 0.10 M NaOH-0.10 M KCl (pH 13) solution. The aqueous receiving phases (a2) were 50 mM NaH_2PO_4 for the extraction of the four-compound mixture and 100 mM NaH_2PO_4 for the rest of studies, both at pH 2.1.

After the 1.60-mL aqueous sample solution was prepared in the 2-mL modified vial with the Teflon ring already in place, 30 μL of *n*-octane membrane-phase was added from a 100-μL Hamilton syringe onto the top of the aqueous sample solution. This

positioned it inside the Teflon ring. The vial was then placed on the bottom of the jacketed water bath and the temperature was maintained at 25.0 ± 0.1 °C.

Before placing the tip of the 1-μL syringe needle in the 2-mL vial, the Teflon stopper and the small Teflon sleeve were slid onto the needle (see Figure 3.1). The syringe was then rinsed and filled with 1.0_0 or 0.50 μL of the receiving aqueous phase. After the needle and the Teflon sleeve were wiped with a Kimwipe, the syringe was positioned, using a clamp, such that the Teflon stopper fitted snugly into the vial and the bottom of the Teflon sleeve was about 0.5 mm above the organic membrane. A gentle push of the jacketed water bath slightly upward made the Teflon sleeve contact the organic membrane phase. Because of the surface-wetting of the sleeve by the organic phase, the central part of the membrane phase was dragged up a little bit as shown in Figure 3.1. The magnetic stirrer was then turned on. A 1- to 3-mm deep vortex was created at the bottom of the organic membrane phase at stirring speeds between 1500 and 2000 rpm (Figure 3.1). The 1.0_0- or 0.50-μL receiving phase (a2) in the syringe needle was then slowly pushed out to form an aqueous microdrop in the organic membrane phase. The presence of the small vortex at the bottom of the membrane phase is necessary to accommodate this microdrop of aqueous receiving phase. Once they are formed, the aqueous drop and the organic membrane are very stable and it is safe to stir at the highest stirring speed attainable with the stirrer (about 2050 rpm). In this design, the small Teflon sleeve is essential in forming the aqueous microdrop. Without the sleeve, the aqueous drop will be lost immediately by climbing up the surface of the stainless steel needle when the aqueous sample solution is stirred.

After the desired extraction time had elapsed, the plunger was slowly withdrawn to take the aqueous microdrop back into the needle while the sample solution was still being stirred. The syringe was removed from the clamp and then the Teflon stopper and

the Teflon sleeve were slid off the needle. To prevent any organic solvent from being injected into the HPLC system, the outside of the needle was first wiped with a Kimwipe. Then, while the needle was pointing upward, a small portion (ca. 0.02 μL) of the liquid in the needle was pushed out. Any organic solvent quickly evaporated. The aqueous liquid was then taken back into the needle, without allowing it to evaporate, and all the aqueous extractant in the needle was injected into the HPLC for quantification.

3.2 Results and Discussions

3.2.1 Kinetics

The relative increase in the concentration (C_{a2}) of the analyte in the aqueous receiving phase at any time during an extraction can be quantified as the enrichment factor (EF):

$$EF = \frac{C_{a2}}{C_{a1,initial}} \tag{3.1}$$

During the course of an extraction, EF increases until it reaches its maximum value at equilibrium which, from eq 2.5, is seen to have the value:

$$EF_{max} = \frac{K_1}{K_2 + K_1 K_2 (V_o/V_{a1}) + K_1 (V_{a2}/V_{a1})} \tag{3.2}$$

where the distribution ratios are given by:

$$K_1 = C_{o,eq}/C_{a1,eq} \tag{3.3}$$

and

$$K_2 = C_{o,eq}/C_{a2,eq} \tag{3.4}$$

If K_2 is very small, so that nearly all of the analyte is in a2 at equilibrium, then the enrichment factor at equilibrium will be:

$$EF_{max} \approx \frac{V_{a1}}{V_{a2}} \qquad (3.5)$$

Equation 3.5 applies to the present experimental conditions because pH_{a2} (= 2.1) is well below the pK_a values (≈ 10) of the conjugate acids of the four compounds, methamphetamine, mephentermine, 2-phenylethylamine and methoxyphenamine, employed in this study.[60]

In the study described in chapter 2, the volume V_{a2} was 200 μL, the volume V_{a1} was 1.0 mL and the interfacial areas A_1 and A_2 were estimated to be 0.8_0 cm^2 and 0.5_2 cm^2, respectively. Under those conditions, it was possible to achieved extraction equilibrium for mephentermine in under 30 min. However, in the presently-described microdrop device, V_{a2} has been decreased from 200 μL to 1 μL or less with the consequence that the o-a2 interfacial area A_2 is about 10 times smaller in the new device and the overall mass transfer rate is reduced. Therefore, it is experimentally impracticable to pursue EF_{max} because the time required to reach equilibrium is long.

A simpler rate expression than the relatively complex set of equations and constants in chapter 2 can be obtained by assuming an irreversible back extraction

$$i_{a1} \underset{k_2}{\overset{k_1}{\rightleftharpoons}} i_o \xrightarrow{k_3} i_{a2} \qquad (3.6)$$

and by invoking the steady-state approximation for the "intermediate" in the organic membrane phase.[73,74] This is justified by the extremely small distribution ratios for the back extraction ($K_2 = 10^{-7}$ to 10^{-8}, see section 2.31) and by the relatively small fraction of sample compound that is present in that phase at any time. The resulting integrated first-

order rate equation is:

$$EF \approx \frac{V_{a1}}{V_{a2}} \{1 - \exp[-k\,(t - t_{lag})]\} \qquad (3.7)$$

in which the first-order rate constant k is related to the individual rate constants by the expression:[73]

$$k \approx \frac{k_1\,k_3}{k_2 + k_3} \qquad (3.8)$$

and in which t_{lag} is the "lag-time"' that is related to the time required to reach steady-state extraction.[74] For periods of time at which the extraction is far-short of equilibrium, it is essential that t_{lag} be included in eq 3.7.

The accuracy with which eq 3.7 approximates the rigorous theoretical rate equation is demonstrated in Figure 3.2. The dashed line and the five points marked on it were generated from the rigorous equation 2.19 in chapter 2. To do this, the values k_1 = 0.053 min^{-1}, k_2 = 0.063 min^{-1} and k_3 = 0.26 min^{-1}, which are needed for equation 2.19, were calculated using the values of $\overline{\beta}_{o1}$, $\overline{\beta}_{a2}$, K_1 and K_2 that were reported in chapter 2 for the extraction of mephentermine, along with the values of $A_1 = 0.3_5$ cm^2, $A_2 = 0.04_4$ cm^2, V_{a1} = 1.60 mL, $V_o = 30 \times 10^{-3}$ mL and $V_{a2} = 1.00 \times 10^{-3}$ mL, which are appropriate to the present 1-μL drop system.

The solid line in Figure 3.2 was generated by non-linear least-square fitting of eq 3.7 to the five points marked on the dashed line, as though they were data points. In this fitting process, with $V_{a1}/V_{a2} = 1.60 \times 10^3$ entered as a known constant, the values of the two fitting parameters were $t_{lag} = 1.8 \pm 0.3$ min and $k = 0.037 \pm 0.001$ min^{-1}. This fitting value for k is close to the value of 0.043 min^{-1} that is calculated from eq 3.8. The agreement between eq 3.7 and eq 2.19 gets even closer if data points from times longer

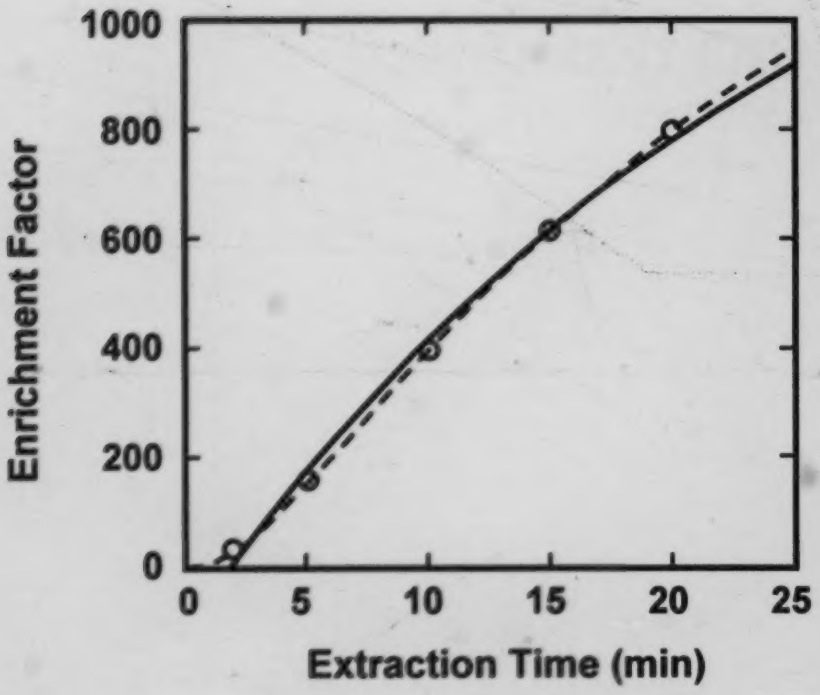

Figure 3.2 Plots of enrichment factor (EF) versus extraction time, showing the non-linear least-square fit (solid line) of the approximate first-order rate equation 3.7 to the five points (○), at 2, 5, 10, 15 and 20 min, generated from equation 2.19 using constants appropriate to the present 1-μL system (dashed line) for the extraction of mephentermine. See text for details.

than the 20-min shown in Figure 3.2 are included in the fitting process, but such long extraction times are not practical in routine analytical determinations. The fit of the solid line to the points in Figure 3.2 demonstrates that, for points collected after the lag-time, eq 3.7 may be used to describe the extraction rate curve.

One goal of the present study is to achieve high preconcentration (i.e. high EF) within a relatively short time. For this purpose, K_2 should be made very small by choosing a suitably low pH in the receiving phase a2 so that at equilibrium, EF = EF_{max}. The system should then be designed to make both EF_{max} (= V_{a1}/V_{a2}) and k as high as is practicable. For a fixed sample volume, V_{a1}, eq 3.5 shows that EF_{max} can be increased by decreasing V_{a2}. The factors which influence k can be appreciated by substituting the definitions in chapter 2 for k_1, k_2 and k_3 into eq 3.8:

$$k = \frac{A_1 A_2 K_1 \overline{\beta}_{o1} \overline{\beta}_{a2}}{V_{a1} (A_1 K_2 \overline{\beta}_{o1} + A_2 \overline{\beta}_{a2})} \qquad (3.9)$$

A larger value of K_1 gives a larger value of k. However, for a given organic solvent (i.e. *n*-octane), the magnitude of K_1 is a property only of the analyte compound and is not amenable to experimental control. More efficient stirring causes k to increase because it increases the mass transfer coefficients $\overline{\beta}_{o1}$ and $\overline{\beta}_{a2}$ by decreasing the thicknesses of the Nernst diffusion films. More efficient stirring can be due either to a faster stirring speed or to an improved circulation pattern in the *n*-octane phase as a result of, for example, a different microdrop volume, V_{a2}. A second effect of microdrop volume arises because it produces a smaller interfacial area A_2, which contributes to a smaller k via eq 8. In this connection, it should be noted that, because of the linear inverse proportionality between EF and V_{a2} in the first term of eq 3.7, the net effect of reducing V_{a2} is always to produce a

larger EF at any time during the extraction, even though a smaller V_{a2} contributes to a smaller rate constant.

A practical demonstration of the enrichment that is readily attainable with SME/BE is presented in Figure 3.3. The chromatograms (a) – (c) are for injections into the liquid chromatograph of 1.0_0 μL of aqueous standard solutions containing increasing concentrations of a mixture of four basic compounds. All four compounds are undetectable in the chromatogram of standard (a). The chromatograms (d) and (e) were obtained by injecting the 1.0_0 μL microdrop of a2 phase after 5- and 15-min of extraction/back-extraction of the standard (a) solution, respectively. It can be seen by comparing peak heights in chromatograms (d) and (c) that, in only 5 min, methamphetamine, mephentermine, and methoxyphenamine have been enriched more than 100 times in the microdrop. Even for 2-phenylethylamine, which has a relatively small distribution ratio (K_1 = 1.08 L/L, see section 2.3.1), an enrichment of 53 times has been achieved in 5 min. In chromatogram (e), which was obtained after 15 min of extraction, the peak heights for all four compounds are higher than in (d), as is expected from eq 3.7. By 15 min, EF for 2-phenylethylamine has increased from 53 to 164.

The experimentally measured rate curves for the extraction of mephentermine and of 2-phenylethylamine from 1.60 mL of 1.0×10^{-5} M aqueous sample solutions with 1.0_0 μL and 0.50 μL of aqueous receiving phase are shown as data points in Figures 3.4 and 3.5. The solid lines in these figures represent the non-linear least-square fit of eq 3.7 to the experimental points. The fitting parameters k and t_{lag} are summarized in Table 3.1. Immediately apparent for each microdrop volume is the effect of K_1 on the extraction rate constant k. At pH_{a1} = 13, the measured values of K_1 are 1.08 L/L and 44.9 L/L for 2-phenylethylamine and mephentermine (see section 2.3.1), respectively, which leads to a larger k for the latter compound. Also obvious is the significant increase in EF for both compounds when the drop size is decreased from 1.0_0 μL to 0.50 μL.

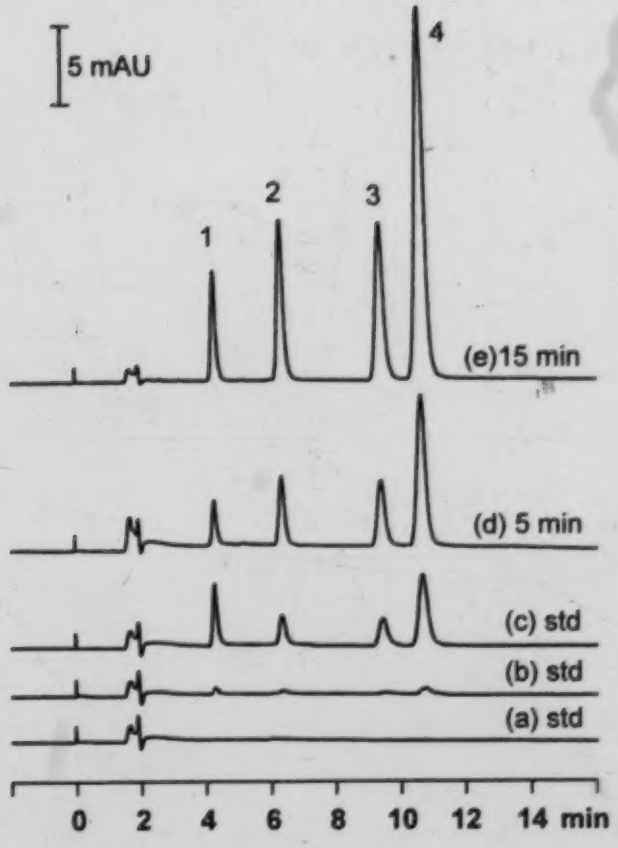

Figure 3.3 Chromatograms of a mixture of 2-phenylethylamine (**1**), methamphetamine (**2**), mephentermine (**3**), and methoxyphenamine (**4**) in standard solutions, (a) 2.0×10^{-6} M **1**, 1.0×10^{-6} M **2**, **3** and **4**, (b) 2.0×10^{-5} M **1**, 1.0×10^{-5} M **2**, **3** and **4**, (c) 2.0×10^{-4} M **1**, 1.0×10^{-4} M **2**, **3** and **4**, prepared in 50 mM NaH_2PO_4 (pH2.5); and chromatograms of 1-μL back-extractants after (d) 5 min and (e) 15 min of extraction from a 1.6-mL sample solution of 2.0×10^{-6} M **1**, 1.0×10^{-6} M **2**, **3**, and **4** at pH 13, stirred at 1900 rpm. Chromatographic conditions: column, 15 cm long × 3.2 mm i.d., 5-μm ODS; detection, UV 220 nm; mobile phase, 25 mM NaH_2PO_4 (pH2.5)/methanol (70/30, v/v); flow rate, 0.5 mL/min; injection volume, 1.0 μL.

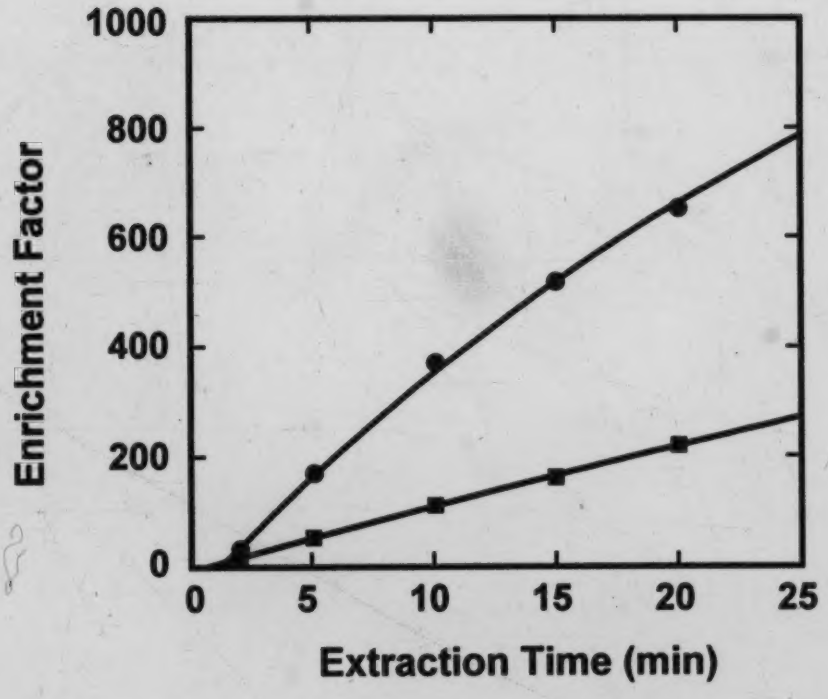

Figure 3.4 Plots of observed EFs of (•) mephentermine and (▪) 2-phenylethylamine in the 1.0_0-μL receiving phase versus extraction time at a stirring speed of 2050 rpm. Points indicate experimental data. Solid lines are fits to eq 3.7. The initial concentration of both compounds in the aqueous sample solution was 1.0×10^{-5} M. Other constants are given in Table 3.1.

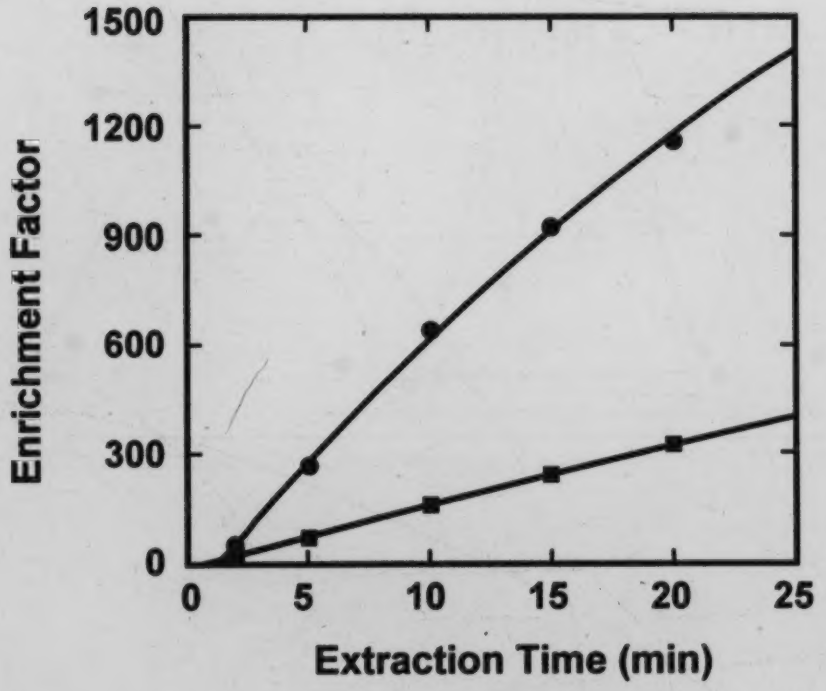

Figure 3.5 Plots of observed EFs of (•) mephentermine and (▪) 2-phenylethylamine in the 0.50-μL receiving phase versus extraction time at a stirring speed of 2050 rpm. Points indicate experimental data. Solid lines are fits to eq 3.7. The initial concentration of both compounds in the aqueous sample solution was 1.0×10^{-5} M. Other constants are given in Table 3.1.

Table 3.1 Fitting parameters (k and t_{lag}) and constants for extraction rate curves of mephentermine and 2-phenylethylamine shown in Figures 3.4 and 3.5.[a]

	V_{a2} (μL)	A_2 (cm^2)	EF_{max}	k (min^{-1})	t_{lag} (min)
Mephentermine	1.0_0	0.04_4	1600	0.028 ± 0.001	1.0 ± 0.2
	0.50	0.02_6	3200	0.024 ± 0.001	1.2 ± 0.2
2-Phenylethylamine	1.0_0	0.04_4	1600	0.0076 ± 0.0001	0.7 ± 0.1
	0.50	0.02_6	3200	0.0056 ± 0.0000_4	0.6 ± 0.1

a. V_{a1} = 1.60 mL; V_o = 30 μL; $A_1 = 0.3_5$ cm^2; 2050 rpm; at 25.0 °C.

Stirring speed was also observed to affect k. For example, for both mephentermine and 2-phenylethylamine, after 20-min of extraction using the 1.0_0-μL drop, EF was about 10% higher at a stirring speed of 2050 rpm than it was at 1700 rpm.

3.2.2 Deviations at High C_{a2}

The rigorous extraction-rate equation in chapter 2 (and therefore the approximate first-order rate equation, eq 3.7) accurately describes the experimentally measured plot of EF versus time over the entire curve of the extraction, provided that the absolute concentration of solute in the aqueous receiving phase does not become too high. For example, in chapter 2 excellent agreement with theory is observed over the whole rate curve when V_{a2} = 200 μL and EF_{max} = 5, for which the highest attained C_{a2} was only 5.0×10^{-4} M for mephentermine and 2-phenylethylamine. However, when V_{a2} is greatly decreased, as in the present study, so that EF becomes very large and C_{a2} becomes high even well before the attainment of extraction equilibrium, then deviations from the theoretical rate equations may be observed (see Figure 3.6) due to interfacial adsorption of the surface-active cationic conjugate species of the sample compounds at the o-a2 liquid-liquid interface.[75-77] Adsorbed solutes may reduce the rate of mass transfer across the liquid-liquid interface either by creating a physical barrier or by reducing convection adjacent to the interface and thereby increasing the diffusion film thicknesses, δ_{o2} and δ_{a2}.[52,69-71,78]

The following evidence exists that an adsorbed solute layer is present on the 1.0_0-μL and 0.50-μL drops when $C_{a2} \geq 10^{-2}$ M, which occurs at times above 20 min: When C_{a2} is low, the microdrop retains its spherical shape during the entire process of being drawn back into the needle; but when C_{a2} is high the last 0.1- to 0.2-μL portion of the microdrop changes shape from spherical to vertically cylindrical as it is being drawn back into the needle. The shape change results from the marked decrease in interfacial

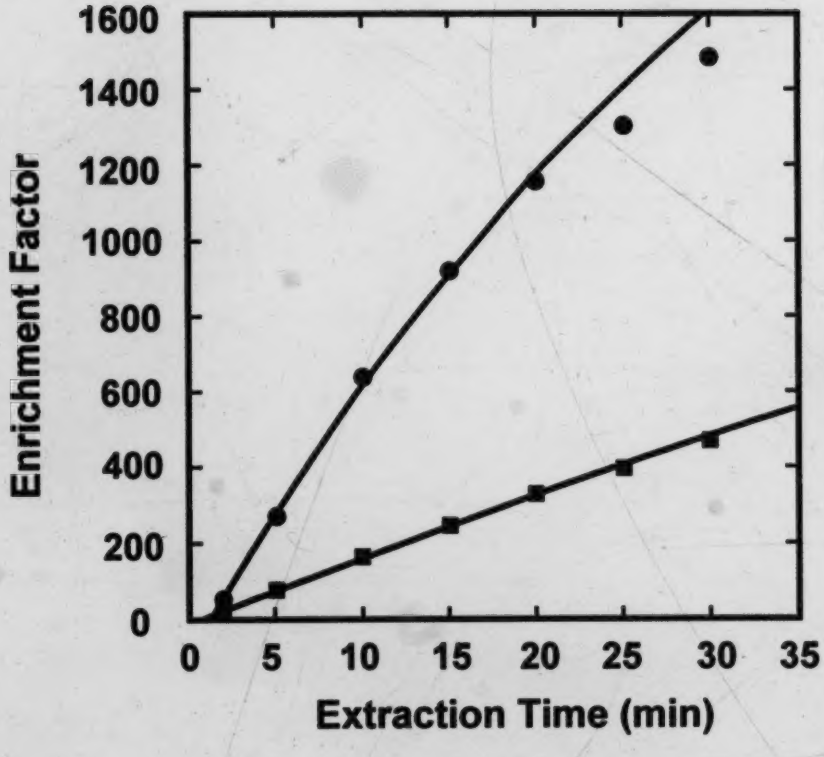

Figure 3.6 Plots of observed EFs of (•) mephentermine and (▪) 2-phenylethylamine in the 0.50-μL receiving phase versus extraction time showing deviations from the theoretical rate equations due to interfacial adsorption. The rest are the same as Figure 3.5.

tension of the last portion of the contracting drop as the surface-concentration of adsorbed solute increases due to compression of the adsorbed layer as the surface area of the drop is decreased.[75]

The extraction rate curves for both mephentermine and 2-phenylethylamine reflect the presence of adsorbed solute at times above which $C_{a2} \geq 10^{-2}$ M. In this high concentration region of the curve, the observed data points fall below the theoretical rate curve which was constructed using data points obtained at $C_{a2} \leq 10^{-2}$ M. In order to acquire a full understanding of the adsorption-induced deviation from the rate theory, it would be necessary to perform quantitative characterization both of solute adsorption at the *n*-octane-aqueous interface in terms of a solute adsorption isotherm, and of the reduction in mass transfer rate as a function of the surface concentration of the adsorbed solute. However, even in the absence of such a detailed characterization, it is possible to conclude that the deviation occurs to a significant extent only when the absolute concentration of the solute in the microdrop is quite high.

3.2.3 Calibration Curves and Analytical Significance

Extraction calibration curves for the preconcentration of mephentermine and 2-phenylethylamine from a 1.60-mL sample solution into a 1.0$_0$-μL drop were obtained by plotting HPLC signal (peak area) vs. $C_{a1,initial}$ for a series of initial sample concentrations, using a 10-min extraction at a stirring speed of 2000 rpm. The calibration curves (see Figure 3.7) were linear up to 2.0×10^{-5} M mephentermine and up to 3.0×10^{-5} M 2-phenylethylamine, with zero intercepts. Their slopes and 95% confidence limits were $(7.49 \pm 0.03) \times 10^{11}$ L/mol and $(1.44 \pm 0.17) \times 10^{11}$ L/mol, and their correlation coefficients (R^2) were 1.0000 and 0.9984, respectively, for mephentermine and 2-phenylethylamine. Typical relative standard deviations for replicate extractions of the same sample were about 2 to 3 % (n=3).

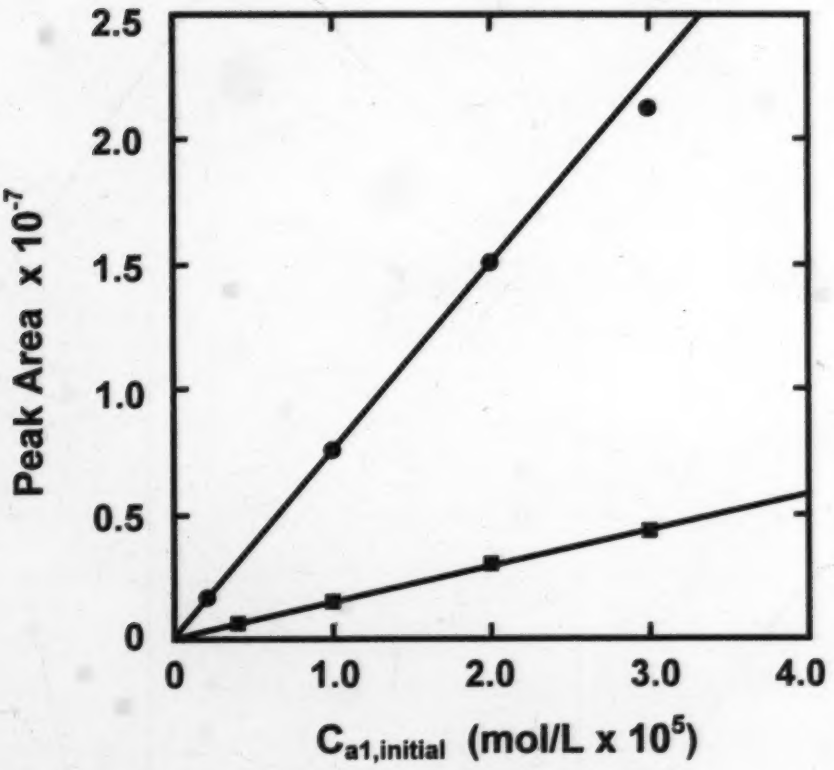

Figure 3.7 Calibration curves for 10-min extractions of (•) mephentermine and (▪) 2-phenylethylamine in a 1.6-mL sample solution into a 1-μL drop, plotted as HPLC peak area versus initial concentrations in the aqueous sample solution. Points were obtained in duplicate. See text for details. The last data point corresponding to very high C_{a2} of mephentermine was not included in the linear regression for the reason discussed in section 3.2.2.

3.2.4 Other Tested Designs

Some other designs have also been tested for preconcentration, which include a Teflon rod probe and a drop-in-drop probe.

3.2.4.1 Teflon Rod Probe

The Teflon rod probe is shown in Figure 3.8. This system differs from the system described in previous sections in that the *n*-octane organic phase is held in a 10-μL recess at the tip of a Teflon rod. The 1-μL LC syringe needle is inserted into the hole drilled at the center of the Teflon rod and the 1-μL aqueous receiving phase is suspended inside the 10-μL organic phase. The advantage of this system is that there is no limitation on the volume of the aqueous source phase. The system has been tested by extracting the model compound mephentermine from a 5-mL sample solution contained in a micro reaction vial. The obtained results are given in Figure 3.9.

The disadvantage of this system is that the organic drop and thus the 1-μL a2 drop are not very stable and can be knocked off at high stirring speeds, which compromises the enrichment factor. The stirring speed is limited to about 1000 to 1200 rpm. Another problem is the bubble generated and trapped inside the organic phase, which can grow during extraction and may knock off the 1-μL a2 drop.

3.2.4.2 Drop-in-Drop Probe

The drop-in-drop probe is shown in Figure 3.10. This system uses only 2 to 3 μL of *n*-octane organic phase, which is held at the tip of a glass tubing with the help of a Teflon ring. Because of the instability of the drops at high stirring speeds, stirring speed is limited to lower than 800 rpm. The observed enrichment factor for mephentermine is about 230 in 10 min.

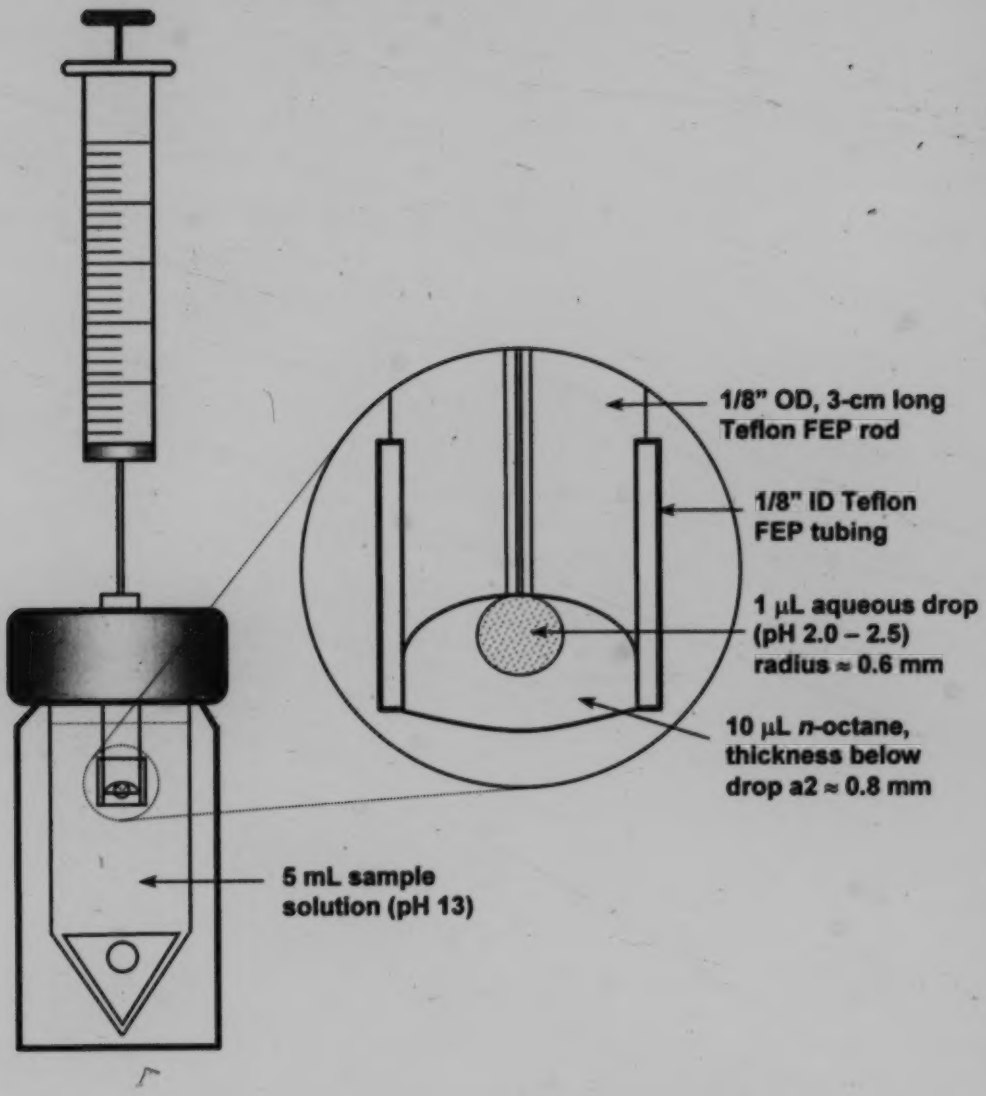

Figure 3.8 The Teflon rod probe system shown for the extraction from 5 mL of aqueous sample solution through a 10-μL *n*-octane organic phase into a 1-μL aqueous receiving drop.

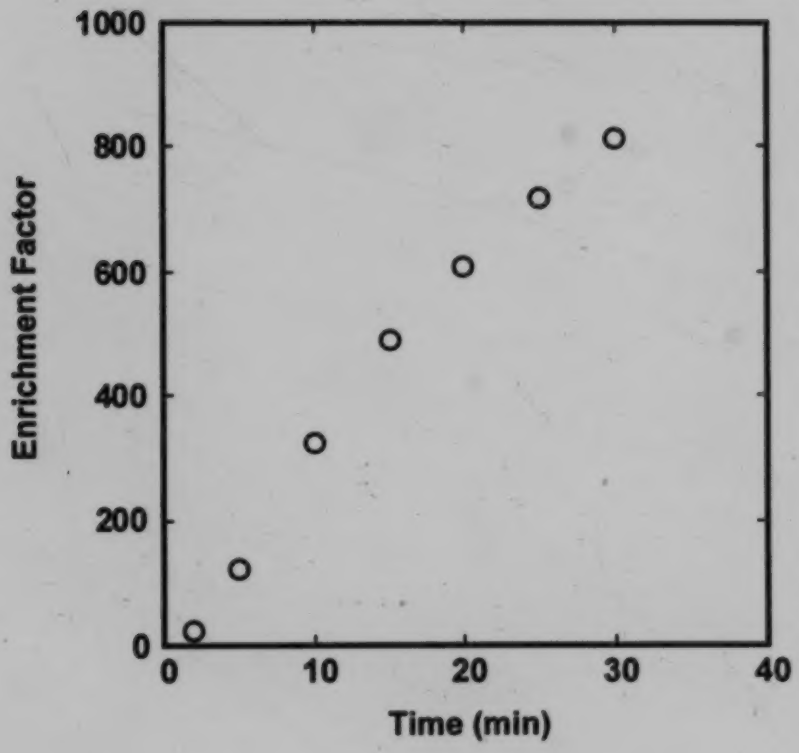

Figure 3.9 Plots of observed EFs of mephentermine in the 1-μL receiving phase versus extraction time at a stirring speed of 1200 rpm. Experimental conditions: $C_{a1,initial} = 1.0 \times 10^{-5}$ M, $V_{a1} = 5$ mL, $V_o = 10$ μL, $V_{a2} = 1.0$ μL, 25.0 °C.

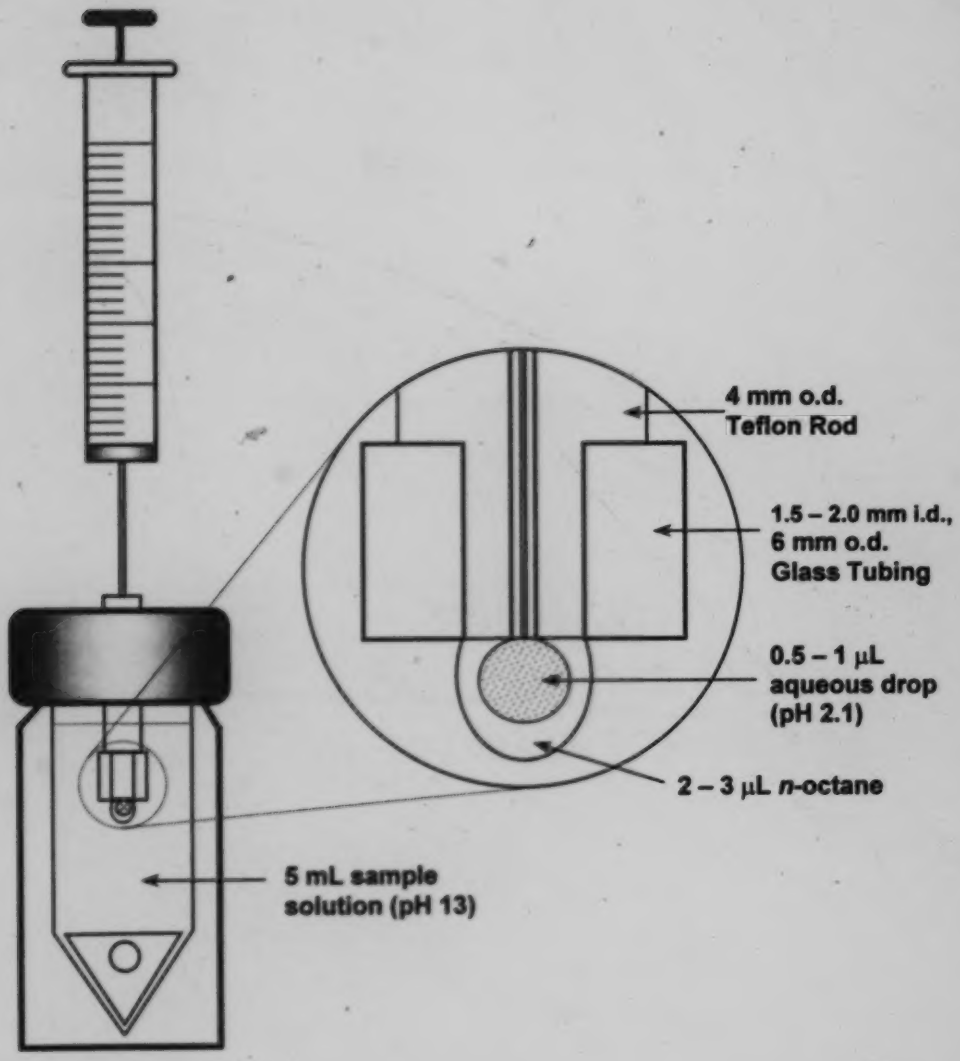

Figure 3.10 The drop-in-drop probe system shown for the extraction from 5 mL of aqueous sample solution through a 10-μL *n*-octane organic phase into a 1-μL aqueous receiving drop.

Chapter 4

Conclusions and Future Work

4.1 Conclusions

The proposed solvent microextraction technique, SME/BE, is attractive in terms of simplicity, analytical precision, overall sample preparation time, cost, and minimization of organic waste. The technique is suitable for ionic and ionizable compounds. Compared with forward extraction alone, SME/BE potentially provides additional clean-up of samples, increased extraction selectivity, and much higher enrichment factor.

Because the forward- and back-extractions are carried out simultaneously, the number of manipulations is minimized. The manual operation is very simple, especially with the design for quantitative extraction. No attention is needed during the extraction and several extraction vials can be stirred simultaneously. The technique is also amenable to automation.

Quantitative extraction can be achieved for compounds with relatively small distribution coefficients using a layer of the aqueous receiving phase. Very high preconcentration is possible using a single microdrop of the aqueous receiving phase. The typical relative standard deviations for this technique are about 1 to 3 % (n=3).

This technique uses only 30 to 80 μL of *n*-octane, the consumption of organic solvent is minimized. Since fresh organic solvent is used for each extraction, there is no memory effect, and since the back extractant is already in aqueous media, there is no need for desorption prior to injection into HPLC. With the design for quantitative

extraction, the volume of the aqueous receiving phase is only 100 or 200 μL, therefore, there is no need for volume reduction by solvent evaporation.

The increase in extraction efficiency which is realized upon reducing V_{a2} from 1-μL to 0.5-μL could be further improved by using even smaller microdrop volumes. The use of $V_{a2} < 0.1$ μL would be worth investigating since such small volumes are compatible with the injection volumes required by capillary electrophoretic and capillary chromatographic separation techniques.

Currently, the most popular phases for SPE are the silica based C18 and C8 phases and the commercially available coatings for SPME are nonpolar or of medium polarity, which are very efficient for hydrophobic analytes. However, enrichment and cleanup of polar or ionic compounds are more difficult in SPE and SPME. On the other hand, the SME/BE technique is designed specifically for analytes that can be ionized in aqueous media. Therefore, SME/BE is a sample preparation technique that should complement the current SPE and SPME.

4.2 Future Work

The present work only proposed and demonstrated the new solvent microextraction technique SME/BE, its usefulness for real-world applications and its advantages over existing extraction techniques are still yet to be demonstrated in the future. Due to its unique characteristics, this technique should find many applications, especially in the fields of pharmaceutical, medical and environmental analysis. The proposed future work is outlined in the following sections.

4.2.1 Applications

4.2.1.1 Basic and Acidic Drugs in Biological Fluids

The analysis of drugs and their metabolites in biological fluids represents an essential role in pharmaceutical and toxicology studies. Because of the complexity of the matrices and low concentrations of drugs, sample preparation is often an inevitable step prior to HPLC or CE separations. Since many drug compounds have basic or acidic groups,[79-83] SME/BE is suitable for the extraction of basic and acidic drugs.

The work presented in this thesis has demonstrated successfully the extraction of several phenylalkylamines. Therefore, this technique should be applicable immediately to the extraction of drugs of abuse. After extraction, the ideal set-up for analysis would be either HPLC-MS or CE-MS. The current method uses GC-MS[84,85] after derivatization and extraction of these basic compounds, although recent development in column technology has made it possible to analyze non-derivatized drugs.[86]

4.2.1.2 Ionic Compounds

For ionic compounds (e.g. those containing quaternary ammonium group[87]) and compounds existing as an ion in a wide range of pH's (e.g. those containing $-SO_3^-$), extraction can be done through ion pairing. The pairing ion is generated by the dissociation of weak acidic or basic groups. In this case, the driving force of the extraction is still the pH difference between the source and the receiving phases as for the extraction of basic and acidic compounds, but the species whose ionic state changes during extraction process is the pairing ion instead of the analyte. The mechanism is illustrated in Figure 4.1 using anion as an example.

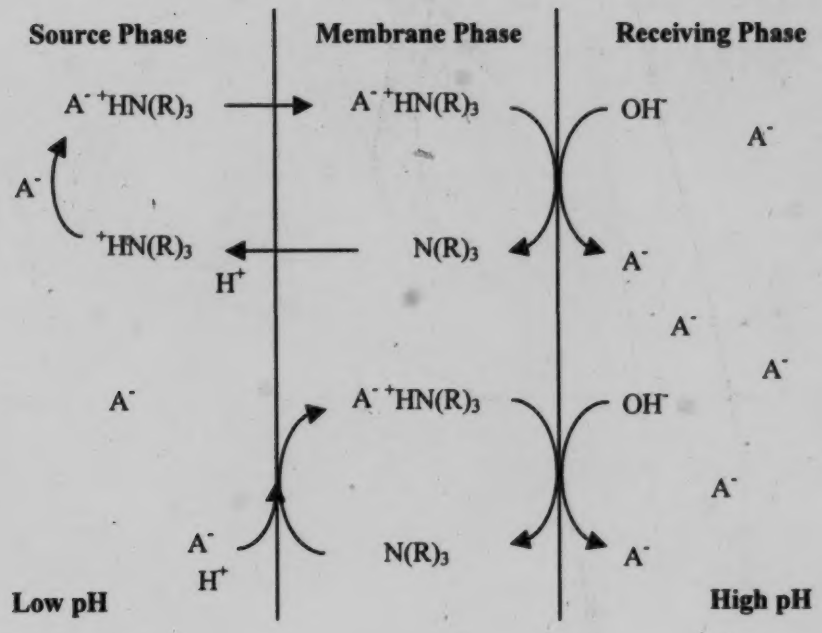

Figure 4.1 Schematic diagram of the extraction of ionic compounds using an ion-pairing reagent through an organic liquid membrane. The extraction of analyte anion A^- is shown as an example. Ion pairing can occur either in the source phase or at the interface.

4.2.1.3 Environmental Water

Although SME/BE is not suitable for the extraction of solid environmental samples such as soil, it can be used to extract ionizable compounds such as phenols and pesticides in environmental water. In this case, trace enrichment is always required. The extraction of phenols in water has been performed using many different extraction techniques such as supercritical fluid extraction[88] and solid phase extraction.[89] The supported liquid membrane technique has also been used to extract pesticides in water.[90-92]

4.2.1.4 Amino Acids

The extraction of amino acids can be performed through ion pairing using either positively or negatively charged pairing ions. This has been demonstrated by using the bulk liquid membrane (BLM) technique[93] and the extraction mechanisms are illustrated in Figure 4.2. BLM transport experiments, typically conducted using U-tube cells with membrane phase volumes ranging from a few milliliters to over 100 ml, are extremely time-consuming due to the thickness of the membrane. It usually takes hours or even longer to see any significant transport of analyte across the membrane; therefore, it has no potential for practical application.[94-96] The use of SME/BE with micro organic membrane should significantly increase the extraction efficiency for most amino acids although for amino acids with very polar side chains, the extraction efficiency might still be low due to very small distribution ratios. Recently, the extraction of dansylated amino acids has been demonstrated by using supported liquid membrane (SLM) techniques.[97]

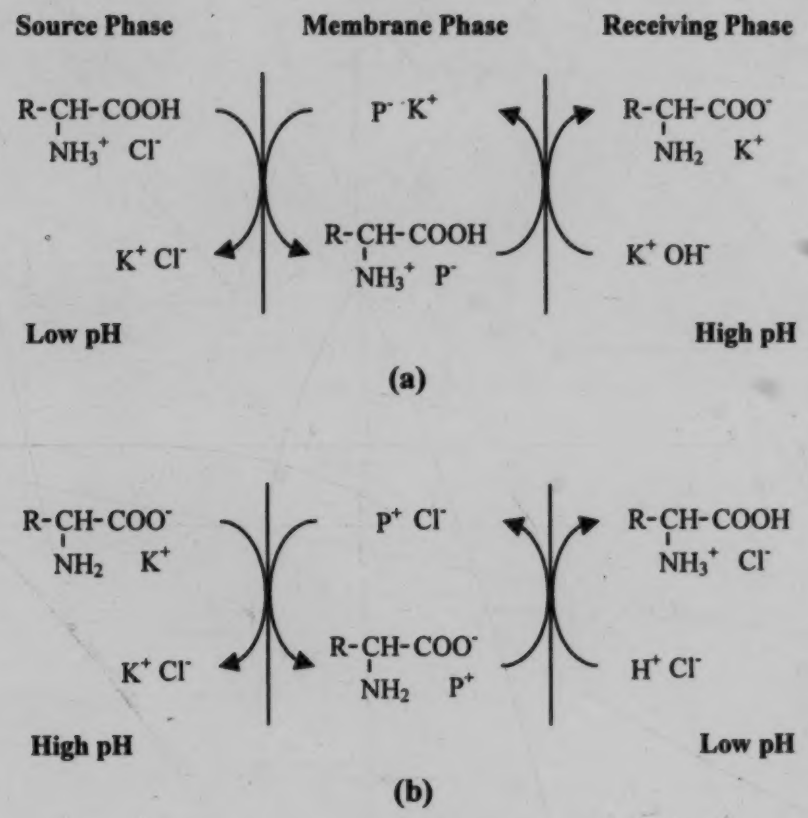

Figure 4.2 Schematic representation of the extraction of amino acids (a) from acidic source to basic receiving phases using a negatively charged pairing ion P^- and (b) from basic source to acidic receiving phases using a positively charged pairing ion P^+.

4.2.1.5 Metal Ions

In order to transport metal ions through the hydrophobic organic liquid membrane, carrier molecules, which can form neutral complexes with metal ions, have to be used to facilitate the transport. With proper choice of carrier molecules and conditions of the source and the receiving phases, selective metal ion extraction and enrichment can be achieved effectively. Illustrated in Figure 4.3 are three different extraction mechanisms with different types of carrier molecules.

In Figure 4.3 (a), the carrier C^- (such as 8-hydroxyquinoline) is a complexing agent that is added to the aqueous source phase to form a neutral complexes with metal ions before it is extracted into the membrane phase. On the receiving side, the metal ions are released using a trapping agent L^{3-} (e.g. EDTA) that forms a stronger complex with the metal ions. In this case, the pH difference between the source and the receiving phases is also a driving force for the transport. In Figure 4.3 (b), the neutral carrier (such as macrocyclic polyethers) is added to the organic membrane phase that forms a complex with metal ions at the source-membrane interface. The complex carrying certain number of counterions such as chloride to maintain electrical neutrality is transported to the receiving side and the metal ions are released at the membrane-receiving interface. In Figure 4.3 (c), the carrier is a liquid anion exchanger such as methyltrioctylammonium chloride (Aliquat-336) and tetraheptylammonium chloride, which is added to the organic membrane phase. In this case, a metal-ligand complex bearing negative charge (MQ_3^-) is formed in the source phase, which is then extracted into the organic membrane phase by ion association with the liquid anion exchanger at the interface. The metal ions are released on the receiving side by using a stronger complexing agent L^{3-} in the receiving phase.

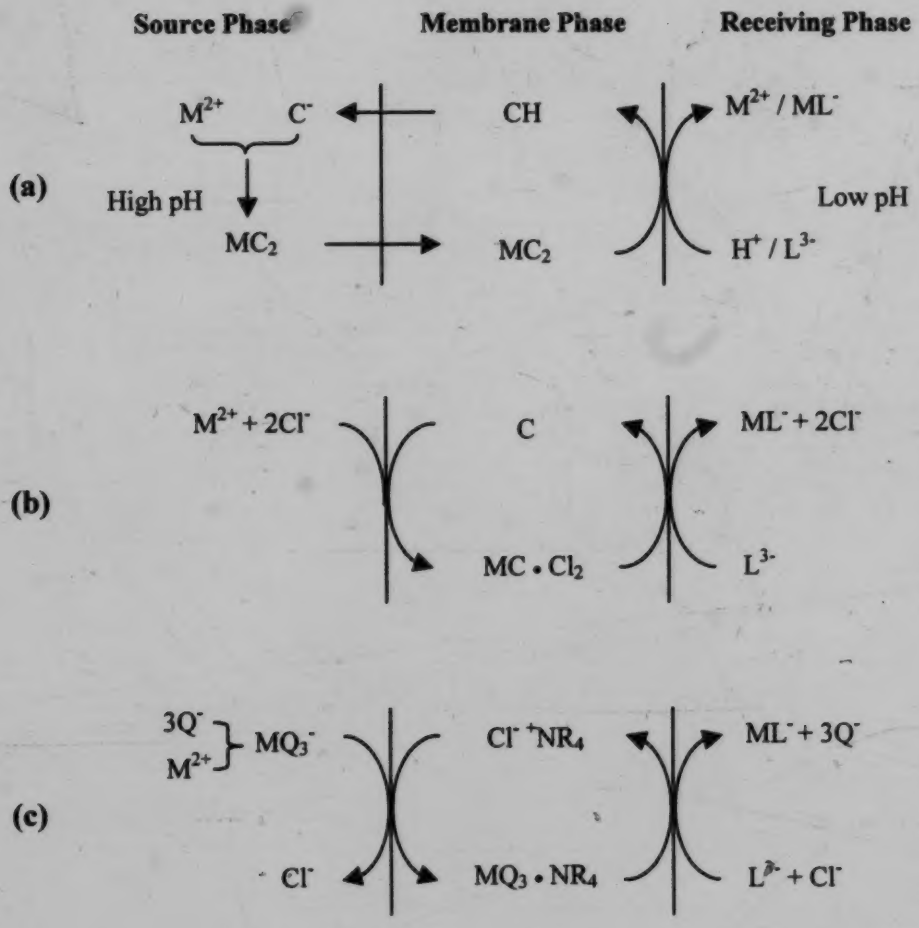

Figure 4.3 Schematic illustration of the transport of metal ions through an organic liquid membrane using carriers: (a) C^- as complexing agent dissolved in the source phase, (b) C as complexing agent dissolved in membrane phase, and (c) $R_4N^+Cl^-$ as liquid anion exchanger dissolved in the membrane phase. Q^- and L^{3-} are complexing agents.

Without trapping agent in the receiving phase, the transport of metal ions is limited by the Donnan equilibrium, e.g. for the case of Figure 4.3 (b):

$$[M^{2+}]_s [Cl]_s^2 = [M^{2+}]_r [Cl]_r^2 \qquad (4.1)$$

where the subscript s and r represent the source and receiving phases, respectively. Although it is possible to obtain higher $[M^{2+}]_r$ than $[M^{2+}]_s$ by using a larger concentration gradient of chloride ion across the membrane, significant enrichment of the metal ion in the receiving phase can only be achieved by using a trapping agent in the receiving phase. The transport of metal ions through organic liquid membranes has been studied extensively using the bulk liquid membrane,[94-96,98-102] supported liquid membrane,[94-96,103-108] and emulsion liquid membrane techniques.[94-96]

4.2.1.6 Evaluating Carrier Performance

Although the bulk liquid membrane technique has no potential for practical applications, it is often used for evaluating or screening the performance of carriers[99,101,109] and for other related fundamental studies of carrier facilitated transport.[98,110,111] Carriers which demonstrate interesting selectivity characteristics can then be investigated in more practical membrane types such as supported liquid membranes and emulsion liquid membranes.[109] However, BLM transport experiments are extremely time-consuming due to the thickness of the membrane. One example is shown in Figure 4.4. Significant time-saving is expected when the SME/BE technique as shown in Figure 2.1 is used to screen the carrier properties. Due to their applications in carrier-based ion-selective electrodes[112-114] and in selective separation of ions[94-96,104,115,116] using liquid membrane and solid phase extraction, the synthesis and the use of more efficient carriers (or more specifically macrocyclic compounds)[117-119] are still the subject of intensive research.

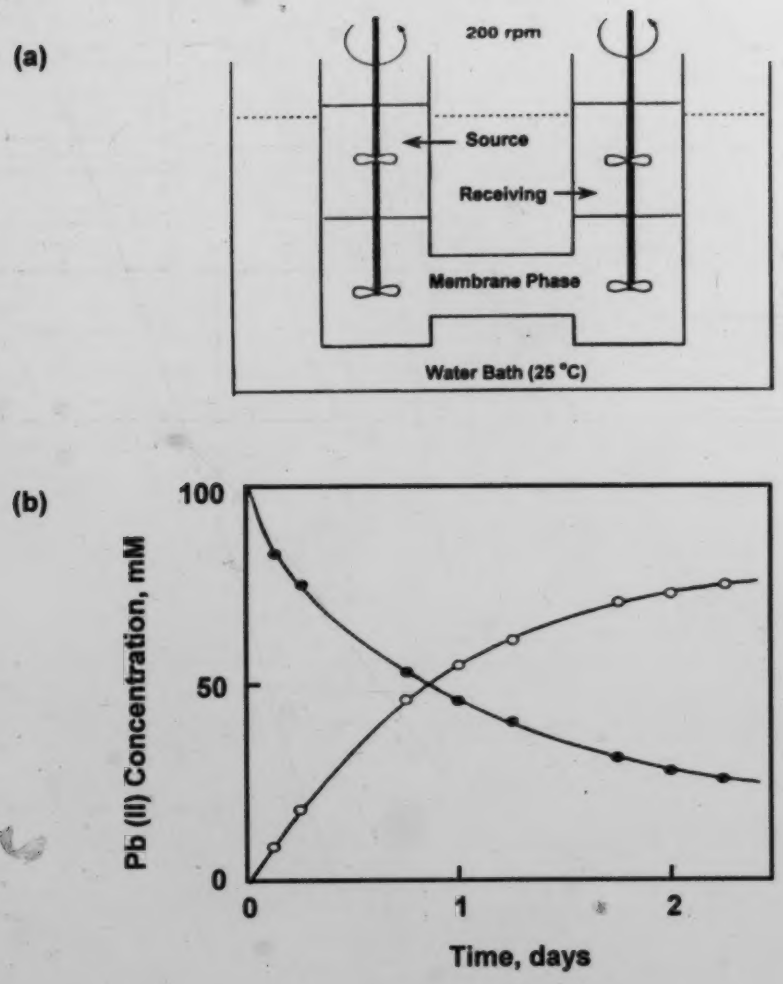

Figure 4.4 (a) BLM cell for measuring metal ion transport across a chloroform membrane. (b) Pb^{2+} concentrations in the source (•) and receiving (o) phases versus time. Initial conditions: source phase, 15 mL of 0.10 M Pb^{2+} in acetate buffer at pH 6.18; membrane phase, 30 mL of 5.0 mM acyclic polyether dicarboxylic acid in chloroform; receiving phase, 15 mL of 0.10 M nitric acid. From reference 101.

4.2.2 Instrumentation

4.2.2.1 On-line Coupling of Microdrop Extraction to HPLC

To couple the microdrop extraction technique on-line to HPLC, a setup such as that shown in Figure 4.5 can be used. In this setup, the microsyringe is replaced by an annular tubular (tubing-in-tubing) drophead similar to a microdialysis probe[120-122] without a dialysis membrane. Actually, the whole setup for on-line coupling of microdialysis to HPLC[123-126] can be adopted for the microdrop extraction experiment with minimal modification. Similar tubing-in-tubing drophead has also been used by Liu and Dasgupta[127] to perform solvent extraction in a microdrop. With such a setup, it is possible to automate the microdrop extraction experiment.

4.2.2.2 Coupling to Capillary Electrophoresis

The coupling of the microdrop extraction to CE should be simple. Instead of using a tubing-in-tubing drophead, the aqueous microdrop can be suspended in the organic membrane phase directly from the tip of the CE capillary. Because the size of the drop is very small (< 0.5 μL), extraction should be very efficient. After extraction, the drop can be injected either hydrostatically or electrokinetically. For the latter injection method, the tip of the CE capillary is sputter-coated with platinum metal, to which a contact wire is attached with silver epoxy adhesive.

Dasgupta's group at Texas Tech is also working on the coupling of microdrop extraction to CE and CEC. In their design, the organic membrane phase is a thin film coated on the microdrop that is also suspended directly from the tip of the CE capillary.[128]

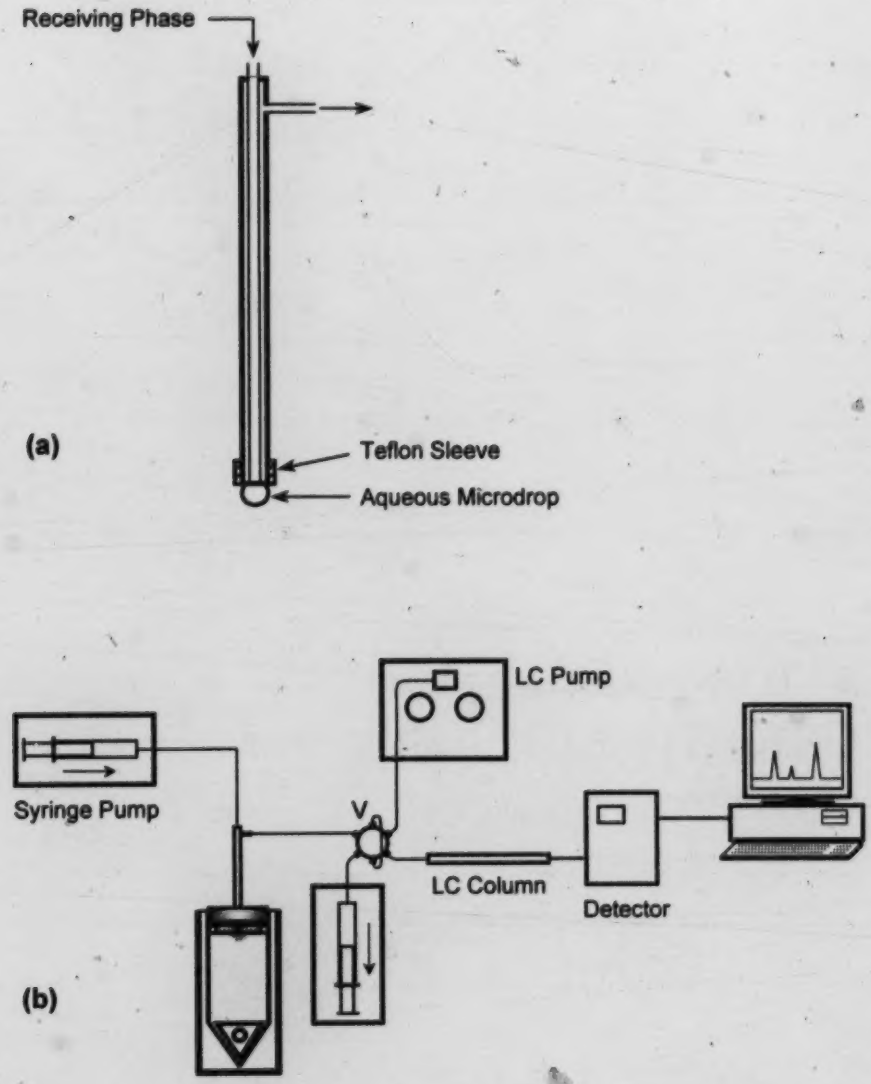

Figure 4.5 Schematic diagrams of (a) the tubing-in-tubing drophead and (b) the on-line microdrop extraction-HPLC system. V: LC injection valve.

4.2.3 Theory

When the adsorption of molecules at the membrane-receiving interface is significant, the observed enrichment factors will be lower than those predicted by the theory. It would be nice to have a kinetic model which includes the effect of adsorption at the interfaces.

Bibliography

(1) Mehta, A.C. *Talanta,* **1986**, *33*, 67-73.

(2) Snyder, L.R.; Kirkland, J.J.; Glajch, J.L. *Practical HPLC Method Development*, 2nd ed.; Wiley-Interscience: New York, 1997; Chapter 4.

(3) Lloyd, D.K. *J. Chromatogr. A* **1996**, *735*, 29-42.

(4) Majors, R.E.; Raynie, D.E. *LC-GC* **1997**, *15*, 1106-1117.

(5) Majors, R.E. *LC-GC* **1996**, *14*, 754-766.

(6) Kubán, V. *Crit. Rev. Anal. Chem.* **1991**, *22*, 477-557.

(7) Clark, G.D.; Whitman, D.A.; Christian, G.D.; and Ruzicka, J. *Crit. Rev. Anal. Chem.* **1990**, *21*, 357-375.

(8) Majors, R.E. *LC-GC* **1996**, *14*, 936-943.

(9) Loeper, J.M. In *Modern Practice of Gas Chromatography*, 3rd ed.; Grob, R. ed.; Wiley-Interscience: New York, 1995; pp.788-791.

(10) Grob, K.; Grob, K.Jr.; Grob, G. *J. Chromatogr.* **1975**, *106*, 299-315.

(11) Murray, D.A.J. *J. Chromatogr.* **1979**, *177*, 135-140.

(12) Ramsey, J.; Campbell, D.B. *J. Chromatogr.* **1971**, *63*, 303-308.

(13) Aggarval, V.; Bath, R.; Sunshine, I. *Clin. Chem.* **1974**, *20*, 307.

(14) Van de Hoff, G.R.; Baumann, R.A.; Brinkman, U.A.Th.; van Zoonen, P. *J. Chromatogr.* **1993**, *644*, 367-373.

(15) Dalluge, J.; Catalina, I.; Vreuls, R.; Brinkman, U.; Pocurull, E. In *Proceedings of Nineteenth International Symposium on Capillary Chromatography and Electrophoresis*, May 18-22, 1997, Wintergreen, Virginia; pp 150-151.

(16) Magni, P.; Munari, F.; Trestianu, S. In *Proceedings of Nineteenth International Symposium on Capillary Chromatography and Electrophoresis*, May 18-22, 1997, Wintergreen, Virginia; pp 388-389.

(17) Liu, H.; Dasgupta, P.K. *Anal. Chem.* **1996**, *68*, 1817-1821.

(18) Jeannot, M.A.; Cantwell, F.F. *Anal. Chem.* **1996**, *68*, 2236-2240.

(19) Jeannot, M.A.; Cantwell, F.F. *Anal. Chem.* **1997**, *69*, 235-239.

(20) Jeannot, M.A.; Cantwell, F.F. *Anal. Chem.* **1997**, *69*, 2935-2940.

(21) He, Y.; Lee, H.K. *Anal. Chem.* **1997**, *69*, 4634-4640.

(22) Berrueta, L.A.; Gallo, B.; Vicente, F. *Chromatographia* **1995**, *40*, 474-483.

(23) Moors, M.; Massart, D.L. McDowall, R.D. *Pure & Appl. Chem.* **1994**, *66*, 277-304.

(24) Majors, R.E.; Raynie, D.E. *LC-GC* **1997**, *15*, 1106-1117.

(25) Lingeman, H.; Hoekstra-Oussoren, S.J.F. *J. Chromatogr. B* **1997**, *689*, 221-237.

(26) He, Y.; Lee, H.K. *Electrophoresis*, **1997**, *18*, 2036-2041.

(27) Nielen, M.W.F.; Frei, R.W.; Brinkman, U.A.Th. In *Selective Sample Handling and Detection in High-performance Liquid Chromatography, Part A*; Frei, R.W.; Zech, K. Eds.; Elsevier:Amsterdam, 1988; pp.5-80.

(28) Huber, R.; Zech, K. In *Selective Sample Handling and Detection in High-performance Liquid Chromatography, Part A*; Frei, R.W.; Zech, K. Eds.; Elsevier:Amsterdam, 1988; pp.81-143.

(29) Tomlinson, A.J.; Benson, L.M.; Guzman, N.A.; Naylor, S. *J. Chromatogr. A* **1996**, *744*, 3-15.

(30) Campins-Falco, P.; Herraez-Hernandez, R.; Sevillano-Cabeza, A. *J. Chromatogr.* **1993**, *619*, 177-190.

(31) Arthur, C.L.; Pawliszyn, J. *Anal. Chem.* **1990**, *62*, 2145-2148.

(32) Zhang, Z.; Yang, M.J.; Pawliszyn, J. *Anal. Chem.* **1994**, *66*, 844A-853A.

(33) Pawliszyn, J. *Solid-Phase Microextraction: Theory and Practice*, Wiley-VCH: New York, 1997.

(34) Eisert, R.; Pawliszyn, J. *Crit. Rev. Anal. Chem.* **1997**, *27*, 103-135.

(35) Chen, J.; Pawliszyn, J. *Anal. Chem.* **1995**, *67*, 2530-2533.

(36) Daimon, H.; Pawliszyn, J. *Anal. Commun.* **1997**, *34*, 365-369.

(37) Jinno, K.; Taniguchi, M.; Hayashida, M.; Ohno, Y. In *Proceedings of Nineteenth International Symposium on Capillary Chromatography and Electrophoresis*, May 18-22, 1997, Wintergreen, Virginia; pp 198-199.

(38) Li, S.; Weber, S.G. *Anal. Chem.* **1997**, *69*, 1217-1222.

(39) Gorecki, T.; Martos, P.; Pawliszyn, J. *Anal. Chem.* **1998**, *70*, 19-27.

(40) Liu, Y.; Lee, M.L.; Hageman, K.J.; Yang, Y.; Hawthorne, S.B. *Anal. Chem.* **1997**, *69*, 5001-5005.

(41) Shelly, D.C.; Rossi, T.M.; Warner, I.M. *Anal. Chem.* **1982**, *54*, 87-91.

(42) Bengtsson, M.; Johansson, G. *Anal. Chim. Acta* **1984**, *158*, 147-156.

(43) Luo, Y.; Al-Othman, R.; Ruzicka, J.; Christian, G.D. *Analyst*, **1996**, *121*, 601-606.

(44) Audunsson, G. *Anal. Chem.* **1986**, *58*, 2714-2723.

(45) Jonsson, J.A.; Mathiasson, L. *Trends Anal. Chem.* **1992**, *11*, 106-114.

(46) Jonsson, J.A.; Lovkvist, P.; Audunsson, G.; Nilve, G. *Anal. Chim. Acta* **1993**, *277*, 9-24.

(47) Lindegard, B.; Bjork, H.; Jonsson, J.A.; Mathiasson, L.; Olsson, A-M. *Anal. Chem.* **1994**, *66*, 4490-4497.

(48) Thordarson, E.; Palmarsdottir, S.; Mathiasson, L.; Jonsson, J.A. *Anal. Chem.* **1996**, *68*, 2559-2563.

(49) Palmarsdottir, S.; Thordarson, E.; Edholm, L.-E.; Jonsson, J.A.; Mathiasson, L. *Anal. Chem.* **1997**, *69*, 1732-1737.

(50) Malcus, F.; Djane, N.-K.; Mathiasson, L.; Johansson, G. *Anal. Chim. Acta* **1996**, *327*, 295-300.

(51) Danesi, P.R.; Chiarizia, R. *CRC Crit. Rev. Anal. Chem.* **1980**, *10*, 1-126.

(52) Davies, J.T.; Rideal, E.K. *Interfacial Phenomena*, 2nd ed.; Academic Press: New York, 1963; Chapter 7.

(53) Cussler, E.L. *Diffusion: Mass Transfer in Fluid Systems*, Cambridge University Press: Cambridge, UK, 1984; chapters 1, 2, 9, 11.

(54) Danesi, P.R. In *Principles and Practices of Solvent Extraction*, Rydberg, J.; Musikas, C.; Choppin, G.R. Eds.; Marcel Dekker: New York, 1992; pp.157-207.

(55) Frost, A.A.; Pearson, R.G. *Kinetics and Mechanism*, 2nd ed.; John Wiley & Sons: New York, 1961; pp 173-177.

(56) Capellos, C.; Bielski, B.H.J. *Kinetic Systems: Mathematical Description of Chemical Kinetics in Solution*; Wiley-Interscience: New York, 1973; pp 35-38.

(57) Szabó, Z.G. In *Comprehensive Chemical Kinetics*, Bamford, C.H.; Tipper, C.F.H. eds.; Elsevier: Amsterdam, 1969; Vol. *2*, pp 29-31.

(58) Jeannot, M.A. Ph.D. Thesis, University of Alberta, Fall 1997; chapter 3.

(59) Liley, P.E.; Reid, R.C.; Buck, E. In *Chemical Engineers' Handbook*, 6th ed.; Perry, R.H.; Green, D.W., Eds.; McGraw-Hill: New York, 1984; chapter 3, pp 258-259.

(60) Vree, T.B.; Muskens, A.Th.J.M.; van Rossum, J.M. *J. Pharm. Pharmac.* **1969**, *21*, 774-775.

(61) Taylor, G. *Proc. R. Soc. Lond. A* **1953**, *219*, 186-203.

(62) Taylor, G. *Proc. R. Soc. Lond. A* **1954**, *225*, 473-477.

(63) Aris, R. *Proc. R. Soc. Lond. A* **1955**, *235*, 67-77.

(64) Ouano, A.C. *Ind. Eng. Chem. Fundam.* **1972**, *11*, 268-271.

(65) Wisnudel, M.B.; Torkelson, J.M. *AIChE J.* **1996**, *42*, 1157-1163.

(66) Cussler, E.L. *Diffusion: Mass Transfer in Fluid Systems*, Cambridge University Press: Cambridge, UK, 1984; chapters 4, 5.

(67) Crank, J. *The Mathematics of Diffusion*, 2nd ed.; Clarendon Press: Oxford, UK, 1975; chapter 10.

(68) Pratt, K.C.; Wakeham, W.A. *Proc. R. Soc. Lond. A* **1974**, *336*, 393-406.

(69) Brown, A.H. *Brit. Chem. Eng.* **1965**, *10*, 622-626.

(70) England, D.C.; Berg, J.C. *Am. Inst. Chem. Eng. J.* **1971**, *17*, 313-322.

(71) Borwankar, R.P.; Wasan, D.T. *Ind. Eng. Chem. Fundam.* **1986**, *25*, 662-668.

(72) Much cheaper stirrers with digital speed control up to 2500 rpm are commercially available such as VWRbrand Stirrer Model 400S.

(73) Frost, A.A.; Pearson, R.G. *Kinetics and Mechanism*, 2nd ed.; John Wiley & Sons: New York, 1961; chapter 8, p.172 and p.195.

(74) Crank, J. *The Mathematics of Diffusion*, 2nd ed.; Oxford University Press: 1975; chapter 4, p.51.

(75) Persaud, G.; Tian, X.M.; Cantwell, F.F. *Anal. Chem.* **1987**, *59*, 2-7.

(76) Amankwa, L.; Cantwell, F.F. *Anal. Chem.* **1990**, *62*, 2270-2274.

(77) Amankwa, L.; Cantwell, F.F. *Can. J. Chem.* **1991**, *69*, 88-93.

(78) Tarasov, V.V.; Yagodin, G.A.; *Ion Exchange and Solvent Extraction*, **1988**, *10*, 141-237.

(79) Roth, H.J.; Eger, K.; Troschutz, R. *Pharmaceutical Chemistry, Volume 2: Drug Analysis*, Ellis Horwood: New York, 1991.

(80) Davies, N.M. *J. Chromatogr.* **1997**, *691*, 229-261.

(81) Smith. R.M.; Hurdley, T.G.; Gill, R.; Osselton, M.D. *J. Chromatogr.* **1987**, *398*, 73-87.

(82) Roos, R.W.; Lau-Cam, C.A. *J. Chromatogr.* **1986**, *370*, 403-418.

(83) McMahon, G.P.; Kelly, M.T. *Anal. Chem.* **1998**, *70*, 409-414.

(84) Zurer, P. *C & EN*, 1997, Jan. 27, p.28.

(85) Marquet, C.B.; Fauconnet, A.L.; Lacassie, E.; Lachatre, G. *J. Chromatogr. Sci.* **1998**, *36*, 1-7.

(86) *Chrompack News*, 1998, No.1, p.10.

(87) Moder, M.; Loster, H.; Herzschuh, R.; Popp, P. *J. Mass Spectrom.* **1997**, *32*, 1195-1204.

(88) Ramsey, E.D.; Minty, B.; McClullagh, M.A.; Games, D.E.; Rees, A.T. *Anal. Commun.* **1997**, *34*, 3-6.

(89) Li, N.; Lee, H.K. *Anal. Chem.* **1997**, *69*, 5193-5199.

(90) Knutsson, M.; Nilve, G.; Mathiasson, L.; Jonsson, J.A. *J. Chromatogr. A*, **1996**, *754*, 197-205.

(91) Nilve, G.; Stebbins, R. *Chromatographia*, **1991**, *32*, 269-277.

(92) Megersa, N.; Jonsson, J.A. *Analyst*, **1998**, *123*, 225-231.

(93) Behr, J-P.; Lehn, J-M. *J. Am. Chem. Soc.* **1973**, *95*, 6108-6110.

(94) Noble, R.D., Way, J.D., Eds.; *Liquid Membranes: Theory and Applications*, ACS Symposium Series 347; American Chemical Society: Washington, DC, 1987.

(95) Araki, T., Tsukube, H., Eds.; *Liquid Membranes: Chemical Applications*; CRC Press: Boca Raton, Florida, 1990.

(96) Bartsch, R.A., Way, J.D., Eds.; *Chemical Separations with Liquid Membranes*, ACS Symposium Series 642; American Chemical Society: Washington, DC, 1996.

(97) Wieczorek, P.; Jonsson, J.A.; Mathiasson, L. *Anal. Chim. Acta*, **1997**, *337*, 183-189.

(98) Lamb, J.D.; Christensen, J.J.; Oscarson, J.L.; Nielsen, B.L.; Asay, B.W.; Izatt, R.M. *J. Am. Chem. Soc.* **1980**, *102*, 6820-6824.

(99) Izatt, R.M.; LindH, G.C.; Bruening, R.L.; Huszthy, P.; McDaniel, C.W.; Bradshaw, J.S.; Christensen, J.J. *Anal. Chem.* **1988**, *60*, 1694-1699.

(100) Hayashita, T.; Bartsch, R.A.; Kurosawa, T.; Igawa, M. *Anal. Chem.* **1991**, *63*, 1023-1027.

(101) Hiratani, K.; Takahashi, T.; Sugihara, H.; Kasuga, K.; Fujiwara, K.; Hayashita, T.; Bartsch, R.A. *Anal. Chem.* **1997**, *69*, 3002-3007.

(102) Safavi, A.; Rastegarzadeh, S. *Talanta*, **1995**, *42*, 2039-2042.

(103) Izatt, R.M.; Bruening, R.L.; Bruening, M.L.; Lindh, G.C.; Christensen, J.J. *Anal. Chem.* **1989**, *61*, 1140-1148.

(104) Asfari, Z.; Bressot, C.; Vicens, J.; Hill, C.; Dozol, J-F.; Rouquette, H.; Eymard, S.; Lamare, V.; Tournois, B. *Anal. Chem.* **1995**, *67*, 3133-3139.

(105) Papantoni, M.; Djane, N-K.; Ndung'u, K.; Jonsson, J.A.; Mathiasson, *Analyst*, **1995**, *120*, 1471-1477.

(106) Malcus, F.; Djane, N-K.; Mathiasson, L.; Johansson, G. *Anal. Chim. Acta*, **1996**, *327*, 295-300.

(107) Djane, N-K.; Bergdahl, I.A.; Ndung'u, K.; Schutz, A.; Johansson, G.; Mathiasson, L. *Analyst*, **1997**, *122*, 1073-1077.

(108) Djane, N-K.; Armalis, S.; Ndung'u, K.; Johansson, G.; Mathiasson, L. *Analyst*, **1998**, *123*, 393-396.

(109) Izatt, R.M.; Lamb, J.D.; Bruening, R.L. *Sep. Sci. Technol.* **1988**, *23*, 1645-1658.

(110) Behr, J-P.; Kirch, M.; Lehn, J-M. *J. Am. Chem. Soc.* **1985**, *107*, 241-246.

(111) Lamb, J.D.; Christensen, J.J.; Izatt, S.R.; Bedke, K.; Astin, M.S.; Izatt, R.M. *J. Am. Chem. Soc.* **1980**, *102*, 3399-3403.

(112) Bakker, E.; Buhlmann, P.; Pretsch, E. *Chem. Rev.* **1997**, *97*, 3083-3132.

(113) Bakker, E.; Pretsch, E. *Anal. Chem.* **1998**, *70*, 295-302.

(114) Tohda, K.; Yoshiyagawa, S.; Kataoka, M.; Odashima, K.; Umezawa, Y. *Anal. Chem.* **1997**, *69*, 3360-3369.

(115) Bradshaw, J.S.; Izatt, R.M. *Acc. Chem. Res.* **1997**, *30*, 338-345.

(116) Majors, R.E.; Raynie, D.E. *LC-GC*, **1997**, *15*, 1106-1117.

(117) Okahara, M.; Nakatsuji, Y. In *Topics in Current Chemistry, Vol. 128;* Royal Chemical Society: London, 1985; pp. 37-59.

(118) Zolotov, Y.A. Ed. *Macrocyclic Compounds in Analytical Chemistry*, Wiley: New York, 1997.

(119) Kral, V.; Gale, P.A.; Anzenbacher, P. Jr.; Jursikova, K.; Lynch, V.; Sessler, J.L. *Chem. Commun.* **1998**, 9-11. Also see *C & EN*, **1998**, February 16, pp.31-32.

(120) Lunte, C.E.; Scott, D.O.; Kissinger, P.T. *Anal. Chem.* **1991**, *63*, 773A-780A.

(121) *CSC 1995-96 Chromatography and Microdialysis Catalogue*, Chromatography Sciences Company (CSC), Quebec, Canada.

(122) *A Handbook for Microdialysis and in vivo Sampling*, Bioanalytical System (BAS) Inc., 1997.

(123) Davies, M.I.; Lunte, C.E. *Chem. Soc. Rev.* **1997**, *26*, 215-222.

(124) Newton, A.P.; Justice, J.B. Jr. *Anal. Chem.* **1994**, *66*, 1468-1472.

(125) Wages, S.A.; Church, W.H.; Justice, J.B. Jr. *Anal. Chem.* **1986**, *58*, 1649-1656.

(126) Buttler, T.; Gorton, L.; Jarskog, H.; Marko-Varga, G.; Hahn-Hagerdal, B.; Meinander, N.; Olsson, L. *Biotechnology and Bioengineering*, **1994**, *44*, 322-328.

(127) Liu, H.; Dasgupta, P.K. *Anal. Chem.* **1996**, *68*, 1817-1821.

(128) Based on Dr. Cantwell's personal communication with Dr. Dasgupta.

Part II

The Changes in Chain Conformation in the ODS Bonded Phase Caused by Sorbed Tetra-*n*-butylammonium Ion (TBA^+) and its Effect on the Sorption of *n*-Butanol

Chapter 5
Introduction

5.1 Reversed-Phase Liquid Chromatography

Reversed-phase liquid chromatography (RPLC) was introduced in 1950 by Howard and Martin[1] in an attempt to separate long chain (C_{12}-C_{18}) fatty acids because the normal mode chromatography, using a polar stationary phase and a non-polar mobile phase, was not applicable to longer chain fatty acids or other lipophilic compounds. To solve the problem, they treated Kieselguhr, a porous support, with dimethyldichlorosilane vapor and then coated this hydrophobic support with a non-polar liquid such as paraffin oil or octane as the liquid stationary phase. By using a polar mobile phase such as aqueous methanol or aqueous acetone, long chain (C_{12}-C_{18}) fatty acids were easily separated. Since both the polarity of the phases and the respective elution order of solutes were reversed from conventional (normal) mode chromatographic system; they named this new mode of chromatography as *reversed-phase partition chromatography*. However, due to its poor column efficiency, unstable stationary liquid, and incompatibility with gradient elution, reversed-phase partition chromatography, had never gained widespread acceptance.[2]

To address these problems, chemically bonded stationary phases, developed first for gas chromatography,[3-6] were introduced to liquid chromatography in the late 1960s.[7-11] Bonded phases were prepared by means of chemical reaction of the hydroxyl (or silanol) group on silica surface with a non-polar modifier such as n-hexadecyltrichlorosilane,[5] yielding a phase in which the non-polar alkyl group was covalently bonded to the solid support through a siloxane (Si-O-Si-R) bond. Due to its high stability and rapid mass transfer, *reversed-phase bonded phases liquid*

chromatography (RPBP-LC) quickly gained popularity and reversed-phase partition chromatography was phased out in the early 1970's. Since then, the application of bonded phase technology has had a tremendous impact in separation science. It has been estimated that 80-90% of modern HPLC separations[12] or 57% of all analytical chromatography[13] utilize bonded reversed-phase stationary phases. In the following sections, the synthesis of bonded phases and some important properties of bonded phases and silica support will be introduced.

5.2 Silica Support

Silica gel is probably the most important single substance involved in modern chromatography. Today more than 90% of column packings used in reversed- and normal-phase LC are based on silica.[14] According to Scott,[15] "*without silica gel there would be no HPLC, no TLC and no bonded phases and separation science would, indeed, be a technically restricted field of interest and of more limited use.*" A brief review of the chemical properties of silica gel is presented here. Detailed treatments of this subject have been done by Berthod,[14] Scott,[15] Unger,[16] and Iler.[17]

The silica used for LC column packings is essentially porous and amorphous with the general formula $SiO_2 \cdot xH_2O$. It does not produce any X-ray diffraction patterns. The lack of crystallinity or the amorphous nature of silica is not difficult to understand considering an average wall thickness of ca. 1-2 nm or 2-6 silicon atoms across for a silica material of 250 - 400 m^2/g.[18,19] Water is chemically bound in a non-stoichiometric amount, forming the Si-OH silanol groups most important for making LC packings. There are three kinds of silanol groups on amorphous silica surface: isolated, vicinal, and geminal silanols.[20-22]

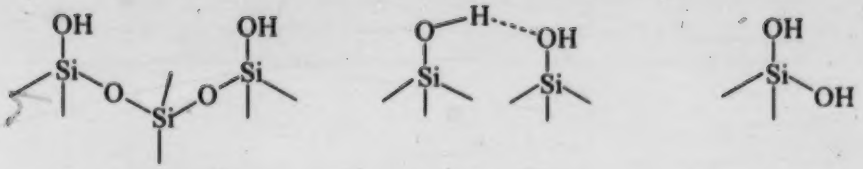

Isolated Silanols Vicinal Silanols Geminal Silanols

The actual existence and relative quantities of different silanol groups on the silica surface are strongly dependent on the thermal and chemical history of the material.

The surface silanol groups serve as attachment points for organic moieties to produce the bonded phases. Silanols are also considered as strong adsorption sites with which polar solvent and solute molecules can interact during the chromatographic separation. This is why it is important to know the total concentration of silanol groups and even the relative concentrations of different types of silanol groups on the silica surface. Although there is controversy over the reliability of the methods used to measure the silanol concentrations,[15] it is generally agreed that a fully hydroxylated surface contains about 8 $\mu mol/m^2$ of silanol groups (or 4.8 silanols per nm^2).[20,21,23,24] Infrared spectroscopy (IR)[21,25-27] can be used to distinguish isolated (sharp band at 3740 cm^{-1}) and hydrogen bonded (broad band around 3600 ($\pm$50) cm^{-1}) silanols, although IR does not provide separate identification of geminal and vicinal silanol groups.[27] Evidence of the existence of geminal silanols is provided by solid state ^{29}Si NMR,[22,27-29] However, NMR is not capable of differentiating vicinal silanols from isolated silanols.

Amorphous silica is soluble in water.[17] Its concentration at saturation is about 100 ppm at room temperature and neutral pH. Solubility increases drastically above pH 9 due to the formation of silicate ions in addition to monosilicic acid:

$$SiO_2 + 2H_2O \rightleftharpoons Si(OH)_4 \overset{OH^-}{\rightleftharpoons} [Si(OH)_5]^- \qquad (5.1)$$

The solubility increases linearly with temperature and exponentially with decreasing particle size.[16]

Although monosilicic acid is a very weak acid with a pKa 9.9,[30]

$$Si(OH)_4 \rightleftharpoons Si(OH)_3O^- + H^+ \qquad (5.2)$$

the measured pKa value for silanol groups on silica surface is 7.1 (±0.5),[31,32] which is much more acidic than the monosilicic acid. At pH 7, silica surface bears negative charges in solution, which is responsible for the cation-exchange properties of silica although its capacity is very low at this pH. In solutions of pH <2, silica should bear a positive charge due to the protonation of silanol groups.[16]

5.3 Synthesis of Bonded Phases

Bonded phases are most commonly prepared through the reaction of silica with *n*-alkylchlorosilanes. *n*-Octadecyl (C_{18}), *n*-octyl (C_8), and *n*-butyl (C_4) are the most popular primary substituents in the reactive silanes. Since silicon has a valence of four, silanes may have up to three reactive functional groups (X) per molecule in addition to the non-reactive *n*-alkyl substituent. They are called monofunctional, difunctional, and trifunctional silanes:

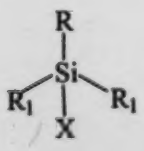

monofunctional

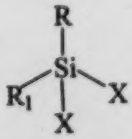

difunctional

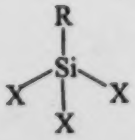

trifunctional

where R is the *n*-alkyl substituent, R_1 usually a methyl group, and X chloro or other functional groups. The reaction mechanism between the silica surface and the silanes was proposed as a nucleophilic substitution of X by the surface ≡Si-O(-H) through a reactive intermediate with a pentavalent silicon atom.[33]

The reaction is commonly carried out in a reaction flask, where the pretreated silica and a predetermined amount of the silane are slurried in a suitable solvent such as toluene along with a base such as pyridine as a catalyst and acid scavenger. The mixture is refluxed with agitation for at least several hours under anhydrous or hydrous conditions. The silanized silica is then filtered, washed with suitable solvents, and finally dried before use. Depending on the type of silanes and reaction conditions employed in the surface modification, both monomeric and polymeric bonded phases (see Figures 5.1 and 5.2) can be prepared.

Monomeric phases result from the reaction between monofunctional silanes and the surface silanol groups because each silane molecule is capable of forming only one siloxane bond with the surface silanol. The reaction is usually carried out under anhydrous conditions. In the presence of water, the reactivity of the monochlorosilane and thus the obtainable surface coverage (or density) of the C_{18} or C_8 ligand will be reduced because of the hydrolysis of monochlorosilane.[33] Monomeric bonded phases can also be prepared by the reaction of silica with di- or trifunctional silanes under anhydrous conditions. In this case, one or two siloxane bonds with the silica surface may be formed per silane molecule. This type of bonded phase is very similar to those prepared from monofunctional silanes except that the former may possess more hydroxyl groups due to the hydrolysis of unreacted leaving groups such as chloro.

Polymeric phases are synthesized using di- or trifunctional silanes in the presence of water.[34] Polymerization occurs at the surface when water is added directly to the silica

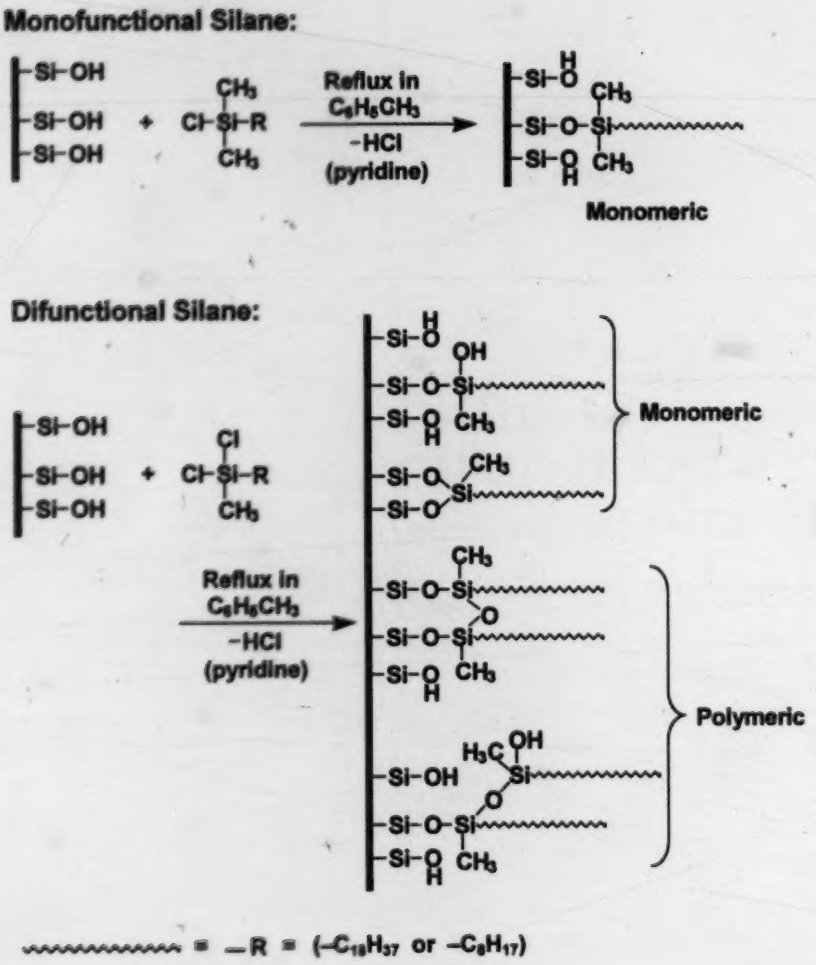

Figure 5.1 Synthesis of octadecylsilyl (ODS) reversed phase bonded phase from mono- and di-functional silanes.

Trifunctional Silane:

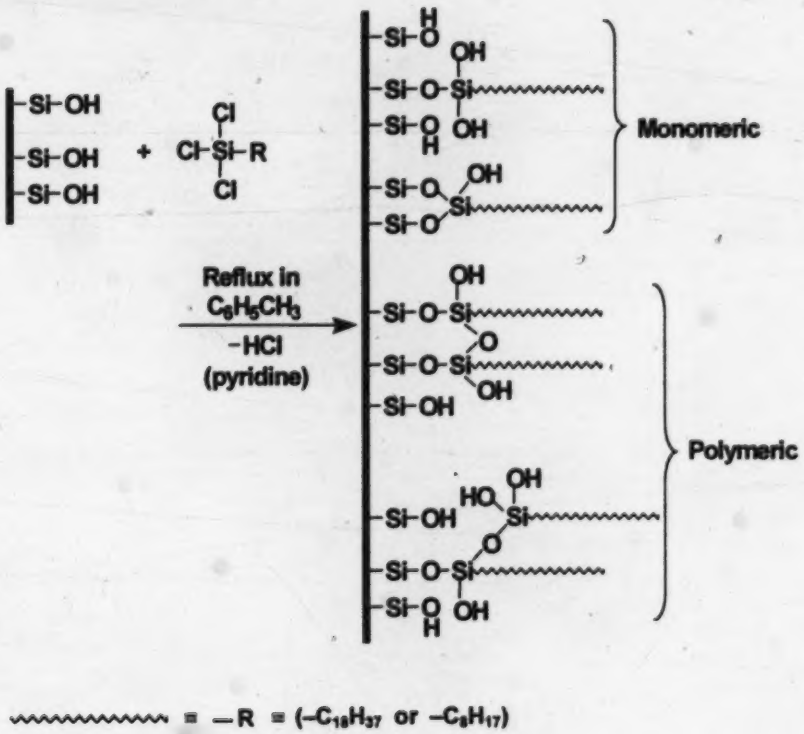

~~~~ = —R = ($-C_{18}H_{37}$ or $-C_8H_{17}$)

Figure 5.2 Synthesis of octadecylsilyl (ODS) reversed phase bonded phase from trifunctional silane.
~~~~

and equilibrated prior to reaction. After a di- or trifunctional silane has bonded to the silica surface, the unreacted leaving groups can be hydrolyzed by water to yield silanols on the silane ligand (called *silane silanols* to differentiate from *silica silanols* – the silanols on the substrate surface). These hydrolyzed silanes will react with leaving groups such as chloro from other silanes, resulting in a polymeric network. This polymerization process may also occur in solution before bonding to the silica surface if water is introduced to a slurry of the silica containing the di- or trichlorosilane. Both procedures have been used by commercial column manufacturers.[34]

The bonded phases obtained using monochlorosilanes in the absence of organic bases have a typical surface coverage between 2.3 and 2.9 $\mu mol/m^2$ for C_{18} and C_8 phases.[35] The surface coverage of monomeric phases can be controlled by varying silane concentration,[36] reaction time and temperature. A surface coverage of as high as 3.5 $\mu mol/m^2$ can be achieved by adding a base such as pyridine to monochlorosilanes under optimal conditions.[37,38] The organic base works as an acid scavenger and also forms a more reactive intermediate (≡Si-N=) with chlorosilanes. The maximum attained surface coverage of 4.1±0.2 $\mu mol/m^2$ was prepared by the use of the most reactive silanes — alkyldimethyl(dimethylamino)silanes.[39] For polymeric phases, surface coverage is controlled by varying the amount of water added to the reaction slurry. In general, the maximum coverage ranges from 4.5 to ca.6.5 $\mu mol/m^2$.[34,40]

The silanol density on a fully hydrated silica surface, as mentioned in the previous section, is ca. 8 $\mu mol/m^2$. Therefore, at least half of the surface silanols are left unreacted for monomeric phases due to steric constraints. For polymeric phases, the free silanol concentration on the surface could be even higher after the hydrolysis of unreacted leaving groups on silane. The existence of these residual silanols may have an undesired effect on column efficiency because some of them may be accessible to solutes for

interaction during chromatographic process, leading to tailing. For this reason, a second silanization step using small silanes such as trimethylchlorosilane (TMCS) and hexamethyldisilazane (HMDS) [$(CH_3)_3SiNHSi(CH_3)_3$] is often carried out to block or "end cap" the most accessible, and thus most active residual silanol groups. Trimethylchlorosilane can react with surface silanols which are not accessible to longer chain silanes; however, it can by no means react with all of the residual silanols. The maximum surface coverage obtained using the most reactive trimethylsilane — trimethyl(dimethylamino)silane is 4.77 μmol/m^2.[39] For bonded phases of close to maximum surface coverage, the changes in surface carbon content made by end-capping are usually negligible.[37,40]

5.4 Some Properties of Bonded Phases

5.4.1 Alkyl Chain Density of the Bonded Phases

The amount of alkylsilane bonded to the silica surface is usually determined by elemental analysis and the result is often referred to as carbon content (P_c) or carbon loading, i.e. the weight percent of carbon (%C) of the *bonded* phase. The carbon content ranges from a few percent up to 20% and higher depending on the length of the ligand, the ligand density, and the specific surface area of the silica.[24,34,40] Carbon content alone, however, is an uninterpretable value because two bonded phases with identical carbon content could have very different surface ligand densities depending on their specific surface areas. The only useful parameter is the alkyl chain (or ligand) density on the surface, expressed in units of μmol of bonded silanes per m^2 of *unbonded* silica or in number of bonded silanes/nm^2.[41]

For monomeric phases, alkyl chain density on silica surface (N) can be calculated from the carbon percentage (P_c) of the *bonded* phase and the specific surface area (S, m^2/g) of the *unbonded* silica commonly measured by the BET method:[42]

$$N\ (\mu mol/m^2) = \frac{10^6\ P_c}{1200\ n_c - P_c(M-1)}\ \frac{1}{S} \qquad (5.3)$$

where n_c is the number of carbons in the bonded silane ligand, M is the molecular weight of the bonded silane ligand, e.g. MW = 311 for the dimethyloctadecylsilyl [$CH_3(CH_2)_{17}Si(CH_3)_2$] group. The conversion between $\mu mol/m^2$ and silanes/nm^2 is simple: N ($\mu mol/m^2$) = 0.6 x N (silanes/nm^2).

Because the degree of polymerization is always unknown for polymeric phases, an assumption must be made about the molecular weight of the bonded species in order to calculate the surface coverage using the above equation. For phases prepared from trichlorosilanes, $CH_3(CH_2)_{17}Si(OH)_2O$- (MW 331) has been used as the representative bonded units.[40] The oxygen atoms in the molecule are introduced as a result of silane hydrolysis during phase synthesis and are considered as part of the bonded phase rather than part of the silica. However, this may overestimate the average molecular weight of the bonded ligands because the average degree of polymerization is always low.

5.4.2 Polymeric Phase vs. Monomeric Phase

Because the bonding chemistry is more complicated when di- and trifunctional silanes are used, the exact structures of such bonded phases are still not clear. However, as mentioned earlier, the maximum attainable surface coverages are about 4 and 6.5 $\mu mol/m^2$ for monomeric and polymeric bonded phases, respectively. Therefore, in the case of uniform distribution of alkyl chains, the average degree of linear polymerization

is low (<2) even for very heavily loaded phases. In the case of non-uniform distribution of alkyl chains, the degree of polymerization could be higher in some regions than others. It is still controversial regarding uniform or non-uniform distribution of the alkyl chains on silica surface.[43,44] Experimental results based on low-angle X-ray reflectivity[45] seem to support the view of uniformly distributed bonded phase.

Too often the column manufacturers do not reveal the bonding chemistry used, and the user is left to guess the nature of the stationary phase. Sander and Wise[40,46] have developed a simple empirical method to probe the relative monomeric or polymeric "character" of a phase, based on the elution order of a three-component polyaromatic hydrocarbon (PAH) mixture: benzo[a]pyrene (BaP; planar shape), phenanthro[3,4-c]phenanthrene (PhPh; nonplanar shape), and tetrabenzonaphthalene (TBN; nonplanar shape). The elution order of these compounds was found to be strongly dependent on the type of phase and the surface coverage. Phases prepared using monomeric surface modification chemistry give the elution order BaP ≤ PhPh < TBN; while phases prepared using polymeric surface modification chemistry give the order PhPh < TBN ≤ BaP. The phase selectivity factor, $\alpha_{TBN/BaP}$, has been used as a quantitative measure of phase shape selectivity

$$\alpha_{TBN/BaP} = \frac{k'_{TBN}}{k'_{BaP}} \qquad (5.4)$$

where k'_{TBN} and k'_{BaP} are the capacity factors for TBN and BaP, respectively. The following classification has been proposed:[46] (a) $\alpha_{TBN/BaP} \leq 1$, "polymeric-like", (b) $1 < \alpha_{TBN/BaP} < 1.7$, "intermediate", and (c) $\alpha_{TBN/BaP} \geq 1.7$, "monomeric-like".

The different shape recognition performance found between polymeric-like and monomeric-like phases is believed to be related to their difference in phase structure.

Although phase structure at the molecular level is difficult to conceptualize, one possibility is that the additional phase loading results from branched structures extending away from the silica surface (vertical polymerization). Another possibility is that phase structure is like a monomeric phase, but with substantially increased phase density (horizontal polymerization). Sander and Wise[47] seem to favor the latter model. They believe that at the molecular level, the two phase types do not appear to be fundamentally different, but instead the differences appear to be a matter of degree and the result of alkyl chain packing density. The improved selectivity for certain compounds offered by polymeric phases is simply a function of the bonding density. This view of polymeric phases seems to be consistent with Wirth and co-workers' experimental results based on their NMR studies of polymeric phases, where the ratio of bonded C_{18} groups to reacted silica silanol is close to 1:1.[48]

For polymeric phases with relatively low bonding densities, the difference between polymeric and monomeric phases seems to be insignificant. Based on their comparative chromatographic studies of bonded phases prepared using mono-, di-, and trifunctional silanes, Verzele and Mussche[49] concluded that a clear distinction between monomeric and polymeric phases is not warranted and that as long as the surface coverage does not exceed 3–3.5 $\mu mol/m^2$ no polymeric bonding is present, even when the silane regent was trifunctional. Therefore, they believed that many commercial phases obtained with trifunctional silanes and therefore with supposedly polymeric character are in fact as monomeric as phases obtained from monofunctional silanes.

The silica gel pore size could also affect the obtained phase structure. In an examination of polymeric C_{18} phases prepared on many dissimilar silicas of different pore sizes, narrow pore substrates consistently yielded phases with monomeric-like selectivity.[50] Typically, only those silica substrates with pore diameters of 150 Å or larger

will produce C_{18} phases with enhanced "polymeric-like" selectivity for PAH isomers. This has been attributed to a size exclusion effect.[47,50] Because smaller silane monomer can diffuse into narrow pores more easily than larger silane polymer molecules, more monomer molecules reach the surface of narrow pore substrates and thus the pore interior is largely monomeric in nature.

5.4.3 Bonded Phase Thickness and Surface Area

The direct determination of bonded phase morphology represents a difficult analytical problem because few analytical techniques can be used for this purpose. The thicknesses of bonded monomeric and polymeric C_{18} phases with pure methanol as solvent have been determined using small angle neutron scattering technique.[51] The measured average thickness for the monomeric C_{18} phase is 17 Å, which is considerably smaller than 26 Å, the length calculated for the most extended (all-*trans*) conformation of the C_{18} chain.[52] Therefore, in a methanol environment most of the alkyl chains are bent or disordered.[51] The average thickness of the polymeric C_{18} phase is 21 Å, only about 25% thicker than the corresponding monomeric phase. Such small increase in chain thickness may be solely attributed to the chain density effect, which is consistent with Sander and Wise's view on polymeric phase structure.[47] Because the polymeric C_{18} phase used has higher phase coverage (5–6.5 $\mu mol/m^2$) than the monomeric C_{18} phase (3–4 $\mu mol/m^2$),[40,51] it is expected that the C18 chains in the denser polymeric phase should be more extended due to van der Waals repulsion. For close-packed C_{18} chains in a horizontally polymerized monolayer, chain thicknesses of 26 Å and 23.6 Å have been measured by Ellipsometry[52] and low-angle X-ray reflectivity method,[53] respectively.

As a result of surface modification, the mean pore diameter is expected to decrease by twice the thickness of the bonded layer. Correspondingly, the specific surface

area of the bonded phases also decreases. The reduction in surface area is dependent on the original pore diameter and the thickness of the bonded layer. Surface areas of the unmodified and the modified silicas are usually measured by the BET method. For silica gels commonly used for HPLC with pore diameters between 60 Å to 150 Å, the reported reduction in surface area ranges from 80% to 30% for C_{18} bonded phases.[54-56]

5.4.4 Alkyl Chain Conformation

Although the details of the molecular conformations of the bonded alkyl chains are still not clear due to the complexity of the bonded-phase system, an understanding of this near-surface region has been gradually developed through the work of many researchers. Both chromatographic[57-59] and spectroscopic methods such as NMR,[60-62] FTIR[63] and fluorescence[64-66] have been used for this purpose. Computer simulation based on molecular dynamics (MD) has also provided important information.[59,67,68] The exact nature of the alkyl chain structure is dependent upon alkyl chain length, chain density, solvent (organic vs. highly aqueous), and thermal conditions. The following is a brief summary of some important features observed using the above techniques:

(1) Alkyl chains have sufficient room to tilt and rotate and possess kinks and bends (see Figure 5.3) because the achievable bonding densities are much lower than that in close-packed alkyl chains (20 $Å^2$ per chain). Kinks and bends decrease with decreasing temperature.

(2) Bound alkyl chains also possess a degree of mobility that increases towards the end of the chain. At low surface chain densities (< 3 $\mu mol/m^2$), there is a tremendous amount of conformational disorder of the bonded chains (see Figure 5.3). However, the first four carbons closest to the silica surface are very rigid and motionally restricted. Increase in chain density causes increased chain ordering and reduced chain mobility.

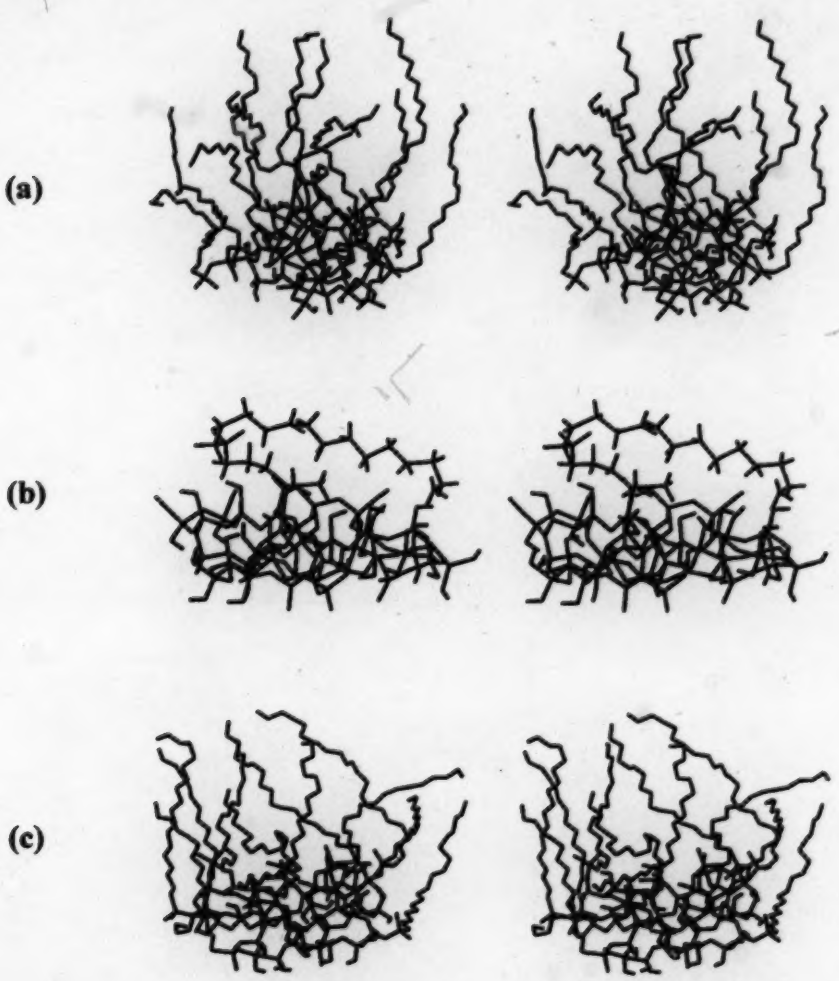

Figure 5.3 Instantaneous ODS chain conformations shown in stereo view obtained by molecular dynamics simulations of an unit cell (32 Å per side) with an average chain density of 2.1 μmol/m^2 at 300 K. (a) Multiple ODS chains with no solvent, (b) a single ODS chain with no solvent, and (c) multiple ODS chains with 20% water-80% methanol at 50 ps of molecular dynamics. Hydrogen atoms in (a) and (c) and solvents in (c) have been removed for easy viewing. These conformations can be viewed in three dimensions using either viewers or naked eyes. (From reference 68.)

(3) In the dry state with low chain densities, the alkyl chains tend to aggregate by hydrophobic interaction and to lie along the silica surface (see Figure 5.3), resulting in a stationary phase significantly thinner than those fully extended. The thickness of the bonded stationary phase increases with increasing surface chain density.

(4) In contact with mobile phases, the thickness of the bonded phase changes as the composition of the solvent is altered. In the presence of pure water, the alkyl chains collapse and lie nearly in the plane of the silica substrate to minimize the area of the alkyl chain/water interface.

(5) In the presence of organic modifier such as alcohol, the alkyl chains assume a more extended configuration and the thickness of the stationary phase increases due to the intercalation of the modifier in alkyl chains (see Figure 5.3). Although it occurs for methanol, this effect is seen most strongly for long-chain alcohols.

(6) In the case of C_{18} bonded phases, non-polar solute molecules can be completely "immersed" in the stationary phase and protected by the C_{18} chains from exposure to bulk solvent.

5.5 Retention Process

Although reversed-phase liquid chromatography enjoys high popularity, our understanding of the retention process is still limited, especially in terms of the microscopic properties of the bonded surface and the complex interplay between solute, solvent and stationary phase. The special issue of the *Journal of Chromatography* published in late 1993 summarized pretty much the current understanding of the retention process and the ongoing debate in RPLC.[69]

There are two fundamental theories which account for the experimental results obtained in RPLC: the solvophobic theory[70,71] adapted to RPLC by Horváth and

coworkers[12,72,73] and the partition theory developed by Dill and co-workers[74-76] following the work of Martire and Boehm[77] and derived from the statistical theory of crystalline lattices.[78] The main difference between these two approaches originates in the fact that the stationary phase plays a passive role in the first case whereas it is active in the second.

According to the solvophobic theory,[12,72,73] the retention of a solute in RPLC can be viewed as a reversible association of the solute with the alkyl chain to form a solute-chain complex. The theory does not presume that retention occurs by a partition mechanism. The solute can bind to alkyl chains in various plausible ways, either penetrating into the interchain space and binding laterally to the alkyl chains or binding at their tips or both depending on the size of the solute molecules and the mobile phase conditions employed. Solute retention is governed by the average value of contact surface area between the solute and the alkyl chains at the chromatographic surface.[12] The main reason for retention and selectivity in RPLC is the solvophobic effect of the solute in the mobile phase, i.e. the mobile phase "drives" the solute toward the stationary phase, rather than any inherently strong attraction between the solute and the stationary phase. This dominant role of the mobile phase in determining the retention behavior in RPLC seems to be confirmed by Horváth and coworkers in a recently published paper[73] for selected groups of nonpolar and weakly polar aliphatic solutes. However, contradicting results have also been found by others.[79] Furthermore, in this solvophobic model, the stationary phase ligand plays no role in the separation process other than providing a sorptive site for retention. Therefore, the solvophobic theory fails to explain experimental observations where the influence of the stationary phase on retention and selection are significant.[76,77,80]

Currently, the most widely accepted retention model is the partition model.[75,76,80] According to the model, retention is a process of transfer of solute from the mobile-phase

environment into the stationary-phase environment and hence depends on the nature of both the mobile and stationary phases. In general, the solute partitions into, rather than adsorbing onto, the bonded phase; that is, it becomes nearly fully embedded within the bonded alkyl chains. Therefore, the bulk-phase partition model, based on the premise that the stationary phase is an amorphous bulk fluid medium and that retention resembles ordinary bulk-phase partitioning, should be a good model for retention. Indeed, the bulk-phase partitioning model can predict several important features of retention process in RPLC.[76] However, the bonded phase is not bulk phase; therefore, the bulk-phase partitioning model has to be refined to include the contribution from alkyl chain organization.

By analogy with other interfacial phases of chain molecules such as surfactant aggregates in monolayers and bilayers, Dill and co-workers[74,75] believe that the bonded phase should have similar molecular organization which exhibits a variation of properties with depth from the surface. This variation of properties with depth contrasts with bulk phases of matter, whose properties, by definition, are invariant with spatial position. Chains in the bulk state have the freedom to explore all possible conformations. Interfacially bonded alkyl chains, however, are prevented from access to all possible conformations by two constraints, the boundary constraint imposed by the silica surface and the steric constraint resulted from lateral interactions among neighboring chains. Both constraints cause bonded alkyl chains to be more ordered than bulk chains. Here, ordering refers to the partial alignment of the chains normal to the silica surface. The model gives two principal predictions for the conformations of the bonded alkyl chains in the absence of penetrant solute or solvent molecules. First, for surface densities that are above approximately one-third of the maximum value, i.e. about 2.7 $\mu mol/m^2$, at which steric constraint among neighboring chains become important, the model predicts a

"disorder gradient", i.e. the alkyl chain segments nearest the silica surface are the most highly ordered, with rapidly increasing disorder toward the chain ends. Second, increasing the surface density of the chains should lead to increased chain ordering.

In conformation with the second law of thermodynamics, the chains should adopt as much disorder as is consistent with the imposed constraints. The partition of solute into a partially ordered bonded phase of fixed surface density leads to further extension and ordering of the alkyl chains. Hence solute partition is an entropically unfavorable process. The principal prediction of the model is that the retention of solute is dependent on the surface density of bonded alkyl chains. At low densities, partitioning of hydrophobic solute should increase linearly with surface coverage of the bonded chains as the surface becomes more fully covered by hydrocarbons and thus become less polar. The partition coefficient should reach a maximum at the point at which interactions among neighboring chains become important. Beyond this critical density, predicted to be about 2.7 $\mu mol/m^2$, further increase in surface density will lead to entropic expulsion of solute by the bonded chains. This theoretical prediction has been verified experimentally by Sentell and Dorsey[81] for the retention of naphthalene in a series of monomeric C_{18} phases with surface coverages of 1.6 – 4.1 $\mu mol/m^2$. Sander and Wise[34] also observed similar retention behavior for various solutes in a series of C_{18} phases, including polymeric phases, with surface coverages of 2.03 – 7.44 $\mu mol/m^2$.

The partition model also predicts that the anisotropy of the bonded alkyl chains at high densities should lead to shape selectivity among solute molecules. Molecules that can most effectively align with the bonded chains are those that are most effectively retained. It cost more free energy to insert each solute substructure that lies parallel to the silica surface than each substructure that aligns with the chains normal to the surface; hence the shape selectivity. This prediction has also been confirmed experimentally by

Sentell and Dorsey[82] who observed increasing selectivity with surface density in a homologous series of phenyl compounds and also for six four-ring PHAs over the bonding density range 1.74 – 4.07 μmol/m^2. Wise and Sander[83] have also demonstrated this effect using four polymeric phases with surface coverages ranging from 2.7 to 5.1 μmol/m^2.

5.6 Scope of This Study

The purpose of this study is to gain more knowledge about how molecules interact with the ODS (C_{18}) bonded phase and how this will affect the retention of other molecules. More specifically, the effect of the sorption of a large hydrophobic organic ion, tetra-*n*-butylammonium ion (TBA^+), on the C_{18} chain conformation and its effect on the sorption of butanol are studied by measuring the amounts of TBA^+ and butanol simultaneously sorbed in the ODS stationary phase using column equilibration technique.

In a previous study on indirect UV detection in LC,[84] Glavina and Cantwell found that the origin of indirect detection of butanol with naphthalene-2-sulfonate (NS^-) is that they compete with one another for space in the ODS stationary phase.[85] However, the situation is more complicated for the indirect detection of TBA^+ with (4-nitrobenzyl)-trimethylammonium ($NBTA^+$). In this case, the sorption of TBA^+ was found to influence the amount of $NBTA^+$ sorbed both by raising interfacial electrical potential and by altering the amount of space available for $NBTA^+$.[86,87] For the second effect, the way in which the sorbed TBA^+ alters the amount of space available for $NBTA^+$ was found to be dependent on ionic strength. At high ionic strength, sorbed TBA^+ decreases the amount of space available by competing with $NBTA^+$. At low ionic strength, however, in addition to space competition, sorbed TBA^+ seems to be able to increase the amount of space

available for $NBTA^+$. This unusual phenomenon, i.e. space creation, was explained in terms of the alteration of the alkyl chain conformation upon TBA^+ sorption.

The goal of this study is to confirm and to better understand this phenomenon. Because the observation in the previous study was complicated by the dominant electrostatic repulsion between the two cations, a neutral molecule, *n*-butanol, instead of $NBTA^+$ is used in this study to eliminate this strong electrostatic effect. *n*-Butanol is chosen because it had previously been studied together with NS^-, and competition for space was found to be the only mechanism.

Chapter 6
Experimental

In this chapter, the details of the experiments that were done in this study are presented. They include the column equilibration technique for measuring the sorption of TBA^+ and butanol in the ODS stationary phase, solvent extraction/flow injection analysis (SE/FIA) technique for quantifying TBA^+, gas chromatographic method for quantifying butanol, and shake-flask method for measuring distribution coefficient of butanol in *n*-hexadecane and aqueous solution.

6.1 Chemicals and Stock Solutions

Whatman Partisil-10 ODS-3 (Batch no. 101409, Whatman, Clifton, NJ) was used as the stationary phase in all experiments. It is a trifunctional octadecylsilane modified reversed-phase stationary phase with a 10 μm particle diameter and 350 m^2/g specific surface area for the unbonded silica. It has a 10.5% carbon loading[88] and the specific surface area of the bonded phase was measured to be 266 m^2/g.[84,86] Partisil ODS-3 is described by the manufacturer as being "highly end-capped" (95% end-capped).

Tetra-*n*-butylammonium chloride (TBA^+Cl^-) hydrate (98%, Aldrich, Milwaukee, WI) was used without further purification. Stock solutions (0.05 to 0.60 mol/L) were prepared by dissolving in Nanopure water and then filtering through a 0.45-μm Nylon filter to remove particulate. The prepared stock solutions were standardized by titration with 0.1 mol/L silver nitrate. Standard solutions of TBA^+ used for SE/FIA were prepared in 1:1 (v/v) methanol:water.

n-Butanol (99.8%, Aldrich, Milwaukee, WI) was used as received. Stock solutions were prepared by dissolving in Nanopure water. Standard solutions of butanol used for GC analysis were prepared in 1:1 (v/v) methanol:water. 2-Pentanol (98%,

Lancaster, Windham, NH) was used as received. Stock solutions were prepared in 1:1 (v/v) methanol:water.

Picric acid (Matheson, Coleman and Bell) was reagent grade and used as received. Solutions were standardized by titration with sodium hydroxide. Chloroform (99.8%, Fisher Scientific, Nepean, ON) and *n*-hexadecane (99%, Aldrich, Milwaukee, WI) were used as received.

Sodium chloride (BDH, Toronto, ON), sodium hydroxide (BDH, Toronto, ON) and glacial acetic acid (BDH, Toronto, ON) were all analytical grade and used as received. Acetate buffer stock solution (0.10 mol/L) was prepared by adding 0.1 mol/L NaOH to 0.10 mol/L acetic acid solution until pH = 5.0.

Methanol (>99.8%, Fisher Scientific, Nepean, ON) and pure ethanol (Commercial Alcohol Ltd.) were distilled before use. Water was purified by the Nanopure system (Barnstead, Dubuque, IA).

6.2 Column Equilibration Technique

In the column equilibration technique, a mobile phase containing a fixed concentration of solute is passed through the column until the effluent contains the same concentration of the solute as the influent. At this point, the stationary phase is at equilibrium with the mobile phase, whose solute concentration is known. The solute sorbed in the stationary phase is then eluted with a different solvent and the amount of sorbed solute is quantitatively measured. In this way, the concentrations of the solute in both the stationary phase and the mobile phase can be determined.[89] In these experiments, the simultaneous sorption of TBA^+ and butanol and the sorption of TBA^+ or butanol alone were studied by measuring the amount sorbed in a short Partisil ODS-3 column at equilibrium. The sorption isotherm for TBA^+ was also measured in the same way.

6.2.1 Column Equilibration Apparatus and Procedure

The column equilibration apparatus is shown in Figure 6.1. It consists of a Waters 501 HPLC pump for loading the sample solution (the mobile phase), a Waters 6000 HPLC pump for eluting the sorbed solute, two in-line filters (2-μm pore), two stainless steel tubing coils (1.0 m long), a Rheodyne 7010 six-port rotary valve for switching between loading and elution, and a short column (2.0 cm long × 0.40 cm i.d.), which was dry-packed with 0.157 g of Partisil-10 ODS-3 packing material. All the connections were made with stainless steel tubing of 1/16" o.d. and either 0.5 mm or 0.25 mm i.d. The column, the valve, and the coils were placed in a water bath whose temperature was maintained at 25.0 ± 0.1 °C by a circulating water bath (Type NBE, Haake, Berlin).

The general procedure for the column equilibration experiment is as follows. With the valve in the "load" position as shown in Figure 6.1 (indicated by the solid lines), the mobile phase containing TBA^+ or butanol or both is pumped through the column at a flow rate of 3 ml/min to the waste until sorption equilibrium is achieved. This is the loading step. The valve is then switched to the "elute" position (indicated by the hollow lines) and the sorbed solutes are eluted by pumping 1:1 (v/v) $MeOH/H_2O$ through the column at a flow rate of 1 mL/min. The eluate is collected in a 10-mL volumetric flask for about 8 min to ensure complete elution and then diluted to volume with 1:1 (v/v) $MeOH/H_2O$. This is the elution step.

For the measurement of TBA^+ isotherms, two series of sample solutions were prepared with water as solvent at total ionic strengths 0.50 M and 0.050 M, respectively. Ionic strengths were adjusted by adding NaCl. The TBA^+ concentration in each series was varied over a wide range, from 1.0×10^{-4} mol/L to 0.24 mol/L and from 5.0×10^{-5} M to 0.050 M for ionic strengths of 0.50 M and 0.050 M, respectively. However, the total concentration of TBA^+Cl^- and NaCl was kept constant, either 0.50 mol/L or 0.050 mol/L.

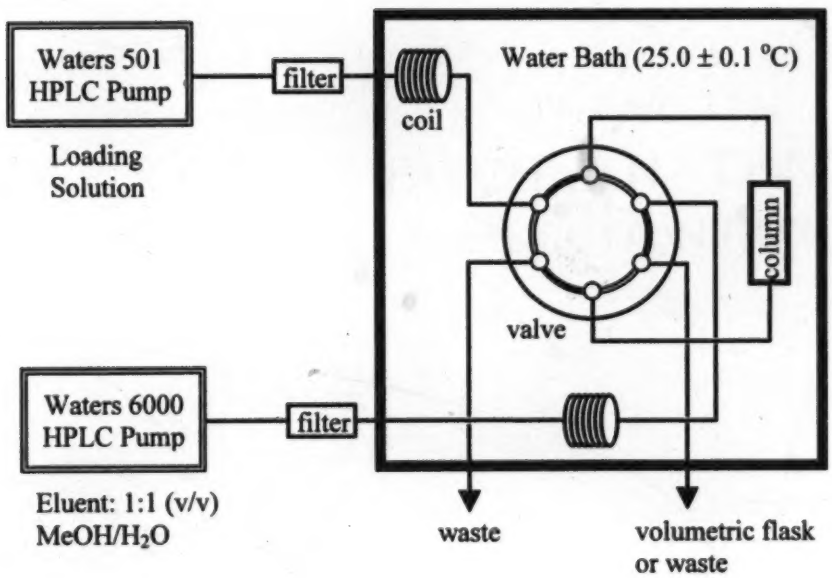

Figure 6.1 Column equilibration apparatus.

All these solutions had a pH of 5.0 controlled by 1×10^{-4} mol/L acetate buffer.

To study the effect of TBA^+ on butanol sorption, the butanol concentration in the mobile phase was kept constant at 1.0×10^{-3} mol/L and the TBA^+ concentrations were varied from 0 to 0.50 mol/L and from 0 to 0.050 mol/L in two series of solutions with total ionic strengths of 0.50 mol/L and 0.050 mol/L, respectively. To study the effect of butanol on TBA^+ sorption, the TBA^+ concentration in the mobile phase was kept constant at 1.0×10^{-4} mol/L and the butanol concentrations were varied from 0 to 0.030 mol/L in two series of solutions with total ionic strengths of 0.50 mol/L and 0.050 mol/L, respectively. Ionic strengths were adjusted by adding NaCl and the total concentration of TBA^+Cl^- and NaCl was kept constant, either at 0.50 or at 0.050 mol/L, and all these solutions had a pH of 5.0 controlled by 1×10^{-4} mol/L acetate buffer.

After the elution step, the total amount of each solute eluted from the column was determined by measuring its concentration in the volumetric flask. For TBA^+, the concentration was measured using SE/FIA technique as described previously,[93,98] in which TBA^+ was extracted into the organic phase (chloroform) as a TBA^+-picrate ion-pair. For butanol, the concentration was determined by gas chromatography on a 3.0 m × 2.0 mm i.d. × 1/8" o.d. stainless steel column packed with 5% w/w Carbowax 20 M (Chromatographic Specialties Ltd.) on Chromosorb WAW-DMCS with a mesh size of 100/120 (Manville). A Perkin-Elmer 8500 gas chromatograph with a flame ionization detector was used. The chromatographic conditions employed were as follows: helium flow rate ≈ 50 ml/min (30 psi), hydrogen pressure = 16 psi, air pressure = 22 psi, injector temperature = 230 °C, detector temperature = 200 °C, and column temperature = 70 °C (2.5 min) → 87 °C, 12 °C/min, → 125 °C, injection volume = 0.6 μL solution + 1 μL air. Because the eluate collected in the volumetric flask contained NaCl, which, as well as the

thermally decomposed product of TBA^+Cl^-, could build up in the injector, the injector glass liner was cleaned daily.

The amount of TBA^+ or of butanol sorbed, n_i (mol), by the ODS stationary phase at equilibrium was calculated by the following equation

$$n_i = n_{T,i} - C_{m,i} V_m \qquad (6.1)$$

where $n_{T,i}$ is the total number of moles eluted including that in the holdup volume V_m. $C_{m,i}$ (mol/L) is the concentration of TBA^+ or butanol in the mobile phase, V_m (L) includes the void volume of the packed bed and frits and the volume of the connecting tubing.

Before column equilibration experiments were performed, the volume of the sample solution that was required to pump through the column to establish sorption equilibrium had to be determined. This was done by measuring the loading curve for each of the sample solutions. The loading curve is a plot of the amount of solute sorbed in the stationary phase vs. the volume of the sample solution pumped through the column. The amount of solute sorbed in the stationary phase usually increases with the sample volume to a limiting plateau, at which point equilibrium (or complete breakthrough) is achieved. To ensure column equilibration condition, a volume larger than the complete breakthrough volume was used for each of the sample solutions. Column equilibrium experiments were performed in triplicate for each solution.

6.2.2 Holdup Volume Measurement

To measure the holdup volume, water was used as an unretained compound and pure ethanol as eluent. With the valve in the "load" position (Figure 6.1), pure water was pumped through the column at a flow rate of 1.0 mL/min for 30 min. The valve was then switched to the "elute" position and pure ethanol was pumped through the column at a

flow rate of 1.0 mL/min into a 10-mL volumetric flask which contained 0.50 mL of pure methanol internal standard and 1.0 mL of ethanol. The eluate was collected up to the 10-mL mark.

The amount of water eluted in the 10-mL flask was determined by gas chromatography on a 3.0 m × 2.2 mm i.d. × 1/8" o.d. stainless steel column packed with 50/80 mesh Porapack QS (Waters). The Perkin-Elmer 8500 gas chromatograph with a thermal conductivity detector was used and the chromatographic conditions used were as follows: helium flow rate ≈ 35 mL/min (30 psig.), detector and injector temperatures = 250 °C, column temperature = 160 °C (1.9 min) → 200 °C, 30 °C/min, 200 °C (0.5 min), injection volume = 1 μL solution + 1 μL air. Standard solutions were prepared by diluting known volumes of water (0 mL, 0.150 mL, 0.250 mL and 0.300 mL) and methanol internal standard (0.500 mL) with ethanol in 10-mL volumetric flasks. The holdup volume determined, with 95% confidence limit, was 0.218 ± 0.003 mL.

6.3 Solvent Extraction/Flow Injection Analysis for Determination of Eluted TBA^+

Solvent extraction/flow injection analysis was developed by Karlberg and Thelander[90] and by Bergamin et al.[91] to automate the conventional liquid-liquid solvent extraction. In a typical SE/FIA system, aqueous sample solution is introduced into a continuous aqueous stream by using an injection valve. The aqueous stream is merged and mixed with a second aqueous stream containing a chemical reagent, which will react with the sample to form an extractable component. The resultant aqueous stream is then segmented with an organic immiscible solvent stream by using a "tee" or other shaped segmenter to produce alternating small droplets of organic and aqueous phases. The droplets move into a long extraction coil, where the extraction process occurs. During extraction, the extractable sample component is transported from aqueous droplet into

organic droplet through their interface. The degree of extraction is a function of the residence time of the extractable component in the extraction coil, which is affected by the coil length and the flow rate. Extraction efficiency in the extraction coil is usually high and extraction is often complete in several seconds.[92] The segments of the aqueous and organic phases then enter a phase separator where a portion of the organic phase is separated and directed to a flow-through UV detector. Porous membrane phase separators are the most popular type of phase separator. They are based on selective permeability to the phase which wets the membrane material. For example, porous Teflon is wetted by organic solvents while porous paper is wetted by aqueous phases.

Figure 6.2 shows the schematic diagram of the SE/FIA system[84,93] used in this study. The reagent solution, organic solvents and water were contained in 2-L reagent bottles which were placed inside sealed aluminum containers (home-made by machine shop). Constant pressure (10 psi) from a nitrogen cylinder (Linde) was applied to the aluminum container to produce solvent flow which can be started or stopped by using 2-way slider valves V1 (Laboratory Data Control, Riviera Beach, FL). Valve V2 (Laboratory Data Control) was a 3-way slider valve which allowed either methanol or chloroform to be selected. Methanol was used to flush and fill the system after SE/FIA experiments. Sample solution was introduced into a water stream through a sample injection valve equipped with a 50-μL sample loop (Cheminert R-6031 SWP, Laboratory Data Control). The aqueous reagent (i.e. picrate solution) was mixed with the aqueous sample stream containing TBA^+ at the tee-fitting T1 (CJ-3031, Laboratory Data Control). The aqueous stream and the organic (chloroform) stream were then segmented at the tee-fitting T2 before passing through a 190-cm long extraction coil EC constructed of 0.8-mm i.d. × 1/16" o.d. Teflon tubing. After extraction, a portion of the organic phase was separated by the phase separator PS, which contained two layers of Teflon membrane

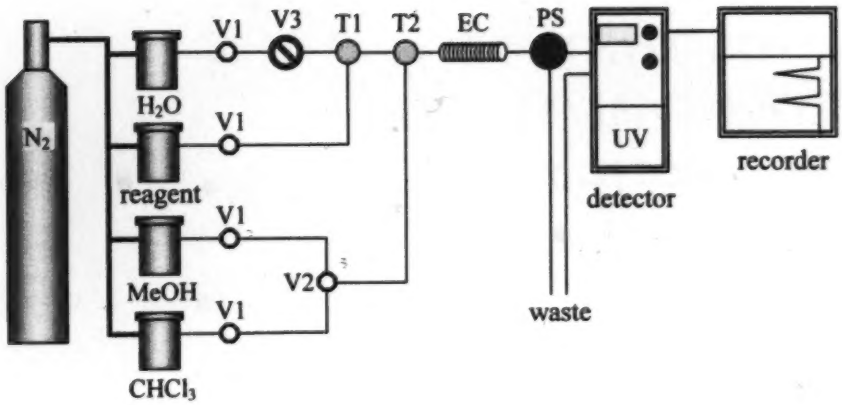

Figure 6.2 Solvent extraction/flow injection analysis system for the determination of TBA^+. V1 is a 2-way slider valve, V2 is a 3-way slider valve, v3 is a sample injection valve, T1 and T2 are tee-fittings, EC is an extraction coil, and PS is a phase separator.

with pore size 10-20 μm (Zitex, Chemplast Inc., Wayne, NJ), and directed to a UV detector (Spectroflow 757, Kratos, Ramsey, NJ) whose wavelength was set to 365 nm. A Recordall Series 5000 recorder R (Fisher Scientific) was used to record the signals.

The flow rates used for the SE/FIA experiments were as follows: total aqueous flow rate = 1.2 mL/min; total chloroform flow rate = 1.3 mL/min; and the chloroform flow rate through the membrane phase separator = 0.5 mL/min. Flow rates were controlled by adjusting the length and inner diameter of the connecting Teflon tubing.

The reagent solution contained 0.005 mol/L sodium picrate and 0.10 mol/L NaCl. Its pH was adjusted to 5 with 1×10^{-4} mol/L acetate buffer. TBA^+ standard solutions (1×10^{-4} mol/L, 2×10^{-4} mol/L, and 3.5×10^{-4} mol/L) were prepared in 1:1 (v/v) $MeOH/H_2O$.

6.4 Shake-flask Method for Measuring Partition Coefficient of Butanol

The conventional shake-flask method[94,95] was used to measure the partition coefficient of butanol between *n*-hexadecane and aqueous solutions, with and without the presence of TBA^+. Four aqueous solutions were prepared, which contained 1.0×10^{-3} mol/L butanol as well as 0.050 mol/L NaCl in solution (1), 0.50 mol/L NaCl in solution (2), 0.45 M NaCl and 0.050 M TBA^+ in solution (3), and 0.50 M TBA^+ in solution (4), respectively. The following is the general procedure used to determine the partition coefficient of butanol. First, 6.0 ml of aqueous solution and 60.0 ml of *n*-hexadecane were pipetted into a clean and dry 125-ml separatory funnel, which has a Teflon stopcock and a glass stopper. To avoid the use of grease, the glass stopper was sealed with Teflon tape and secured by parafilm. The drip tip and the stopcock were also wrapped with parafilm to keep them dry and clean during shaking. The separatory funnel was then placed in a constant temperature shaking water bath (MSB-1122A-1, Blue M Electric Co., Blue Island, IL) maintained at 25.0 ± 0.1 °C and shaken at a speed of about 90 rpm.

After eight hours of shaking, the funnel was taken out of the shaking bath and the aqueous phase was drained into a small 10-mL beaker. A 3.00-mL aliquot of the aqueous phase was pipetted into a 5-mL volumetric flask and after adding 2-pentanol as internal standard the solution was diluted to mark with water. The butanol concentration in the 5-mL flask was then determined by gas chromatography in the same way as outlined in section 6.2.1. The amount of butanol partitioned into the *n*-hexadecane organic phase was calculated by mass balance. The measurement of partition coefficients was performed in triplicate for each aqueous solution.

Chapter 7

Results and Discussions

7.1 Determination of Loading Volumes for TBA^+ and Butanol

In column equilibration experiments, the volume of the mobile phase required to pump through the column to establish equilibrium between the mobile and the stationary phases has to be first determined by measuring loading curves. Shown in Figure 7.1 are the TBA^+ loading curves obtained by pumping a varying volume of the 3.062×10^{-4} mol/L TBA^+ solutions through the column. The solutions were buffered at pH 5.0 and had ionic strengths of 0.050 mol/L or 0.50 mol/L. Two flow rates (1 and 3 mL/min) were used for each solution and data were collected both before and after equilibrium was established. The loading curves are plotted as peak height of TBA^+ measured by SE/FIA versus loading volume of the solutions.

It can be seen from Figure 7.1 that regardless of the flow rate used, equilibrium is established after about 40 mL and 60 mL of solutions at ionic strengths of 0.050 M and 0.50 M, respectively, have been pumped through the column. Obviously, the sorption process for TBA^+ in the ODS stationary phase is not controlled by the sorption kinetics, but by the supply of TBA^+. Therefore, for sample solutions with lower concentrations of TBA^+, larger volumes have to be pumped through the column to reach equilibrium. This makes it necessary to determine the loading volume required for each sample solution at different concentrations. Typical loading curves measured for TBA^+ or butanol alone and both together are shown in Figure 7.2 and 7.3 for low and high ionic strengths, respectively. Minimum loading volumes required to reach equilibrium and loading volumes actually used in this study are given in Table 7.1. Because the loading volumes for butanol at all the concentrations used for this study, ranging from 5×10^{-4} mol/L to 3×10^{-2} mol/L, are less than 30 mL, the minimum loading volumes required to establish

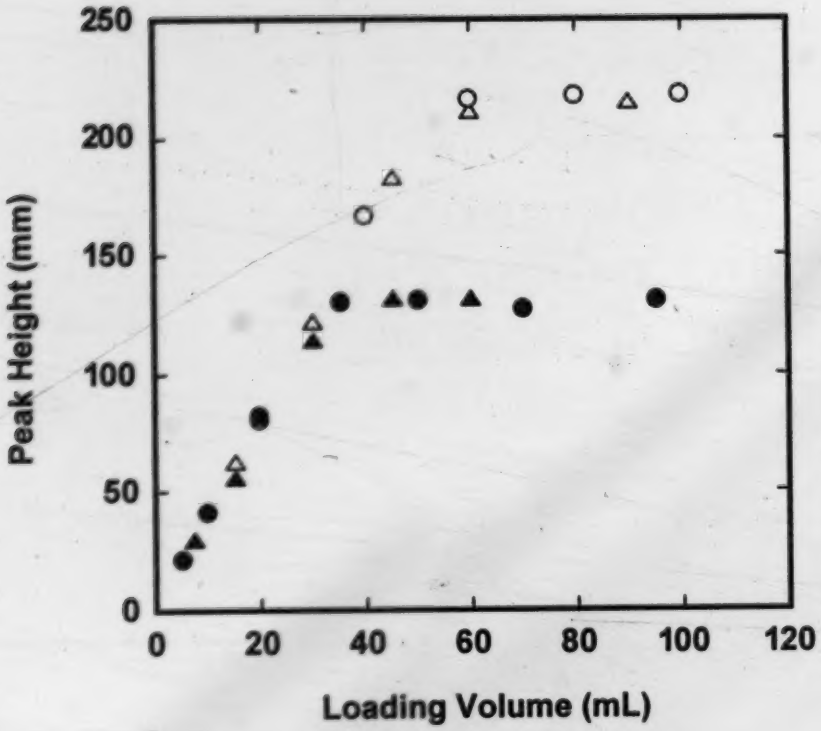

Figure 7.1 TBA^+ loading curves for 3.062×10^{-4} mol/L TBA^+ in pH 5.0 buffer at ionic strengths of 0.050 mol/L at flow rates 1 mL/min (●) and 3 mL/min (▲) and of 0.50 mol/L at flow rates 1 mL/min (○) and 3 mL/min (△).

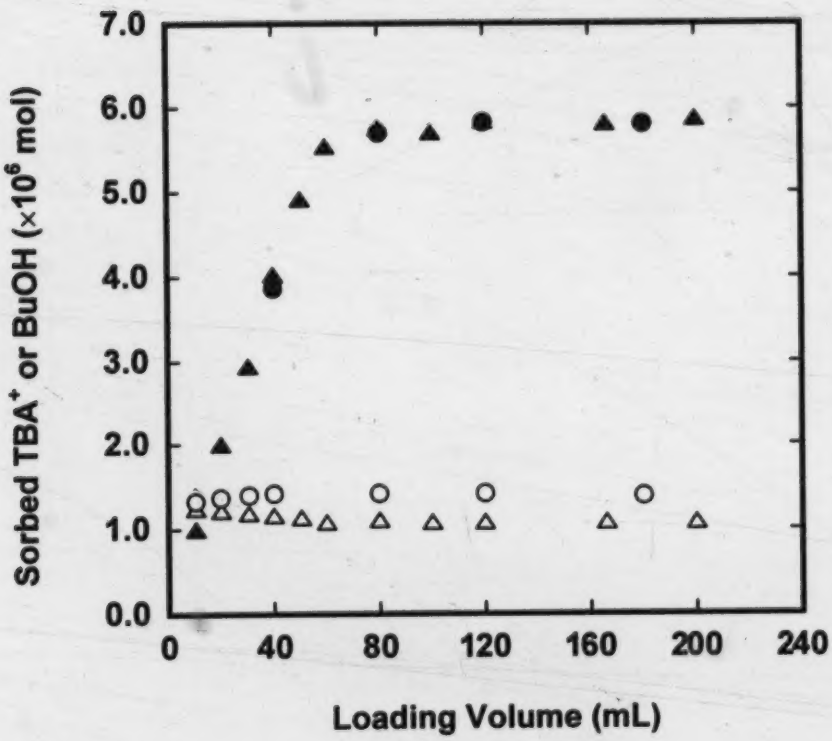

Figure 7.2 Loading curves for 1.021×10^{-4} mol/L TBA^+ alone (●) and in the presence of 5.00×10^{-4} mol/L butanol (▲), and for 5.00×10^{-4} mol/L butanol alone (○) and in the presence of 1.021×10^{-4} mol/L TBA^+ (△). Sample solution is buffered at pH 5.0 with an ionic strength of 0.050 mol/L.

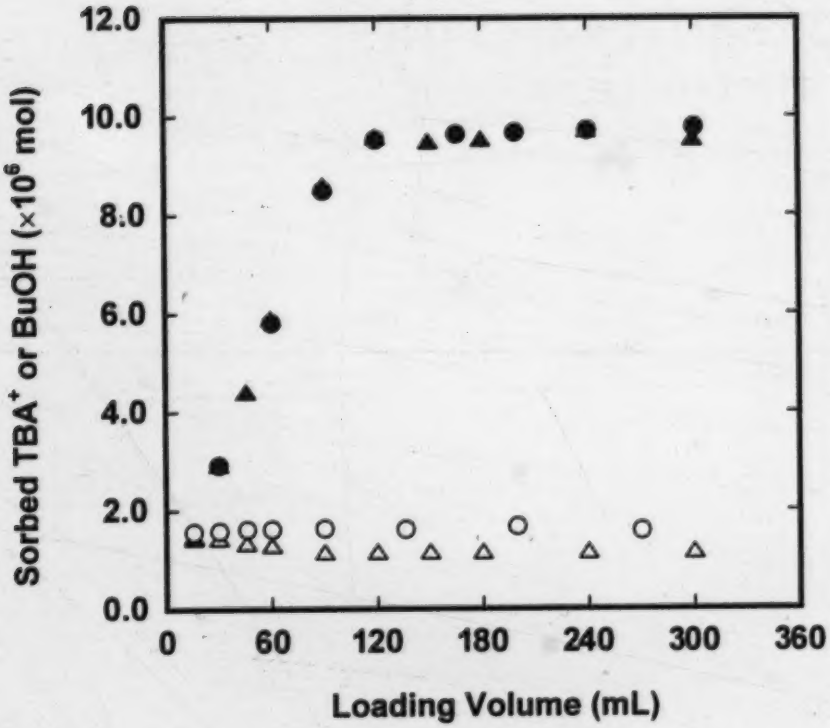

Figure 7.3 Loading curves for 1.021×10^{-4} mol/L TBA^+ alone (●) and in the presence of 5.00×10^{-4} mol/L butanol (▲), and for 5.00×10^{-4} mol/L butanol alone (○) and in the presence of 1.021×10^{-4} mol/L TBA^+ (△). Sample solution is buffered at pH 5.0 with an ionic strength of 0.50 mol/L.

Table 7.1 Minimum loading volumes required to reach equilibrium and loading volumes actually used in this study for the ionic strengths (IS) 0.50 and 0.050 mol/L.

$[TBA^+]$ in mobile phase	Loading Volume (mL)			
	IS = 0.50 mol/L		IS = 0.050 mol/L	
mol/L	minimum	actual	minimum	actual
0	< 15	60	< 10	60
1×10^{-2}	< 30	60	< 30	60
5×10^{-3}	< 30	60	< 30	60
1×10^{-3}	30	60	30	60
5×10^{-4}	80	120	40	90
1×10^{-4}	160	240	80	150
5×10^{-5}	240	330	120	210

equilibrium are determined solely by the TBA^+ concentration in the mobile phase.

It is also obvious from Figure 7.1 that at higher ionic strength more TBA^+ is sorbed in the ODS stationary phase. This effect has been quantitatively explained by the Stern-Guoy-Chapman (SGC) model of the electrical double layer.[96-99] According to the model, the surface density of a sorbed ionic species is proportional to the square root of ionic strength.

In column equilibration experiments, the elution step has to ensure a complete elution of the sorbed solutes. In this study, 1:1 (v/v) methanol:water was used to elute both sorbed TBA^+ and sorbed butanol. The completeness of elution of TBA^+ and butanol has been determined previously by Glavina.[84] It was found that both TBA^+ and butanol were almost completely eluted in 2 mL of eluent. In this study, more than 8 mL of eluent was often collected to ensure the completeness of the elutions.

7.2 Sorption Isotherms

A sorption isotherm is a plot of the solute concentration in the stationary phase, $C_{s,i}$ (mol/kg or mol/m^2), versus the solute concentration in the mobile phase, $C_{m,i}$ (mol/L), at constant temperature. Sorption isotherm describes quantitatively the equilibrium distribution of a solute between the two phases. A typical sorption isotherm is shown in Figure 7.4. The distribution coefficient of a solute, $K_{D,i}$, is defined by

$$K_{D,i} = \frac{C_{s,i}}{C_{m,i}} \qquad (7.1)$$

Its value can be determined from the sorption isotherm, for any solute concentration in the mobile phase, by calculating the slope of the straight line drawn through the origin and the point on the isotherm corresponding to the particular mobile phase concentration. This is illustrated in Figure 7.4. The value of the distribution coefficient is dependent on

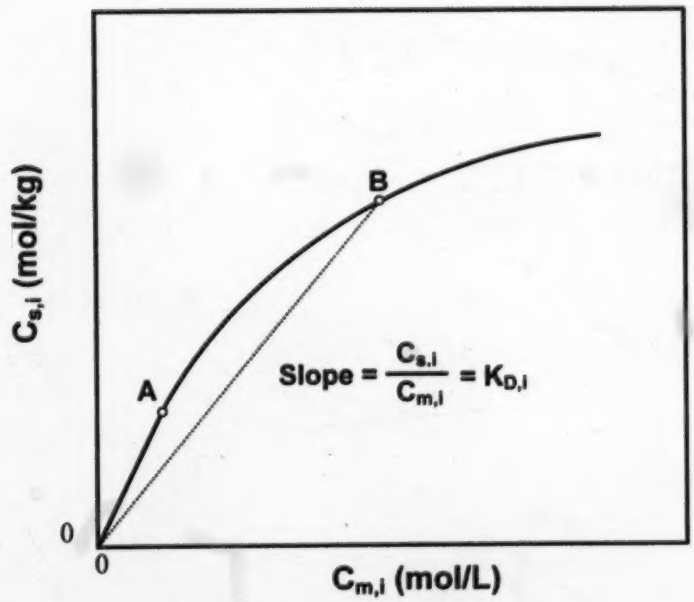

Figure 7.4 A hypothetical sorption isotherm (solid line). The distribution coefficient, $K_{D,i}$, at any point of the isotherm is the ratio of $C_{s,i}/C_{m,i}$.

the solute concentration in the mobile phase. However, in the low concentration region, isotherms are often found to be linear as shown in Figure 7.4 from the origin to point A. In this region, the distribution coefficient is a constant and independent of the solute concentration in the mobile phase.

A comprehensive examination of sorption isotherms may yield information about solvent, solute and the stationary phase as well as their interactions involved in the sorption process. In many instances measurement of sorption isotherms is the only way of probing these interactions.[100] The study of isotherms has played a key role in preparative chromatography, where solutes are commonly separated under nonlinear-isotherm conditions because high solute concentrations are required to achieve high throughputs.[101] Another beneficial aspect of the study of isotherms is the possibility of interpreting the sorption process in terms of phenomena on the molecular scale.[102-104] The Langmuir-type isotherm is the classic example.

7.2.1 Langmuir Isotherm

The earliest attempts to describe sorption isotherm analytically were entirely empirical. It was found that the following equation

$$C_{s,i} = a\, C_{m,i}^{b} \qquad (7.2a)$$

where a and b are constants, gives a concise analytical expression for many experimental data, especially those measured using sorbents with heterogeneous sorption sites. This empirical equation, known as the Freundlich isotherm, however, does not have any physical meaning regarding the sorption mechanism. In 1916, Langmuir proposed the first theoretical treatment of an isothermal sorption equilibrium.[105]

In the Langmuir-type distribution,[105] the solute molecules are assumed to sorb onto a limited number of active sites on the surface of the sorbent. When these sites are all occupied, solute can no longer sorb and the isotherm therefore approaches a limiting plateau. It is described by the Langmuir equation:[105,106]

$$C_{s,i} = \frac{C_{s,i,max} K_i C_{m,i}}{1 + K_i C_{m,i}} \qquad (7.2)$$

where $C_{s,i,max}$ is the maximum concentration of solute i (sorbed as a monolayer) on the sorbent and K_i is the sorption equilibrium constant for solute i.

The Langmuir isotherm was first developed to describe the adsorption of gas molecules on solid sorbent. Implicit in the development of the Langmuir equation are the following assumptions:[107] (1) the gas molecule in the bulk gas phase behaves as an ideal gas; (2) the amount adsorbed is confined to a monomolecular layer; (3) every part of the surface has the same energy of adsorption; (4) there is no interactions between sorbed molecules; and (5) the adsorbed molecules are localized. These assumptions, especially the third and fourth assumptions are unlikely to be true in most sorption situations. Deviations from Langmuir sorption behavior are often found in experimentally measured isotherms. However, the Langmuir equation is still widely used because the Langmuir isotherm is convenient for quantitative analysis of sorption process and has a physical basis and also because it often provides a simple and adequate correlation with experimental data even for situations where the Langmuir-type sorption is unlikely.[100] In the latter case, caution should taken in assigning physical meaning to the parameters in the equation.

To account for the deviations from the Langmuir sorption behavior, a number of more sophisticated models have been suggested, such as the Fowler,[103,108] the Temkin,[109,110] the BET,[111,112] the bilayer,[103] and the bilangmuir,[113] in which several

phenomena ignored by the Langmuir model have been taken into account. For example, both the Fowler and the Temkin isotherms take into account the molecule-molecule interactions. The Fowler isotherm introduces an empirical interaction energy parameter, while the Temkin assumes a linear relationship between the heat of adsorption and the surface coverage. The BET isotherm deals with multilayer adsorption, in which vertical interactions between sorbed molecules in successive layers are introduced while lateral interactions are omitted. The bilayer isotherm applies when adsorption proceeds in two adsorption layers instead of a monolayer. The bilangmuir isotherm assumes two different adsorption sites, with different heat of adsorption, on the surface of sorbent. In the following sections, the Temkin and the bilayer isotherms are presented in more details because they will be used to describe the TBA^+ isotherm measured in this study and the butanol isotherm measured previously by Glavina.[84] Although the Fowler equation also addresses the effect of molecule-molecule interactions, it cannot be formulated as an explicit expression for $C_{s,i}$ and is awkward to handle. Therefore, the Fowler equation was not used in this study.

7.2.2 Temkin Isotherm

The original Temkin equation,[109,110] when applied to the sorption at the solid/liquid interface, can be written as

$$\theta = \frac{C_{s,i}}{C_{s,i,max}} = (1/f) \ln (a\, C_{m,i}) \qquad (7.3)$$

where θ is the fraction of the surface covered with sorbed molecule, f and a are constants. Obviously, this equation is not applicable either at high or at low surface coverage, since it does not reduce to $\theta = 0$ for $C_{m,i} = 0$, nor to $\theta = 1$ for very large values

of $C_{m,i}$. Therefore, the above equation is valid only in the middle range of the sorption isotherm. An equation, which is valid for the entire sorption isotherm, was later derived by Brunauer, Love, and Keenan,[110] which we call the extended Temkin equation.

The derivation of the extended Temkin equation was based on the Langmuir equation with the assumption that the heat of sorption is a linear function of the surface coverage. The derived equation is written as[110]

$$\theta = \frac{C_{s,i}}{C_{s,i,max}} = b \ln\left(\frac{1 + a C_{m,i}}{1 + a \exp(-1/b) C_{m,i}}\right) \qquad (7.4)$$

where b is a constant. In the range of sorption where $(a C_{m,i}) >> 1 >> [a \exp(-1/b) C_{m,i}]$, eq 7.4 can be reduced to eq 7.3 if b is set to be equal to 1/f.

7.2.3 Bilayer Isotherm

The bilayer isotherm[103] was derived based on a kinetic argument by assuming a kind of multilayer sorption: on top of a sorbed molecule in the first layer, a second molecule can sorb with different affinity. It also assumes that molecules sorbed as the first layer compete with each other for sorption sites, while for molecules sorbed on top of the first layer two possibilities are considered: with or without competition for sorption sites between molecules sorbed in the second layer. The competition assumption leads to a four-parameter quadratic equation, while the no-competition assumption gives a three-parameter equation, which can be expressed as the sum of a Langmuir-type expression and a linear partition-type term:[103]

$$C_{s,i} = \frac{a_1 C_{m,i}}{1 + K_{1,i} C_{m,i}} + a_2 C_{m,i} \qquad (7.5)$$

where the parameters a_1 and a_2 are given by

$$a_1 = (K_{1,i} - K_{2,i})\, C_{s,i,max} \quad (7.6)$$

$$a_2 = K_{2,i}\, C_{s,i,max} \quad (7.7)$$

Here, $K_{1,i}$ and $K_{2,i}$ are the sorption equilibrium constants for solute sorbed in the first monolayer and the second layer, respectively, and $C_{s,i,max}$ is the maximum surface concentration of solute sorbed in the first layer. The authors[103] call equation 7.5 the associative bilayer isotherm to distinguish from the competitive bilayer isotherm.

An isotherm, which is similar to eq 7.5, has been previously derived by Enderby[114] to describe water absorption by cellulose. In that derivation, water is assumed to adsorb on two types of sites: the primary sites which allow only monolayer adsorption and the secondary sites, which, when occupied, provide a similar site for an additional water molecule, i.e. multilayer adsorption is allowed on the secondary sites. These assumptions are quite similar to those used in deriving eq 7.5 except that only two layers are considered in eq 7.5.

7.2.4 TBA^+ Sorption Isotherms

The number of moles of TBA^+ apparently sorbed at the Partisil ODS-3 stationary phase, n_{TBA}, measured at varying TBA^+ concentrations in the mobile phase, $C_{m,TBA}$, are given in Table 7.2 for two different ionic strengths. The experimentally measured value n_{TBA} as calculated by eq 6.1, however, may not represent the number of moles of TBA^+ actually sorbed in the ODS stationary phase, $n_{s,TBA}$, due to the fact of co-ion exclusion.[86,87,97] Co-ion exclusion occurs because the sorption of positively charged TBA^+ at the nonionic stationary phase creates an electrical double layer and co-ions, Na^+ and TBA^+, are repelled from the diffuse layer. It means that in the diffuse layer the TBA^+ and the Na^+ concentrations are lower than those in the bulk solution (i.e. the mobile phase). As a result of co-ion exclusion, the experimentally measured n_{TBA}, as calculated

by eq 6.1, tends to underestimate the number of moles of TBA^+ actually sorbed in the ODS stationary phase.

The relationship between n_{TBA}, and $n_{s,TBA}$ and the number of moles of TBA^+ excluded from the diffuse layer, $n_{DL,TBA}$, is

$$n_{TBA} = n_{s,TBA} + n_{DL,TBA} \qquad (7.8)$$

Since $n_{DL,TBA}$ has a negative value, n_{TBA} is smaller than $n_{s,TBA}$. To correct this underestimation, a knowledge of $n_{DL,TBA}$ is required. The value of $n_{DL,TBA}$ can be calculated from the experimentally measured value of n_{TBA} by an iterative process which follows the same steps that have been described in detail in the Appendix of ref 97. (Note: error in eq b; should be $(c^{1/2})^{-1}$). The results are given in Table 7.2.

Shown in Figure 7.5 and 7.6 are the TBA^+ sorption isotherms measured at two different ionic strengths. For the reason mentioned in section 7.1, the amount of TBA^+ sorbed increases at higher ionic strength. The TBA^+ isotherms do not follow the Langmuir equation nor the empirical Freundlich equation. This non-Langmuir behavior is expected because the Langmuir isotherm contains no term for electrostatic interactions between sorbed ionic species. By using the extended Temkin equation,[110] however, good fits (shown as solid lines in Figure 7.5 and 7.6) have been obtained and the fitting parameters used are given in Table 7.3. Because the data points attainable at ionic strength 0.050 mol/L are not adequate to define the curve, the predicted value of $C_{s,TBA,max}$ is not reliable. This is reflected by the extremely large values of error (std. dev.) for $C_{s,TBA,max}$ and b obtained from the nonlinear least-square fit to the data for the ionic strength 0.050 mol/L (see Table 7.3).

A number of workers have studied the sorption of TBA^+ on ODS packings.[98,115-118] Some reported that TBA^+ isotherms follow the Langmuir[98,115] or Freundlich[116] equations, while others[117,118] found that they do not follow either of the above equations.

Table 7.2 Experimental data of TBA^+ sorption isotherms on Partisil ODS-3 at 25.0 °C.

Ionic Strength (mol/L)	$C_{m,TBA}$ (mol/L)	n_{TBA} 10^6 (mol)	$n_{DL,TBA}$ 10^6 (mol)	$n_{s,TBA}$ 10^6 (mol)	$C_{s,TBA}$[1] (mol/kg)
0.50	5.10×10^{-5}	0.72	0.00	0.72	0.046
0.50	1.02×10^{-4}	0.87	0.00	0.87	0.055
0.50	5.10×10^{-4}	1.52	0.00	1.52	0.097
0.50	1.02×10^{-3}	1.77	0.00	1.77	0.113
0.50	2.04×10^{-3}	2.17	0.00	2.17	0.138
0.50	5.10×10^{-3}	2.66	-0.01	2.67	0.170
0.50	1.02×10^{-2}	3.00	-0.01	3.01	0.192
0.50	2.04×10^{-2}	3.31	-0.03	3.34	0.213
0.50	3.06×10^{-2}	3.50	-0.06	3.56	0.227
0.50	4.08×10^{-2}	3.70	-0.08	3.78	0.241
0.50	5.10×10^{-2}	3.81	-0.10	3.91	0.249
0.50	6.09×10^{-2}	3.84	-0.13	3.97	0.253
0.50	9.14×10^{-2}	3.94	-0.20	4.14	0.264
0.50	0.122	4.02	-0.28	4.30	0.274
0.50	0.152	4.05	-0.35	4.40	0.280
0.50	0.183	4.00	-0.41	4.41	0.281
0.50	0.213	4.00	-0.49	4.49	0.286
0.50	0.244	4.00	-0.57	4.57	0.291
0.050	5.37×10^{-5}	0.38	0.00	0.38	0.024
0.050	1.07×10^{-4}	0.53	0.00	0.53	0.034
0.050	5.37×10^{-4}	0.94	0.00	0.94	0.060
0.050	2.15×10^{-3}	1.39	-0.01	1.40	0.089
0.050	5.37×10^{-3}	1.74	-0.05	1.79	0.114
0.050	1.07×10^{-2}	2.03	-0.09	2.12	0.135
0.050	2.15×10^{-2}	2.34	-0.19	2.53	0.161
0.050	3.22×10^{-2}	2.44	-0.29	2.73	0.174
0.050	4.30×10^{-2}	2.53	-0.37	2.90	0.185
0.050	5.01×10^{-2}	2.52	-0.46	2.98	0.190

1. Calculated by $n_{s,TBA}/0.157 \times 10^{-3}$ kg of Partisil ODS-3 used.

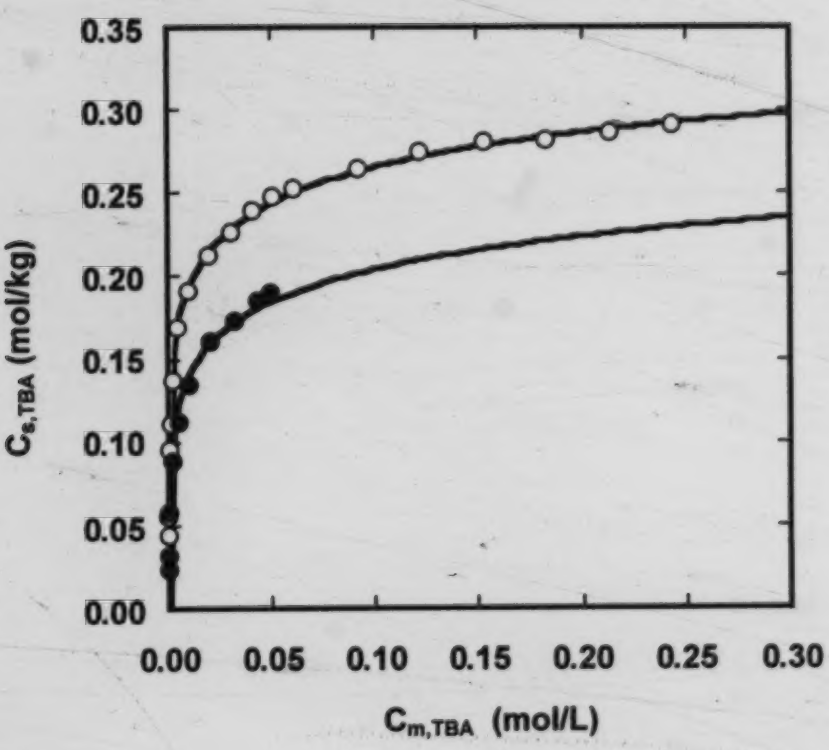

Figure 7.5 TBA^+ sorption isotherms on Partisil-10 ODS-3 from pH 5 aqueous solutions at two ionic strengths: 0.50 M (○) and 0.050 M (●). Solid lines are fits to the extended Temkin equation with fitting parameters given in Table 7.3.

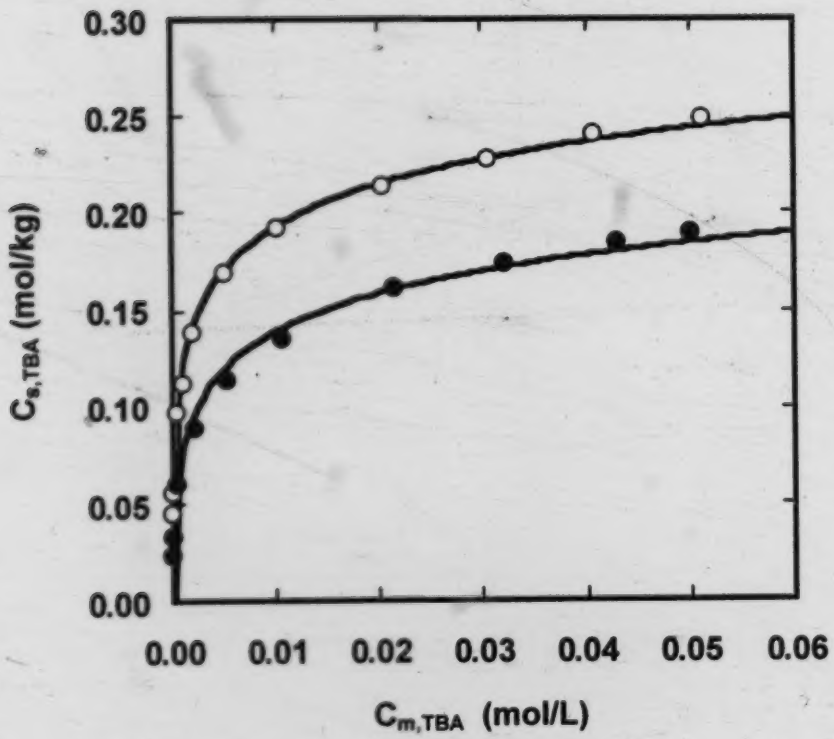

Figure 7.6 TBA^+ sorption isotherms expanded from Figure 7.5 to show the region with TBA^+ concentrations lower than 0.060 mol/L.

Table 7.3 Fitting parameters used to fit the TBA^+ isotherm to the extended Temkin equation.

Ionic Strength (mol/L)	$C_{s,TBA,max}$ (mol/kg)	a	b
0.50	0.36 ± 0.04	40,100 ± 5,100	0.0885 ± 0.012
0.050	0.53 ± 2900[a]	13,500 ± 5,400	0.0532 ± 293[a]

a. See text for comment on large uncertainties at 0.050 mol/L ionic strength.

The discrepancy reported in the literature is probably due to the fact that only a narrow range of solute concentrations was studied by many workers. As pointed out by others,[119] in many cases non-Langmuir isotherms could closely resemble the Langmuir isotherm within a certain range of solute concentrations.

By taking into account the surface potential created by the sorption of ionic species, Stahlberg[118] derived a surface-potential-modified Langmuir isotherm equation, which is similar to that derived previously by Davies,[120,121] to describe the sorption of ionic species. The sorption of TBA^+ was reported to follow the modified Langmuir isotherm.[118] In the Temkin isotherm used in this study, a simple linear relationship between the heat of sorption and the surface coverage is assumed. Although this simple assumption might not be completely true, the satisfactory fitting of the extended Temkin isotherm to the experimentally measured sorption data seems to indicate that this is a reasonable assumption. In fact, Davies[120,121] has shown that when surface potential is small (< 25 mV), the energy of sorption varies linearly with surface coverage and the sorption should also obey the Temkin isotherm.

7.2.5 Butanol Sorption Isotherm

The butanol isotherm is shown in Figure 7.7, which was measured previously by Glavina[84,85] on the same Partisil-10 ODS-3 stationary phase. Because the isotherm does not approach a plateau, a smooth curve through all data points was generated by Stineman interpolation and no attempt was make to fit the entire set of data to a isotherm model.[84,85] Instead, a double-reciprocal plot of $1/C_{s,BuOH}$ versus $1/C_{m,BuOH}$ was made, and the points for which $1/C_{m,BuOH} > 12$ L/mol (i.e. $C_{m,BuOH} < 0.08$ mol/L) were found to be linear. This was taken as an indication of a Langmuir-type behavior at low butanol concentrations. From the slope and intercept of the straight line, the sorption equilibrium

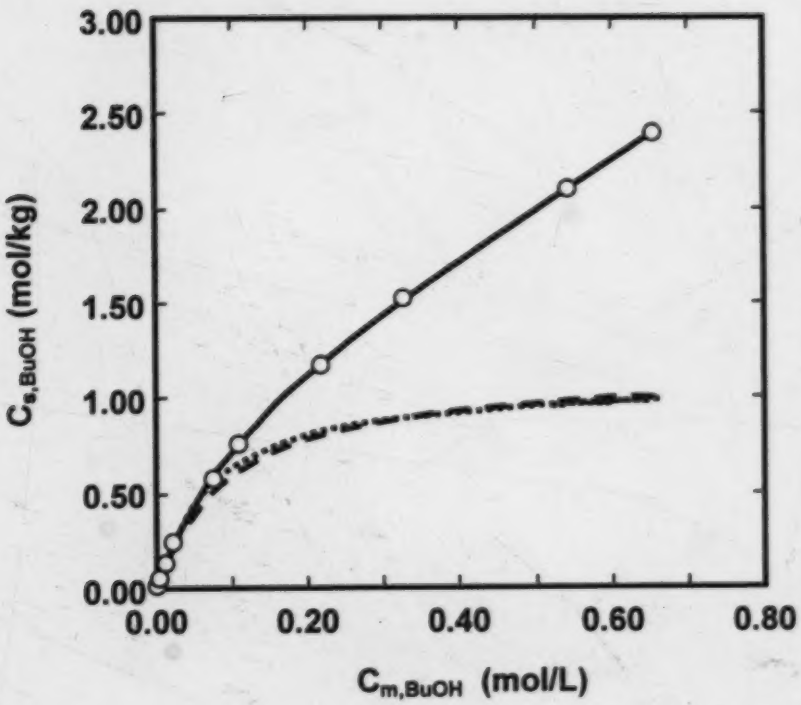

Figure 7.7 BuOH sorption isotherms on Partisil-10 ODS-3 from pH 2 aqueous solutions. The solid line is the fit of the experimental data (O) to the bilayer equation with fitting parameters given in Table 7.4. The data are from reference 84. The dashed and the dotted lines are the Langmuir plots based on the values of $C_{s,TBA,max}$ and $K_{1,\ BuOH}$ obtained from the bilayer model and the double-reciprocal-plot in reference 84 (see Table 7.4), respectively.

Table 7.4 Fitting parameters used in this study to fit the entire BuOH isotherm to the associative bilayer model and those obtained from double-reciprocal plot of $1/C_{s,BuOH}$ versus $1/C_{m,BuOH}$ for the concentration range 0 to 0.08 mol/L.[84,85]

	$C_{s,TBA,max}$ (mol/kg)	$K_{1,BuOH}$ (L/mol)	$K_{2,BuOH}$ (L/mol)
bilayer	1.16 ± 0.06	10.6 ± 0.9	2.1 ± 0.2
Langmuir	1.1 ± 0.6	13 ± 7	—

constant for butanol, K_{BuOH}, and the monolayer concentration of butanol, $C_{s,BuOH,max}$, were calculated to be 13 ± 7 L/mol and 1.1 ± 0.6 mol/kg, respectively.[84,85]

In the present study, it was found that the entire butanol isotherm could be fitted to the associative bilayer model[103] as shown in Figure 7.7 (solid line). The fit is excellent and the fitting parameters used are given in Table 7.4. It can be seen from Table 7.4 that the values of $C_{s,TBA,max}$ and $K_{1,BuOH}$ obtained from the bilayer model are very close to those previously obtained from the double-reciprocal plot of $1/C_{s,BuOH}$ versus $1/C_{m,BuOH}$ for the concentration range from 0 to 0.08 mol/L.[84,85] The Langmuir plots based on the values of $C_{s,TBA,max}$ and $K_{1,BuOH}$ obtained from the bilayer model (dashed line) and from the double-reciprocal-plot (dotted line) are also shown in Figure 7.7.

7.3 Effect of Butanol on TBA^+ Sorption

To study the effect of butanol on the sorption of TBA^+, the TBA^+ concentration in the mobile phase was kept low and constant at 1.0×10^{-4} mol/L, and the butanol concentration was varied from 0 to 0.030 mol/L. Figure 7.8 shows the plot of the number of moles of TBA^+ sorbed, $n_{s,TBA}$, versus the number of moles of butanol sorbed, $n_{s,BuOH}$. It is obvious from Figure 7.8 that the number of moles of TBA^+ sorbed decreases linearly with the number of moles of butanol sorbed. The slopes are –0.087 ± 0.003 and -0.057 ± 0.002 mole of TBA^+ sorbed/mole of butanol sorbed and the calculated *x*-intercepts are $(1.10 \pm 0.03) \times 10^{-4}$ and $(9.8 \pm 0.3) \times 10^{-5}$ mol of butanol sorbed for ionic strengths of 0.50 and 0.050 mol/L, respectively. Such a linear relationship has also been found in a previous study for the effect of butanol on the sorption of naphthalene-2-sulfonate (NS^-) and for the effect of NS^- on butanol sorption.[85] In the previous work, a theoretical model was developed to describe this linear relationship in terms of a competition between NS^- and butanol for available space in the ODS stationary phase.[85] Because the model should

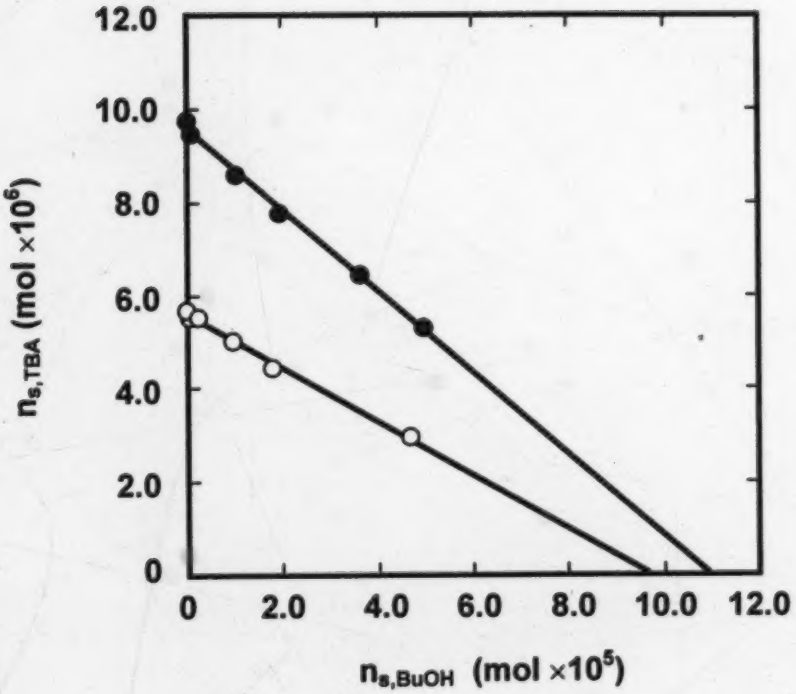

Figure 7.8 Plot of the number of moles of TBA^+ sorbed versus the number of moles of BuOH sorbed in the ODS stationary phase at two ionic strengths: 0.50 mol/L (●) and 0.050 mol/L (○). The TBA^+ concentration in the mobile phase is kept constant at 1.0×10^{-4} mol/L and the butanol concentration is varied from 0 to 0.030 mol/L. Solid lines are the linear least-square fits.

also be applicable to the effect of butanol on the sorption of TBA^+, the same model is presented as follows.

The distribution coefficient of TBA^+, $K_{D,TBA}$, is given by

$$K_{D,TBA} = \frac{C_{s,TBA}}{C_{m,TBA}} = \frac{n_{s,TBA}}{A_{s,TBA}\, C_{m,TBA}} \qquad (7.9)$$

where $A_{s,TBA}$ is the space available in the stationary phase for TBA^+ sorption. When butanol is also present in the mobile phase, the available space for TBA^+ sorption is decreased as a result of "blockage" of some of the surface by sorbed butanol. This is expressed as

$$A_{s,TBA} = A_{s,t,TBA} - A_{s,BuOH} \qquad (7.10)$$

Here, $A_{s,t,TBA}$ is the total space available for TBA^+ sorption in the absence of sorbed butanol and $A_{s,BuOH}$ is the space occupied by butanol.

Sorbed TBA^+ and butanol may reside at different distances from the silica surface in different sorption planes depending upon ODS chain conformation as discussed later. Due to its more or less spherical shape, the thickness of the TBA^+ sorption plane is roughly constant. However, the thickness of the butanol sorption plane depends upon its angular orientation to the surface. The extent of overlap of sorbed TBA^+ and butanol depends upon how far apart and how thick their sorption planes are. Based on these assumptions, the space occupied by butanol, $A_{s,BuOH}$, can be expressed as

$$A_{s,BuOH} = \bar{A}_{BuOH}\, n_{s,BuOH} \qquad (7.11)$$

where $\bar{A}_{BuOH}$ is the space in the TBA^+ sorption plane that is effectively occupied per mol of butanol sorbed and $n_{s,BuOH}$ is the number of moles of butanol sorbed in the stationary

phase. By combining eqs 7.9 – 7.11, the number of moles of TBA^+ sorbed in the stationary phase in the presence of butanol is

$$n_{s,TBA} = (K_{D,TBA}\, C_{m,TBA}\, A_{s,t,TBA}) - (K_{D,TBA}\, C_{m,TBA}\, \bar{A}_{BuOH})\, n_{s,BuOH} \qquad (7.12)$$

Assuming that $K_{D,TBA}$ is a constant over the butanol concentration range used in this study and $\bar{A}_{BuOH}$ is independent of the fraction coverage of the stationary phase by butanol, eq 7.12 predicts a linear relationship between $n_{s,TBA}$ and $n_{s,BuOH}$ since $C_{m,TBA}$ was kept constant in all the experiments. The linearity of the plot shown in Figure 7.8 suggests that these assumptions are reasonable and a competition for space is occurring. A constant $K_{D,TBA}$ means that neither the solvent strength of the mobile phase nor the sorbent strength of the stationary phase changes significantly over the butanol concentration range used in this study.

It is obvious from Figure 7.8 that the number of moles of TBA^+ sorbed at the ionic strength 0.50 mol/L is much higher than that at the ionic strength 0.050 mol/L. This is understandable because, as mentioned in section 7.24, the sorption of ionic species in the ODS stationary phase is significantly influenced by the ionic strength of the mobile phase. The number of moles of TBA^+ sorbed, $n_{s,TBA}$, or the distribution coefficient of TBA^+, $K_{D,TBA}$, is expected to increase with the increase in ionic strength. It is also obvious from Figure 7.8 that the straight line for the higher ionic strength has a larger negative slope than does the line for the lower ionic strength. According to eq 7.12, such dependence of the slope on ionic strength is explicable because $K_{D,TBA}$ is larger at higher ionic strength. By assuming the same $A_{s,TBA}$ for both ionic strengths in the absence of butanol (see eq 7.9), the ratio of the distribution coefficients of TBA^+ at the two ionic strengths can be expressed as the ratio of the numbers of moles of TBA^+ sorbed at the two ionic strengths in the absence of butanol

$$\frac{K_{D,TBA,0.50}}{K_{D,TBA,0.050}} = \frac{n_{s,TBA,0.50}}{n_{s,TBA,0.050}} \qquad (7.13)$$

Based on the data in Figure 7.8, the ratio is estimated to be 1.7 ± 0.1, which is very close to 1.5 ± 0.1, the ratio of the slopes of the two straight lines.

7.4 Effect of TBA^+ on Butanol Sorption

7.4.1 Non-linear relationship between $n_{s,BuOH}$ and $n_{s,TBA}$

To study the reverse effect, i.e. the effect of TBA^+ on the sorption of butanol, the butanol concentration in the mobile phase was kept constant at a concentration of 1.0×10^{-3} mol/L and the TBA^+ concentration was varied from 0 to 0.50 mol/L and from 0 to 0.050 mol/L for the ionic strengths of 0.50 mol/L and 0.050 mol/L, respectively. The plots of the number of moles of butanol sorbed, $n_{s,BuOH}$, versus the number of moles of TBA^+ sorbed, $n_{s,TBA}$, are shown in Figure 7.9 for both ionic strengths. It can be seen from Figure 7.9 that although the amount of butanol sorbed decreases when more TBA^+ is sorbed, there is no linear relationship between $n_{s,BuOH}$ and $n_{s,TBA}$ as was seen in the previous section for the effect of butanol on the sorption of TBA^+.

If the same procedure is followed as in the previous section, an equation similar to eq 7.12 can be derived. Like eq 7.9, the distribution coefficient of butanol, $K_{D,BuOH}$, can be written by

$$K_{D,BuOH} = \frac{C_{s,BuOH}}{C_{m,BuOH}} = \frac{n_{s,BuOH}}{A_{s,BuOH}\, C_{m,BuOH}} \qquad (7.14)$$

where $A_{s,BuOH}$ is the space available in the stationary phase for butanol sorption, which can be expressed, in a similar way as $A_{s,TBA}$ in eqs 7.10 and 7.11, as

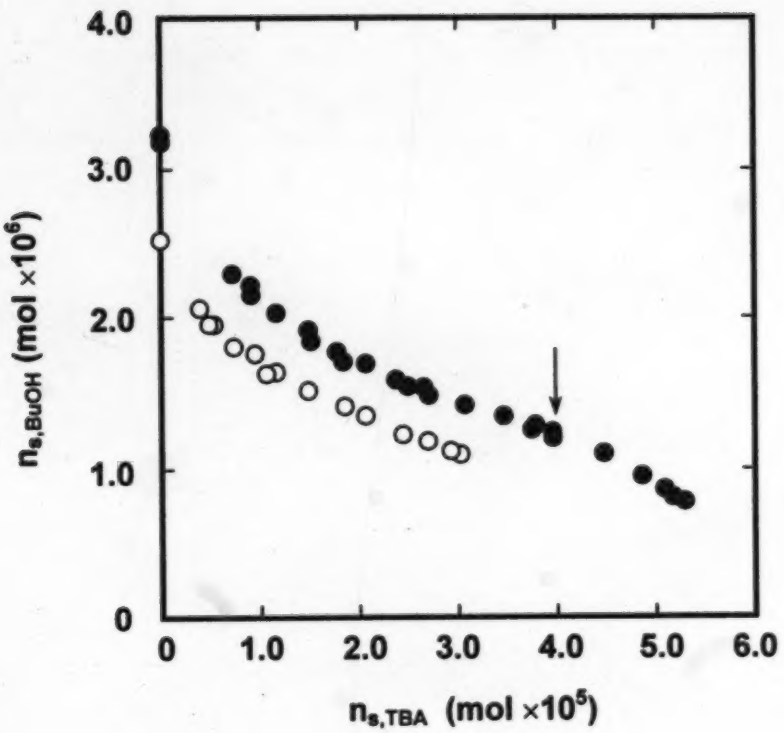

Figure 7.9 Plot of the number of moles of butanol sorbed versus the number of moles of TBA^+ sorbed in the ODS stationary phase at two ionic strengths: 0.50 mol/L (●) and 0.050 mol/L (○). The butanol concentration in the mobile phase is kept constant at 1.0×10^{-3} mol/L and the TBA^+ concentration is varied from 0 to 0.50 or 0.050 mol/L for ionic strengths 0.50 and 0.050 mol/L, respectively.

$$A_{s,BuOH} = A_{s,t,BuOH} - \bar{A}_{TBA}\, n_{s,TBA} \qquad (7.15)$$

Here, $A_{s,t,BuOH}$ is the total space available for butanol sorption in the absence of sorbed TBA^+, $\bar{A}_{TBA}$ is the space in the butanol sorption plane that is effectively occupied per mol of TBA^+ and $n_{s,TBA}$ is the number of moles of TBA^+ sorbed in the stationary phase. A combination of eqs 7.14 and 7.15 will give

$$n_{s,BuOH} = (K_{D,BuOH}\, C_{m,BuOH}\, A_{s,t,BuOH}) - (K_{D,BuOH}\, C_{m,BuOH}\, \bar{A}_{TBA})\, n_{s,TBA} \qquad (7.16)$$

which is similar to eq 7.12 except that the above equation is for the reverse effect. Since $C_{m,BuOH}$ is kept constant in all the experiments, a non-linear relationship between $n_{s,BuOH}$ and $n_{s,TBA}$ could mean that, in this case, $K_{D,BuOH}$ or $A_{s,t,,BuOH}$ or $\bar{A}_{TBA}$, or all of them are no longer constant.

7.4.2 Possible Explanations

A varying $K_{D,BuOH}$ can be caused by a change in sorbent strength, or solvent strength, or both. Although it is difficult to determine if there is a change in sorbent strength when more TBA^+ is sorbed, it is relatively simple to test if the solvent strength has been changed over the range of TBA^+ concentrations used in this study. TBA^+ is a hydrophobic organic ion and butanol is capable of hydrophobic interactions. Therefore, the presence of a high concentration of TBA^+ could cause the so-called salting-in effect[122-125] on butanol, which would result in a higher concentration of butanol in the mobile phase at equilibrium. In other words, it would cause a decreased distribution coefficient for butanol. By determining the vapor composition at equilibrium with an ethanol-water mixture containing various salts, it has been found that $(n\text{-}C_3H_7)_4NBr$ and $(n\text{-}C_4H_9)_4NBr$ are effective in salting in ethanol while small ions such as NH_4Br and $(CH_3)_4NBr$ are effective in salting out ethanol.[126]

To determine if there is a salting-in effect over the range of TBA^+ concentrations used, the *n*-hexadecane-aqueous partition coefficient of butanol, $K_{BuOH,C16/aq}$, was measured using the conventional shake-flask method.[94,95] The measured partition coefficients are given in Table 7.5. The partition coefficient of butanol (0.107) measured at the ionic strength 0.050 mol/L in this study is in good agreement with those measured by the generator column method (0.109[127]) and by other methods (0.114[128] and 0.112[129]) in the literature, where pure water was used as the aqueous phase. According to the measured partition coefficients given in Table 7.5 for the ionic strength 0.50 mol/L, it is obvious that the partition coefficient of butanol is a constant (i.e. there is no salting-in effect on butanol) at TBA^+ concentrations at least up to 0.050 mol/L. Only at very high concentrations of TBA^+ does the salting-in effect become significant, as indicated by a smaller partition coefficient obtained at 0.50 mol/L of TBA^+.

With 0.050 mol/L of TBA^+ and 1.0×10^{-3} mol/L of butanol in the mobile phase at ionic strength 0.50 mol/L, the experimentally measured number of moles of TBA^+ sorbed in the stationary phase at equilibrium is about 4.0×10^{-5} mol (indicated by the vertical arrow in Figure 7.9). Because there is no salting-in effect on butanol in the mobile phases in which the TBA^+ concentration ranges from 0 mol/L up to at least 0.050 mol/L, the solvent strength for butanol should be the same for data points ranging from 0 mol up to at least 4.0×10^{-5} mol of sorbed TBA^+. It can be seen from Figure 7.9 that the range of sorbed TBA^+ from 0 to 4.0×10^{-5} mol covers most of the plot. It means that no significant change in solvent strength has occurred up to at least $n_{s,TBA} = 4.0 \times 10^{-5}$ mol. If there is a change in $K_{D,BuOH}$, it must be caused by the change in sorbent strength.

A change in sorbent strength, and perhaps also in $A_{s,t,BuOH}$ and $\bar{A}_{TBA}$, upon the sorption of TBA^+, is possible considering the difference in molecular shape between TBA^+ and butanol. Although such changes may be produced by TBA^+ sorption, they are

Table 7.5 *n*-Hexadecane-aqueous distribution coefficients of butanol measured with the aqueous solutions containing 1.0×10^{-3} mol/L butanol and varying concentrations of TBA^+ and NaCl at the ionic strengths 0.50 mol/L and 0.050 mol/L at 25.0 °C.

Ionic Strength	$K_{BuOH,C16/aq}$		
(mol/L)	$[TBA^+] = 0$ mol/L	0.050 mol/L	0.50 mol/L
0.50	0.130 ± 0.001	0.133 ± 0.003	0.108 ± 0.003
0.050	0.107 ± 0.001	—[a]	—[a]

a. not measured.

not produced by butanol sorption. When linear (e.g., butanol) or planar molecules are sorbed in the ODS stationary phase, the original ODS chain structure or conformation seems to be largely retained as long as the amount sorbed in the stationary phase is not too large, because these molecules are able to adopt to the original chain conformation while being sorbed in between ODS chains. Because no significant change in chain conformation occurs in the stationary phase, the values of $A_{s,t,,BuOH}$, $\bar{A}_{TBA}$ and $K_{D,BuOH}$ are expected to be more or less the same when linear or planar solutes are sorbed. This explains both the linear effect of butanol on TBA^+ sorption as shown in Figure 7.8 and the linear mutual effect of butanol and NS^- found in the previous work.[85] Two more examples of such linear competition between two linear molecules were found in the literature by replotting the original data.[130] Shown in Figure 7.10 (a) and 7.11 (a) are the original plots from ref 130. When those solid lines in Figure 7.10 (a) and 7.11 (a) are digitized and replotted as surface excess of 1-propanol versus surface excess of octane-1-sulphonate and dodecane-1-sulphonate, linear relationships were found for both plots (see Figure 7.10 (b) and 7.11 (b)). Although the authors did not make correction for co-ion exclusion for their surface excess data, the errors are expected to be insignificant.

Previous fluorescence spectroscopic study also supports the above explanation. By using the hydrophobic molecule, *p*-bis(*o*-methyl)-styrylbenzene (bis-MSB), as a fluorescent probe, Wirth and co-workers[64,65] investigated the orientational distribution of the ODS chains upon the sorption of aliphatic alcohols. They found that the sorption of a monolayer of short-chain alcohols such as *n*-propanol only tilts the ODS chains about 10° further toward the surface normal; that is, from the original 80° from the surface normal with pure water as mobile phase to 70° from the surface normal with 5% *n*-propanol as mobile phase. Although long-chain alcohols such as *n*-octanol and *n*-decanol are more efficient in tilting the ODS chains toward the surface normal, the ODS chains are still

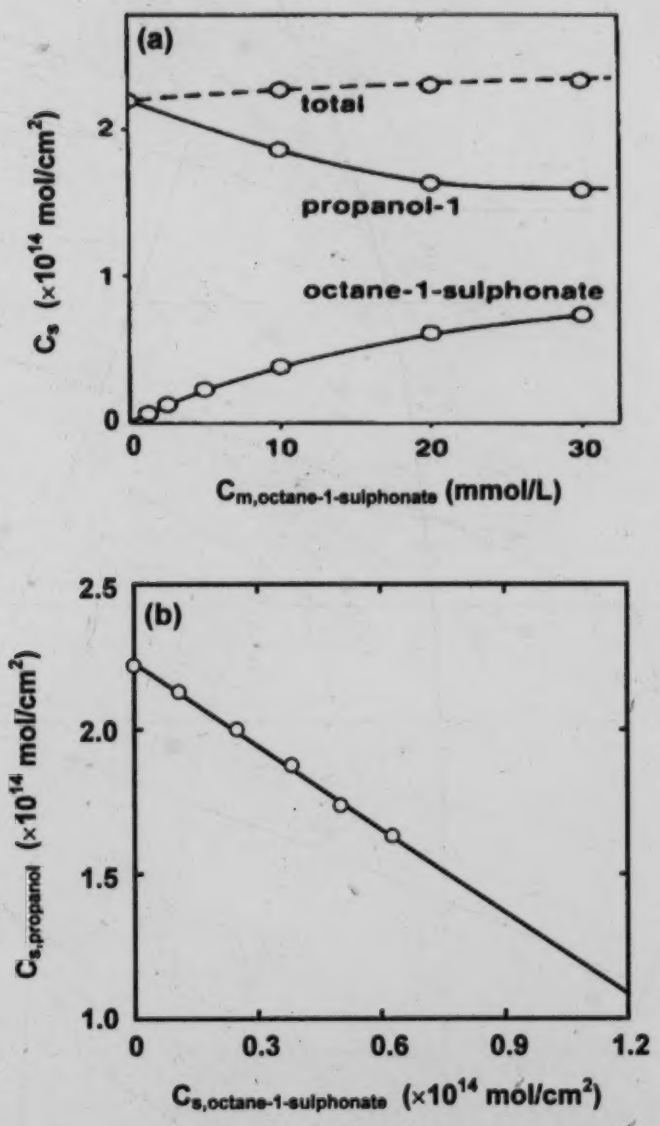

Figure 7.10 Simultaneous sorption of 1-propanol and octane-1-sulphonate in ODS stationary phase from pH3.0 phosphate buffer containing 2 % 1-propanol and varying concentrations of octane-1-sulphonate (a) (From reference 130). The solid lines in (a) are digitized and replotted as $C_{s,propanol}$ versus $C_{s,octane\text{-}1\text{-}sulphonate}$ (b). Temperature: 40 °C.

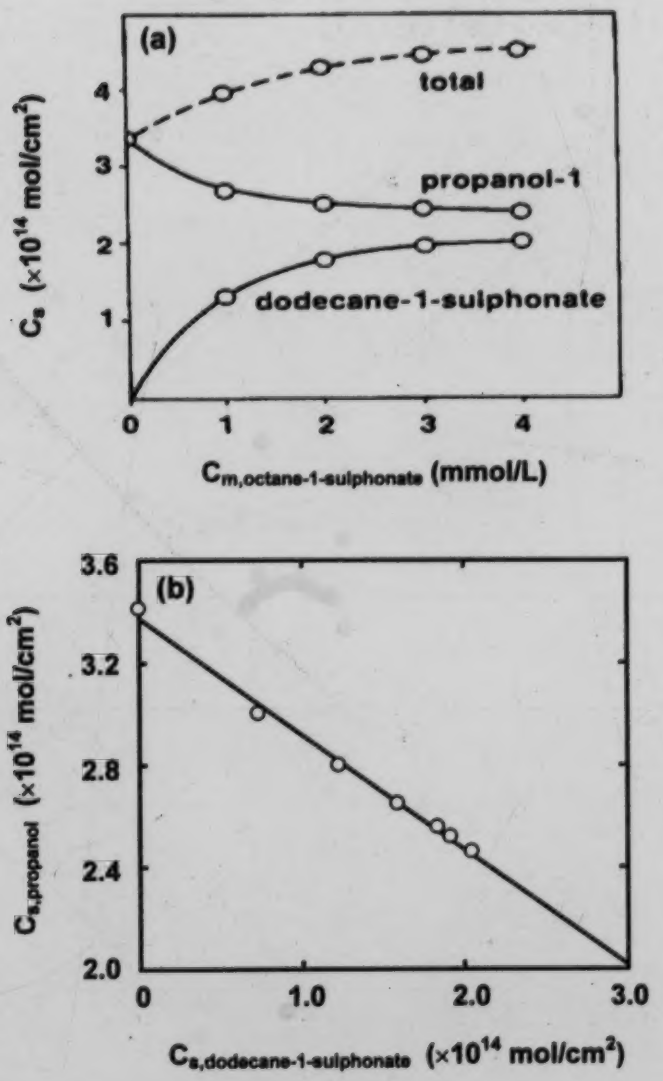

Figure 7.11 Simultaneous sorption of 1-propanol and octane-1-sulphonate in ODS stationary phase from pH3.0 phosphate buffer containing 10 % 1-propanol and varying concentrations of dodecane-1-sulphonate (a) (From reference 130). The solid lines in (a) are digitized and replotted as $C_{s,propanol}$ versus $C_{s,dodecane\text{-}1\text{-}sulphonate}$ (b). Temperature: 40 °C.

tilted more than 50° from the surface normal even when a saturated monolayer of long-chain alcohols are sorbed.

Unlike the molecules of linear or planar shape, TBA^+ is relatively bulky and roughly spherical with a radius of about 4.7 Å. Previous studies on the sorption of TBA^+ by both competitive sorption based on an electrical triple layer model[86,87] and fluorescence spectroscopy[131] have shown that TBA^+ is able to penetrate deep into the ODS stationary phase because of its hydrophobic nature. There, it causes "unfolding" of the ODS chains. Due to the difference in molecular shape, the disturbance of the originally collapsed ODS chains is expected to be much more significant for the sorption of TBA^+ than for the sorption of linear or planar molecules. Such significant disturbance or unfolding of the ODS chains could expose more ODS chain "surface" for the sorption of butanol, thus a varying $A_{s,t,BuOH}$. Because of the unfolding of the ODS chains, butanol may also be sorbed in a different orientation and at a different distance from the silica surface than it is in the absence of sorbed TBA^+, which would result in differences in both $\bar{A}_{TBA}$ and $K_{D,BuOH}$.

7.4.3 Theoretical Model

Presented in this section is the theoretical model developed to describe the relationship between $n_{s,BuOH}$ and $n_{s,TBA}$ as shown in Figure 7.9. The model assumes that the sorption process involves not only a competition for space between sorbed butanol and sorbed TBA^+, but also an alteration of the ODS chain conformation by sorbed TBA^+.

In the model, the changes in $A_{s,t,BuOH}$ and $\bar{A}_{TBA}$ are assumed to be linear functions of the amount of sorbed TBA^+, $n_{s,TBA}$:

$$A_{s,t,BuOH} = A_{s,t,BuOH,init} + k_2\, n_{s,TBA} \qquad (7.17)$$

$$\bar{A}_{TBA} = \bar{A}_{TBA,init} + k_3\, n_{s,TBA} \qquad (7.18)$$

where $A_{s,t,BuOH,init}$ is the total space initially available for the sorption of butanol in the absence of sorbed TBA^+, $\bar{A}_{TBA,init}$ is the space occupied per mole of TBA^+ sorbed, extrapolated to $n_{s,TBA} = 0$, and k_2 and k_3 are constants. The above assumptions are based on the following arguments: (1) Extended ODS chains are expected to have more space (i.e. more accessible chain surface) for the sorption of butanol than folded ODS chains, and the number of ODS chains unfolded by sorbed TBA^+ is directly proportional to the number of moles of TBA^+ sorbed. Here, it should be pointed out that due to the decrease in $K_{D,BuOH}$ upon the unfolding of ODS chains as discussed later, the overall number of moles of butanol sorbed actually decreases with the increase in the number of moles of TBA^+ sorbed, as shown in Figure 7.9. (2) When ODS chains are extended, the extent of overlap or competition for space between sorbed butanol and sorbed TBA^+ is expected to decrease because butanol tends to sorb near the interface between the bonded phase and the aqueous solution with the –OH group directed toward the aqueous solution,[64,65] while TBA^+ may stay deep in the bonded phase.[86,87] If the extent of overlap is decreased, a negative value of k_3 is expected. These arguments are illustrated in Figure 7.12.

Probably, it is necessary to clarify the new meaning of the term $A_{s,t,,BuOH}$. Now $A_{s,t,,BuOH}$ is the total space available, in the absence of sorbed TBA^+, for the sorption of butanol in the ODS stationary phase whose chain conformation has been altered equivalently by $n_{s,TBA}$ mol of sorbed TBA^+. This is an imaginary state. In other words, if the ODS chains could remain extended even after the removal of sorbed TBA^+ (an imaginary state), the total space available for the sorption of butanol in the ODS stationary phase in this imaginary state would be $A_{s,t,,BuOH}$.

In terms of ΔG_{BuOH}, the free energy of transfer of butanol from the mobile phase to the ODS stationary phase, the distribution coefficient of butanol can be expressed as

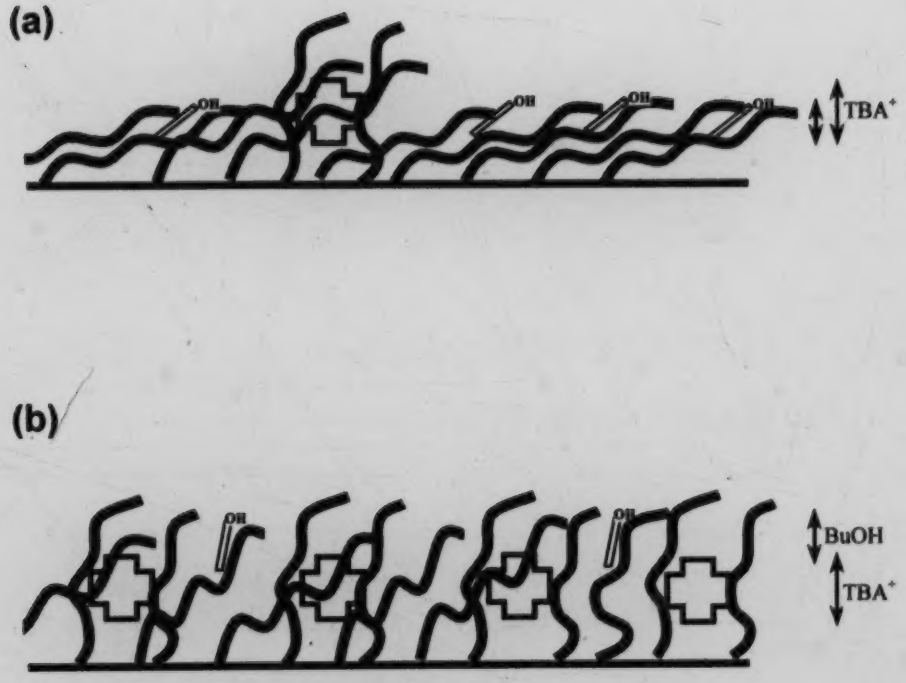

Figure 7.12 Cartoons of ODS bonded stationary phase with sorbed TBA^+ ( ) and butanol (OH) at (a) low and (b) high surface concentrations of sorbed TBA^+. The vertical arrows on the right side represent the sorption planes of TBA^+ and butanol.

$$K_{D,BuOH} = e^{-\Delta G_{BuOH}/RT} \quad (7.19)$$

ΔG_{BuOH} is directly proportional to the contact area between butanol and ODS chains.[12,132] Because the unfolding of ODS chains will increase the distance between the neighboring ODS chains,[65] the contact area between butanol and ODS chains is expected to decrease, i.e. the chance of one butanol molecule in contact with more than one ODS chain is decreased (see Figure 7.12). Because the extent of unfolding of ODS chains is directly proportional to the amount of sorbed TBA^+, it is reasonable to assume that ΔG_{BuOH} is also a linear function of $n_{s,TBA}$,

$$\Delta G_{BuOH} = \Delta G_{BuOH,init} + k_1 n_{s,TBA} \quad (7.20)$$

where $\Delta G_{BuOH,init}$ is the free energy of transfer of butanol in the absence of sorbed TBA^+ and k_1 is a constant. For a weaker interaction (i.e. smaller contact area) between butanol and ODS chains, a positive value of k_1 is expected. By combining eqs 7.19 and 7.20, $K_{D,BuOH}$ can be rewritten as

$$K_{D,BuOH} = K_{D,BuOH,init}\, e^{-k_1 n_{s,TBA}/RT} \quad (7.21)$$

where $K_{D,BuOH,init}$ is the distribution coefficient of butanol in the absence of TBA^+:

$$K_{D,BuOH,int} = e^{-\Delta G_{BuOH,init}/RT} \quad (7.22)$$

By combining eqs 7.17, 7.18, 7.21 with eq 7.16, the relationship between $n_{s,BuOH}$ and $n_{s,TBA}$ can be written as

$$n_{s,BuOH} = e^{-k_1 n_{s,TBA}/RT} [(K_{D,BuOH,init} C_{m,BuOH} A_{s,t,BuOH,init} + K_{D,BuOH,init} C_{m,BuOH} k_2 n_{s,TBA}) - (K_{D,BuOH,init} C_{m,BuOH} \bar{A}_{TBA,init} + K_{D,BuOH,init} C_{m,BuOH} k_3 n_{s,TBA}) n_{s,TBA}] \quad (7.23)$$

The model also assumes that the extent of such changes in $A_{s,t,BuOH}$, $\bar{A}_{TBA}$ and ΔG_{BuOH} with $n_{s,TBA}$ should decrease and almost stop after some critical amount of TBA^+, $n_{s,TBA,crit}$, has been sorbed in the ODS stationary phase because after sorbed TBA^+ reaches this critical concentration, the unfolding of the originally collapsed ODS chains is mostly done and the sorption of more TBA^+ would not significantly alter the unfolded ODS chain conformation. Of course, competition for space between butanol and TBA^+ will continue. According to this assumption, eq 7.23 can only be applied up to $n_{s,TBA,crit}$. After the critical amount of TBA^+ has been sorbed in the ODS stationary phase, changes in $K_{D,BuOH}$, $A_{s,t,BuOH}$ and $\bar{A}_{TBA}$ are assumed to be insignificant and the following equation should be used

$$n_{s,BuOH} = e^{-k_1 n_{s,TBA,crit}/RT} [(K_{D,BuOH,init} C_{m,BuOH} A_{s,t,BuOH,init} + K_{D,BuOH,init} C_{m,BuOH} k_2 n_{s,TBA,crit}) - (K_{D,BuOH,init} C_{m,BuOH} \bar{A}_{TBA,init} + K_{D,BuOH,init} C_{m,BuOH} k_3 n_{s,TBA,crit}) n_{s,TBA}] \quad (7.24)$$

Since $n_{s,TBA,crit}$ is a constant, eq 7.24 represents a linear competition for space between butanol and TBA^+ in the ODS stationary phase which has been unfolded almost completely by sorbed TBA^+.

In the absence of TBA^+, both eq 7.23 and eq 7.24 can be reduced to

$$n_{s,BuOH} = (K_{D,BuOH,init} C_{m,BuOH} A_{s,t,BuOH,init}) \quad (7.25)$$

the number of moles of butanol initially sorbed in the ODS stationary phase in the absence of TBA^+, which corresponds to the two initial data points in Figure 7.9, 3.20×10^{-6} and 2.52×10^{-6} mol butanol sorbed, for ionic strengths 0.50 and 0.050 mol/L, respectively. Therefore, this term in eqs 7.23 and 7.24 is a known constant. The term ($K_{D,BuOH,init}\ C_{m,BuOH}\ \bar{A}_{TBA,init}$) is also a constant. However, the value of $\bar{A}_{TBA,init}$ is unknown and the value of $K_{D,BuOH,init}$ is also uncertain because $A_{s,BuOH}$ (in eq 7.14) is difficult to determine. Therefore, this term is designated as a fitting parameter. Those terms, which include k_1, k_2 and k_3, are also designated as fitting parameters. Thus, in terms of fitting parameters (m_1, m_2, m_3 and m_4), eq 7.23 and 7.24 can be rewritten as

$$n_{s,BuOH} = e^{-m_1 n_{s,TBA}} \left[(6.20 \times 10^{-6} + m_2 n_{s,TBA}) - (m_3 + m_4 n_{s,TBA}) n_{s,TBA}\right] \quad (7.26)$$

$$n_{s,BuOH} = e^{-m_1 n_{s,TBA,crit}} \left[(6.20 \times 10^{-6} + m_2 n_{s,TBA,crit}) - (m_3 + m_4 n_{s,TBA,crit}) n_{s,TBA}\right] \quad (7.27)$$

for the ionic strength 0.50 mol/L, where

$$m_1 = k_1/RT \quad (7.28)$$

$$m_2 = K_{D,BuOH,init}\ C_{m,BuOH}\ k_2 \quad (7.29)$$

$$m_3 = K_{D,BuOH,init}\ C_{m,BuOH}\ \bar{A}_{TBA,init} \quad (7.30)$$

$$m_4 = K_{D,BuOH,init}\ C_{m,BuOH}\ k_3 \quad (7.31)$$

Similar equations can be written for the ionic strength 0.050 mol/L by replacing 6.20×10^{-6} mol with 2.52×10^{-6} mol.

The non-linear least-square fitting of the above model into the data shown in Figure 7.9 was performed using KaleidaGraph (Synergy Software, Reading, PA).

Because the model involves two equations, a conditional test on the following Boolean expression is used:

$$\text{if } n_{s,TBA} < n_{s,TBA,crit} \quad \text{eq 7.26} \quad \text{else} \quad \text{eq 7.27} \tag{7.32}$$

Since the value of $n_{s,TBA,crit}$ is unknown, it has to be determined by curve fitting. However, the value of $n_{s,TBA,crit}$, 1.9×10^{-5} mol, obtained automatically as the fifth adjustable fitting parameter from the curve fitting for 0.50 mol/L ionic strength is not reliable because the obtained fitted curve shows obvious discontinuity. It was found that the correlation coefficients (R^2) are almost the same even when very different values of $n_{s,TBA,crit}$ are used (see Table 7.6) and the thus obtained fitted curves appear differently (see Figures 7.13, 7.14 and 7.15). However, comparing Figure 7.13 to 7.15, it is seen that when the trial value of $n_{s,TBA,crit}$ is low the deflection is in the upward direction, but when the trial value of $n_{s,TBA,crit}$ is high the deflection is in the downward direction. Therefore, the best fit value of $n_{s,TBA,crit}$ is determined by trial and error, employing a trial-series of $n_{s,TBA,crit}$ values (see Table 7.6) using the visual criteria of minimum deflection in either the upward or the downward direction.

For 0.50 mol/L ionic strength, it was found that the fitted curves are not smooth until the testing value of $n_{s,TBA,crit}$ is increased to about 2.2×10^{-5} mol (contrast Figures 7.13 and 7.14) and after this point the quality of the fitting did not improve significantly with higher values of $n_{s,TBA,crit}$. The obtained fitting parameters, m_1, m_2, m_3 and m_4, were also found to be more or less constant after this critical number of moles of TBA^+ have been sorbed (see Table 7.6). This is exactly expected by the theory. The small changes in the values of the obtained fitting parameters as seen in Table 7.6 for test values of $n_{s,TBA,crit} > 2.6 \times 10^{-5}$ mol are most likely caused by overestimation of $n_{s,TBA,crit}$. When test values larger than 3.0×10^{-5} mol are used, the overestimation is so significant that a

Table 7.6 The values of $n_{s,TBA,crit}$ tested and the fitting parameters obtained from the nonlinear least-square fitting of the model to the data obtained at 0.50 mol/L ionic strength.

$n_{s,TBA,crit}$ (mol)	$m_1 \times 10^{-4}$	m_2	m_3	$m_4 \times 10^{-3}$	R^2
1.6×10^{-5}	11 ± 2	0.65 ± 0.23	0.55 ± 0.23	-25 ± 12	0.9987
1.7×10^{-5}	1.0 ± 1	0.54 ± 0.17	0.45 ± 0.16	-18 ± 8	0.9988
1.8×10^{-5}	9.1 ± 1.2	0.45 ± 0.14	0.38 ± 0.13	-14 ± 5	0.9989
1.9×10^{-5}	8.4 ± 1.1	0.40 ± 0.12	0.34 ± 0.10	-12 ± 4	0.9990
2.0×10^{-5}	7.4 ± 1.1	0.32 ± 0.10	0.28 ± 0.08	-8.5 ± 3.1	0.9989
2.1×10^{-5}	6.7 ± 1.0	0.26 ± 0.09	0.24 ± 0.07	-6.8 ± 2.3	0.9989
2.2 × 10-5	6.3 ± 0.8	0.25 ± 0.07	0.23 ± 0.06	-6.2 ± 1.8	0.9989
2.3 × 10-5	6.1 ± 0.7	0.24 ± 0.06	0.23 ± 0.05	-5.7 ± 1.5	0.9989
2.4 × 10-5	5.9 ± 0.7	0.23 ± 0.06	0.23 ± 0.05	-5.4 ± 1.3	0.9989
2.5 × 10-5	5.8 ± 0.6	0.23 ± 0.05	0.23 ± 0.04	-5.2 ± 1.1	0.9989
2.6 × 10-5	5.7 ± 0.6	0.24 ± 0.05	0.23 ± 0.04	-5.0 ± 1.0	0.9989
2.7 × 10-5	5.6 ± 0.5	0.24 ± 0.05	0.24 ± 0.04	-4.9 ± 0.9	0.9989
2.8 × 10-5	5.6 ± 0.5	0.25 ± 0.05	0.25 ± 0.04	-4.9 ± 0.9	0.9988
2.9 × 10-5	5.5 ± 0.5	0.25 ± 0.04	0.25 ± 0.04	-4.8 ± 0.9	0.9988
3.0 × 10-5	5.5 ± 0.4	0.26 ± 0.04	0.26 ± 0.04	-4.7 ± 0.8	0.9988

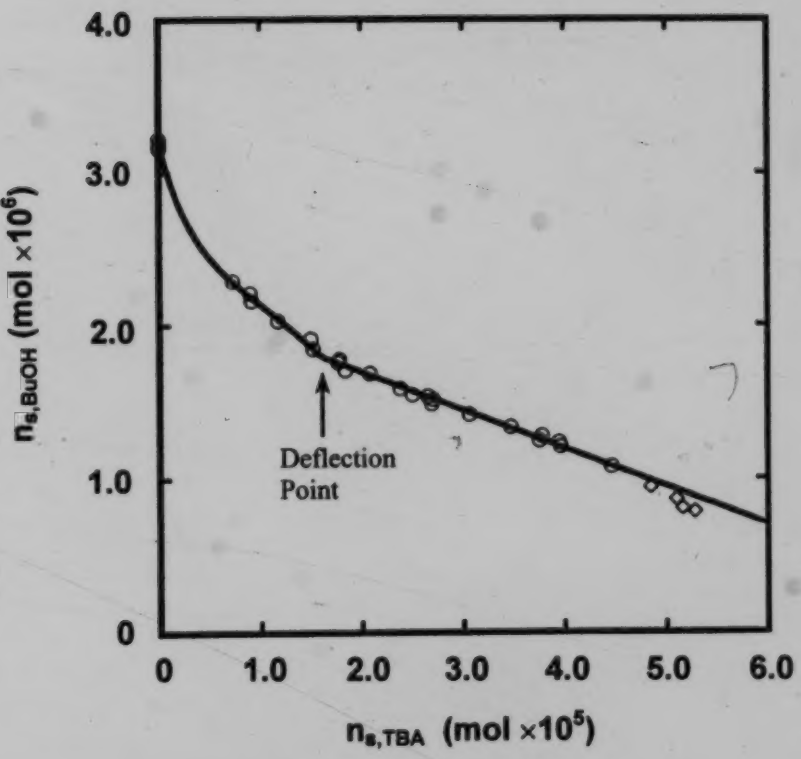

Figure 7.13 Nonlinear least-square fit of the model to the experimental data (○) obtained at the ionic strength 0.50 mol/L with a testing value of $n_{s,TBA,crit}$ = 1.6×10^{-5} mol. The last four data points (◇) are not included in the fitting because of the significant salting-in effect at high concentrations of TBA^+ in the mobile phase.

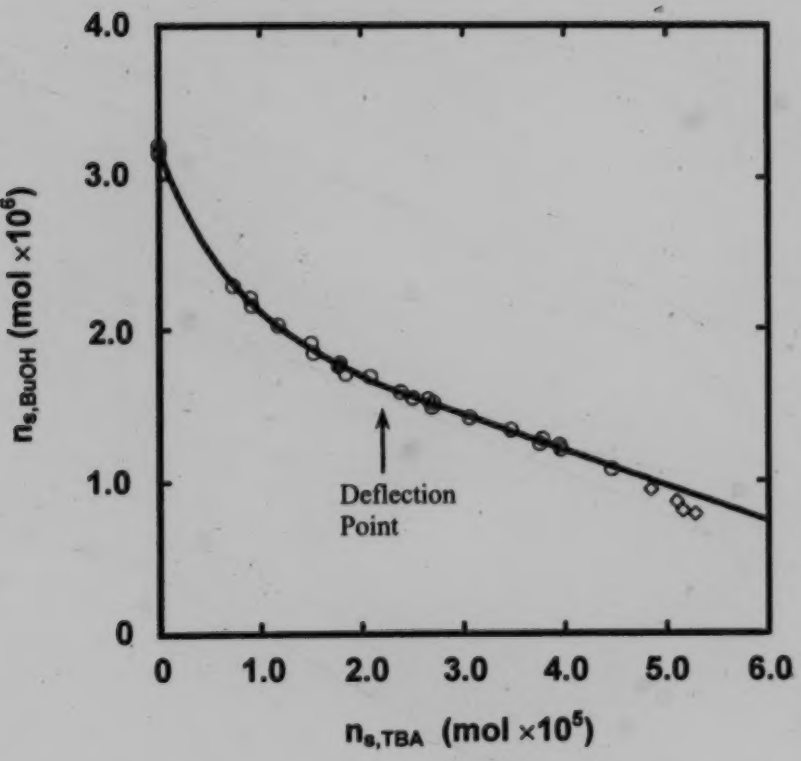

Figure 7.14 Nonlinear least-square fit of the model to the experimental data (O) obtained at the ionic strength 0.50 mol/L with a testing value of $n_{s,TBA,crit}$ = 2.2×10^{-5} mol. The last four data points (◇) are not included in the fitting because of the significant salting-in effect at high concentrations of TBA^+ in the mobile phase.

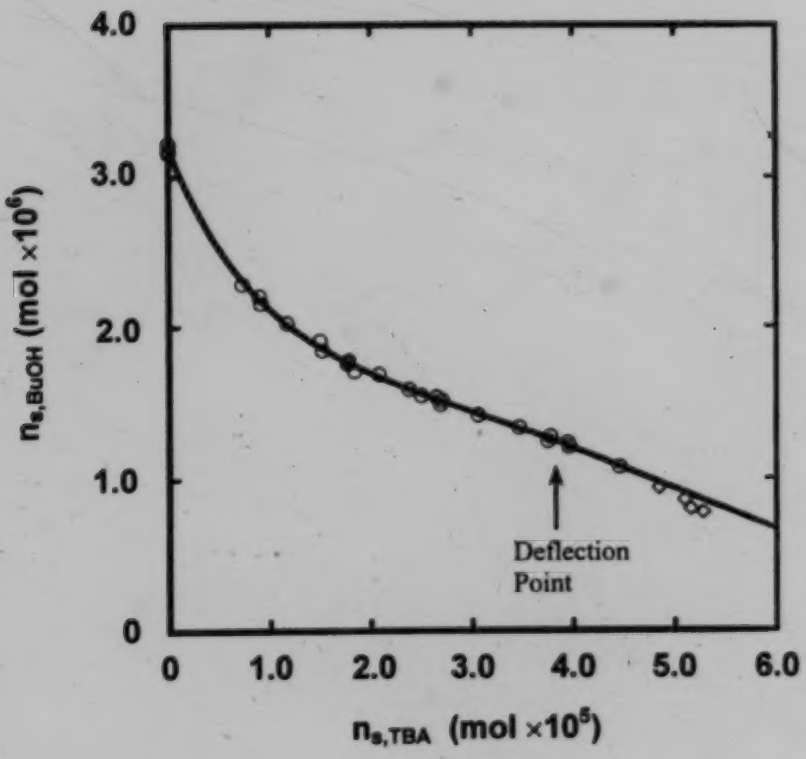

Figure 7.15 Nonlinear least-square fit of the model to the experimental data (○) obtained at the ionic strength 0.50 mol/L with a testing value of $n_{s,TBA,crit}$ = 3.8×10^{-5} mol. The last four data points (◇) are not included in the fitting because of the significant salting-in effect at high concentrations of TBA^+ in the mobile phase.

discontinuity becomes visible on the obtained fitting curves. Therefore, $n_{s,TBA,crit}$ is most likely to be around 2.2×10^{-5} mol.

For 0.050 mol/L ionic strength, the limited number of data points available at high $n_{s,TBA}$ makes it difficult to estimate the value of $n_{s,TBA,crit}$ in the same way as for 0.50 mol/L ionic strength. However, as shown in Figure 7.9, the experimental data for 0.050 mol/L ionic strength are more or less parallel with those for 0.50 mol/L ionic strength. The behavior of the ODS stationary phase towards the sorption of TBA^+ and butanol seems to be very similar for both ionic strengths. Therefore, it is reasonable to assume a similar value of $n_{s,TBA,crit}$ for both ionic strengths. When 2.2×10^{-5} mol is also used as an estimation of $n_{s,TBA,crit}$ for 0.050 mol/L ionic strength, the fitted curve is shown in Figure 7.16 and the obtained values of the fitting parameters are $m_1 = (6.7 \pm 0.8) \times 10^4$, $m_2 = 0.26 \pm 0.06$, $m_3 = 0.24 \pm 0.05$, and $m_4 = -(5.7 \pm 1.4) \times 10^3$. It can be seen from Figure 7.16 that the fitting is very good. The obtained values of the fitting parameters are very close to those obtained for ionic strength 0.50 mol/L given in Table 7.6.

With $n_{s,TBA,crit} = 2.2 \times 10^{-5}$ mol TBA^+ sorbed, the ratio of the number of moles of ODS chains in the stationary phase to the number of moles of TBA^+ sorbed, at both ionic strengths, is

$$\frac{n_{ODS}}{n_{s,TBA,crit}} = \frac{7.6 \times 10^{-5}\ \text{mol}}{2.2 \times 10^{-5}\ \text{mol}} = 3.5 \qquad (7.33)$$

where the value of n_{ODS}, 7.6×10^{-5} mol ODS chains, is estimated based on the 10.5 % (w/w) carbon load of the Partisil ODS-3 packing[88] and the weight of the packing (0.157 g) used. This ratio indicates that after each TBA^+ is surrounded by, on average, between three and four ODS chains, the unfolding of collapsed ODS chains is almost complete and no significant change in chain conformation will occur upon the sorption of more TBA^+.

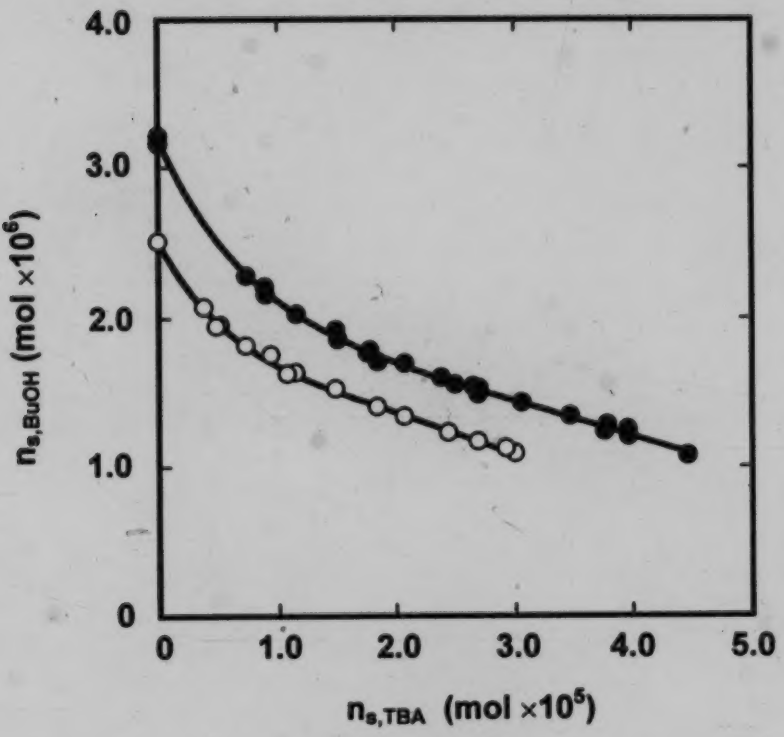

Figure 7.16 Plot of the number of moles of butanol sorbed versus the number of moles of TBA^+ sorbed in the ODS stationary phase at two ionic strengths: 0.50 mol/L (●) and 0.050 mol/L (○). The butanol concentration in the mobile phase is kept constant at 1.0×10^{-3} mol/L and the TBA^+ concentration is varied from 0 to 0.50 and 0.050 mol/L for ionic strengths 0.50 and 0.050 mol/L, respectively. Solid lines are the nonlinear least-square fits of the model to data with $n_{s,TBA,crit} = 2.2 \times 10^{-5}$ for both ionic strengths. The last four data points for ionic strength 0.50 mol/L as shown in Figure 7.9 are not included in the fitting because of the significant salting-in effect at high concentrations of TBA^+ in the mobile phase.

Based on the fitting parameters obtained at $n_{s,TBA,crit}$, the extent of the changes in $K_{D,BuOH}$, $A_{s,t,BuOH}$ and $\bar{A}_{TBA}$ can be estimated. At $n_{s,TBA,crit} = 2.2 \times 10^{-5}$ mol, the obtained m_1's are 6.3×10^{4} and 6.7×10^{4} for the ionic strength 0.50 and 0.050 mol/L, respectively. Therefore, according to eq 7.21, the distribution coefficients of butanol at $n_{s,TBA,crit}$ are

$$K_{D,BuOH,crit} = K_{D,BuOH,init}\, e^{-m_1 n_{s,TBA,crit}} \qquad (7.34)$$

$$= 0.25\, K_{D,BuOH,init} \qquad \text{for 0.50 mol/L ionic strength}$$

and

$$= 0.23\, K_{D,BuOH,init} \qquad \text{for 0.050 mol/L ionic strength}$$

i.e., the distribution coefficient of butanol at $n_{s,TBA,crit}$ is decreased to about one quarter of its initial value for both ionic strengths. This is reasonable because, as mentioned earlier, unfolded ODS chains are expected to be farther apart from each other[65] so that the contact area (i.e. the free energy of interaction) between butanol and ODS chains are reduced.

According to eq 7.17, the total space created by chain unfolding at $n_{s,TBA,crit}$ is (k_2 $n_{s,TBA,crit}$). However, the value of k_2 cannot be estimated from the obtained fitting parameter m_2 because the latter includes $K_{D,BuOH,init}$ that is an unknown constant. Nevertheless, the space increased relative to the initial total space available for butanol sorption can still be calculated

$$\frac{k_2\, n_{s,TBA,crit}}{A_{s,t,BuOH,init}} = \frac{K_{D,BuOH,init}\, C_{m,BuOH}\, k_2\, n_{s,TBA,crit}}{K_{D,BuOH,init}\, C_{m,BuOH}\, A_{s,t,BuOH,init}} \qquad (7.35)$$

$$= \frac{m_2\, n_{s,TBA,crit}}{3.20 \times 10^{-6}} = 1.7 \qquad \text{for 0.50 mol/L ionic strength}$$

$$= \frac{m_2\, n_{s,TBA,crit}}{2.52 \times 10^{-6}} = 2.3 \qquad \text{for 0.050 mol/L ionic strength}$$

The negative value of m_4 means that competition for space between TBA^+ and butanol becomes less important when ODS chains are unfolded. This is reasonable because when the ODS chains are extended, the overlap between butanol and TBA^+ is expected to be reduced. The decrease in competition is about 50–60%:

$$\frac{k_3\, n_{s,TBA,crit}}{\bar{A}_{TBA,init}} = \frac{K_{D,BuOH,init}\, C_{m,BuOH}\, k_3\, n_{s,TBA,crit}}{K_{D,BuOH,init}\, C_{m,BuOH}\, \bar{A}_{TBA,init}} \qquad (7.36)$$

$$= \frac{m_4\, n_{s,TBA,crit}}{m_3} = 0.60 \quad \text{for 0.50 mol/L ionic strength}$$

$$= \frac{m_4\, n_{s,TBA,crit}}{m_3} = 0.52 \quad \text{for 0.050 mol/L ionic strength.}$$

Chapter 8

Conclusions and Future Work

8.1 Conclusions

This work demonstrated that bulky molecules such as TBA^+ behave differently when sorbed in the ODS stationary phase compared with planar or linear molecules such as naphthalene-2-sulphonate and butanol. When TBA^+ is sorbed in the ODS stationary phase, it not only competes for space with butanol, but also creates more space for butanol sorption by unfolding the originally collapsed ODS chains. However, because the unfolded ODS chains are less favorable for the sorption of butanol due to the decreased contact area between butanol and ODS chains, the amount of butanol actually sorbed after taking the created space into account is still less than the amount of butanol sorbed in the originally collapsed ODS stationary phase. Also the overlap between TBA^+ and butanol seems to decrease upon the unfolding of ODS chains by sorbed TBA^+. The experimental data demonstrate that the extent of space creation, the change in the distribution coefficient of butanol and the reduction in overlap between sorbed TBA^+ and sorbed butanol should decrease and almost stop after TBA^+ concentration in the ODS stationary phase reaches a critical level. After this, the effect of the sorption of more TBA^+ on the constants, $A_{s,t,BuOH}$, $K_{D,BuOH,init}$ and $\bar{A}_{TBA}$, becomes insignificant and its only remaining effect is competition for space with sorbed butanol. At this critical level, the ratio of ODS chains to sorbed TBA^+ is found to be between three and four.

8.2 Future Work

The following are several suggestions for future work:

(1). ODS bonded stationary phase is a very complicated system. Depending on the bonding chemistry, the bonding density, the type and the purity of the parent silica used, the obtained ODS phases can behave differently for the same solute molecule. Future work should take this into consideration. It would be interesting to see how TBA^+ or other bulky molecules behave when sorbed in ODS phases of different bonding densities. With very high bonding densities, bulky molecules may not be able to penetrate into the space between ODS chains.

(2). Solvent plays a very important role in determining the conformation of the ODS stationary phase. At higher concentrations of organic modifier in the mobile phase, the ODS chains are expected to be solvated and extended more towards surface normal. Therefore, the effect of the sorption of bulky molecules on the conformation of the ODS phases under this condition should be significantly decreased.

(3). It would be interesting to see how TBA^+ behaves when bonded phases with much shorter alkyl chains such as C8 and C4 are used. In this case, the retention of TBA^+ could be mainly due to adsorption instead of partition; therefore, the change in chain conformation caused by the sorption of TBA^+ should be minimized.

(4). The slopes for the linear effect of butanol on the sorption of TBA^+ as shown in Figure 7.8 are –0.087 and –0.057 mol of TBA^+ sorbed per mol of butanol sorbed for ionic strengths of 0.50 and 0.050 mol/L, respectively. In the previous work in which the effect of butanol on naphthalene-2-sulfonate (NS^-) and the effect of NS^- on butanol sorption were both linear, the slopes were found to be –0.013 mol of NS^- sorbed per mol of butanol sorbed and –0.015 mol of butanol sorbed per mol of NS^- sorbed, respectively.[85] All these slopes are much smaller than those obtained from the linear

plots in Figures 7.10 and 7.11: –0.95 mol of propanol sorbed per mol of octane-1-sulphonate sorbed and –0.45 mol of propanol sorbed per mol of dodecane-1-sulphonate sorbed. It is still not clear what could cause such a big difference in slope. (In addition to the difference in molecular shape, the ODS stationary phases used are obviously different.)

(5). Very recentely, Hu and Haddad[133] reported that low molecular weight alcohols such as 1-butanol can be immobilized onto ODS stationary phase. With pure water as the mobile phase, the alcohol-modified stationary phase gave more rapid elution and improved resolution for two groups of target analytes than unmodified stationary phase. The alcohol-modified ODS stationary phases were found to be very stable. The RSD was found to be less than 1.5 % for both the retention time and peak area for all of the tested analytes over a three month period. This phenomenon is really surprising and worth further investigating. The column equilibrium technique could be used to measure or monitor the actual amount of alcohols trapped in the ODS stationary phase.

(6). In order to avoid any complication caused by bonding chemistry, ODS phases prepared using monofunctional silane (monomeric phases) should be used in future work except for ODS phases with extremely high densities, which can only be prepared using trifunctional silanes.

Bibliography

1. Howard, G.A.; Martin, A.J.P. *Biochem. J.* **1950**, *46*, 532-538.
2. Colin, H.; Guiochon, G. *J. Chromatogr.* **1977**, *141*, 289-312.
3. Rossi, C.; Munari, S.; Cengarle, C.; Tealdo, G.F. *Chim. e Ind. (Milan)* **1960**, *42*, 724.
4. Rehak, V.; Smolkova, E. *Chromatographia*, **1976**, *9*, 219-229.
5. Abel, E.W.; Pollard, F.H.; Uden, P.C.; Nickless, G. *J. Chromatogr.* **1966**, *22*, 23-28.
6. Aue, W.A.; Hastings, C.R. *J. Chromatogr.* **1969**, *42*, 319-335.
7. Stewart, H.N.M.; Perry, S.G. *J. Chromatogr.* **1968**, *37*, 97-98.
8. Halasz, I.; Sebestian, I. *Angew. Chem. Intern. Ed. Engl.* **1969**, *8*, 453-454.
9. Kirkland, J.J.; Destefano, J.J. *J. Chromatogr. Sci.* **1970**, *8*, 309-314.
10. Kirkland, J.J. *J. Chromatogr. Sci.* **1971**, *9*, 206-214.
11. Majors, R.E. *Anal. Chem.* **1972**, *44*, 1722-1726.
12. Melander, W.R.; Horváth, Cs. in *High Performance Liquid Chromatography, Advances and Perspectives*; Horváth, Cs., Ed.; Academic Press: New York, 1980; Vol. 2, pp.113-319.
13. Majors, R.E. *LC-GC Mag.* **1988**, *6*, 298.
14. Berthod, A. *J. Chromatogr.* **1991**, *549*, 1-28.
15. Scott, R.P.W. *Silica Gel and Bonded Phases*; John Wiley & Sons: Chichester, 1993.
16. Unger, K.K. *Porous Silica*; Elsevier: Amsterdam, 1979.
17. R.K. Iler, *The Chemistry of Silica*, Wiley-Interscience: New York, 1979.
18. Verzele, M.; Dewaele, C.; Duquet, D. *J. Chromatogr.* **1985**, *329*, 351-357.
19. Nawrocki, J. *Chromatographia*, **1991**, *31*, 177-192; 193-205.
20. Berendsen, G.E.; Galan, L.de, *J. Liq. Chromatogr.* **1978**, *1*, 403-426.
21. Kiselev, A.V.; Lygin, A.I. *Infrared Spectra of Surface Compounds*, Wiley-Interscience: New York, 1975.
22. Sindorf, D.W.; Maciel, G.E. *J. Am. Chem. Soc.* **1983**, *105*, 1487-1493.

23. Sander, L.C. and Wise, S.A. *CRC Crit. Rev. Anal. Chem.* **1987**, *18*, 299-415.
24. Unger, K.K. in *Packings and Stationary Phases in Chromatographic Techniques*; Unger, K.K. Ed.; Marcel Dekker: New York, 1990; pp.251-470.
25. Mauss, M.; Engelhardt, H. *J. Chromatogr.* **1986**, *371*, 235-242.
26. Boudreau, S.P.; Cooper, W.T. *Anal. Chem.* **1989**, *61*, 41-47.
27. Kohler, J.J.; Chase, D.B.; Farlee, R.D.; Vega, A.J.; Kirkland, J.J. *J. Chromatogr.* **1986**, *352*, 275-305.
28. Maciel, G.E.; Sindorf, D.W. *J. Am. Chem. Soc.* **1980**, *102*, 7606-7607.
29. Pfleiderer, B.;Albert, K.; Bayer, E.; van de Ven, L.; de Haan, J.; Cramers, C. *J. Phys. Chem.* **1990**, *94*, 4189-4194.
30. Greenberg, S.A. *J. Am. Chem. Soc.*, **1958**, *80*, 6508-6511.
31. Hair, M.L. and Hertl, W. *J. Phys. Chem.* **1970**, *74*, 91-94; Hair, M.L. *in Silicon Chemistry*; Corey, E.R., Corey, J.Y., and Gaspar, P.P. Eds.; Ellis Horwood: Chichester, 1988; Ch.44, pp.481-489.
32. Strazhesko, D.N., Strelko, V.B., Belyakov, V.N., and Rubanik, S.C. *J. Chromatogr.* **1974**, *102*, 191-195.
33. Lork, K.D.; Unger, K.K.; Kinkel, J.N. *J. Chromatogr.* **1986**, *352*, 199-211.
34. Sander, L.C.; Wise, S.A. *Anal. Chem.* **1995**, *67*, 3284-33292.
35. Staroverov, S.M.; Fadeev, A.Yu. *J. Chromatogr.* **1991**, *544*, 77-98.
36. Sander, L.C.; Wise, S.A. *Adv. Chromatogr.* **1986**, *25*, 139-218.
37. Buszewski, B.; Jurasek, A.; Garaj, J.; Nondek, L.; Novak, I.; Berek, D. *J. Liq. Chromatogr.* **1987**, *10*, 2325-2336.
38. Kinkel, J.N.; Unger, K.K. *J. Chromatogr.* **1984**, *316*, 193-200.
39. Szabo, K.; Ha, N.L.; Schneider, P.; Zeltner, P.; Kovats, E.sz. *Helv. Chim. Acta*, **1984**, *67*, 2128-2142.
40. Sander, L.C.; Wise, S.A. *Anal. Chem.* **1984**, *56*, 504-510.
41. Unger, K.K.; Becker, N.; Roumeliotis, P. *J. Chromatogr.* **1976**, *125*, 115-127.

42. Berendsen, G.E.; Galan, L.de, *J. Liq. Chromatogr.* **1978**, *1*, 561-586.

43. Lochmuller, C.H.; Colborn, A.S.; Hunnicutt, M.L.; Harris, J.M. *J.Am. Chem. Soc.* **1984**, *106*, 4077-4082.

44. Dorsey, J.G.; Dill, K.A. *Chem. Rev.* **1989**, *89*, 331-346.

45. Wasserman, S.R.; Whiteside, G.M.; Tidswell, I.M.; Ocko, B.M.; Pershan, P.S.; Axe, J.D. *J. Am. Chem. Soc.* **1989**, *111*, 5852-5861.

46. Sander, L.C.; Wise, S.A. *J. High Resolut. Chromatogr. Chromatogr. Commun.* **1988**, *11*, 383-387.

47. Sander, L.C.; Wise, S.A. in *Retention and Selectivity in Chromatography*, Smith, R.M. Ed.; Elsevier: Amsterdam, 1995; chapter 10, pp.337-369.

48. Fatunmbi, H.O.; Bruch, M.D.; Wirth, M.J. *Anal. Chem.* **1993**, *65*, 2048-2054.

49. Verzele, M.; Mussche, P. *J. Chromatogr.* **1983**, *254*, 117-122.

50. Sander, L.C.; Wise, S.A. *J. Chromatogr.* **1984**, *316*, 163-181.

51. Sanser, L.C.; Glinka, C.J.; Wise, S.A. *Anal. Chem.* **1990**, *62*, 1099-1101.

52. Wasserman, S.R.; Tao, Y-T., Whitesides, G.M. *Langmuir*, **1989**, *5*, 1074-1087.

53. Tidswell, I.M.; Ocko, B.M.; Pershan, P.S.; Wasserman, S.R.; Whitesides, G.M.; Axe, J.D. *Phys. Rev. B*, **1990**, *41*, 1111-1128.

54. Sander, L.C.; Wise, S.A. *Adv. Chromatogr.* **1986**, *25*, 139-218.

55. Unger, K.K.; Becker, N.; Roumeliotis, P. . *J. Chromatogr.* **1976**, *125*, 115-127.

56. Eble, J.F.; Grob, R.L.; Antle, P.E.; Snyder, L.R. . *J. Chromatogr.* **1987**, *384*, 45-79.

57. Gilpin, R.K. *J. Chromatogr. Sci.* **1984**, *22*, 371-377.

58. Tanaka, N.; Kimata, K.; Hosoya, K.; Miyanishi, H.; Araki, T. *J. Chromatogr. A.* **1993**, *656*, 265-287.

59. Wheeler, J.F.; Beck, T.L.; Klatte, S.J.; Cole, L.A.; Dorsey, J.G. *J. Chromatogr. A.* **1993**, *656*, 317-333.

60. Sindorf, D.W.; Maciel, G.E. *J. Am. Chem. Soc.* **1983**, *105*, 1848-1851.

61. Albert, K.; Bayer, E. *J. Chromatogr.* **1991**, *544*, 345-370.

62. Sentell, K.B. *J. Chromatogr. A.* **1993**, *656*, 231-263.

63. Sander, L.C.; Callis, J.B.; Field, L.R. *Anal. Chem.* **1983**, *55*, 1068-1075.

64. Montgomery, M.E., Jr.; Green, M.A.; Wirth, M.J. *Anal. Chem.* **1992**, *64*, 1170-1175.

65. Montgomery, M.E., Jr.; Wirth, M.J. *Anal. Chem.* **1994**, *66*, 680-684.

66. Rutan, S.C.; Harris, J.M. *J. Chromatogr. A.* **1993**, *656*, 197-215.

67. Yarovsky, I.; Aguilar, M-I.; Hearn, M.T.W. *Anal. Chem.* **1995**, *67*, 2145-2153.

68. Schure, M.K. In *Chemically Modified Surfaces*, Pesek, J.J.; Leigh, I.E. Eds.; Royal Society of Chemistry: Cambridge,1994; pp.181-189.

69. *J. Chromatogr. A.* **1993**, *656*, 1-615

70. Sinanoglu, O. In *Molecular Associations in Biology*; Pullman, B., Ed.; Academic Press: New York, 1968, pp.427-445.

71. Halicioglu, T.; Sinanoglu, O. *Ann. N.Y. Acad. Sci.* **1969**, *158*, 308-317.

72. Horváth, Cs.; Melander, W.R.; Molnar, I. *J. Chromatogr.* **1976**, *125*, 129-156.

73. Vailaya, A.; Horváth, Cs.; *J. Phys. Chem.* **1997**, *101*, 5875-5888.

74. Marqusee, J.A.; Dill, K.A. *J. Chem. Phys.* **1986**, *85*, 434-444.

75. Dill, K.A. *J. Phys. Chem.* **1987**, *91*, 1980-1988.

76. Dorsey, J.G.; Dill, K.A. *Chem. Rev.* **1989**, *89*, 331-346.

77. Martire, D.E.; Boehm, R.E. *J. Phys. Chem.* **1983**, *87*, 1045-1062.

78. Locke, D.C. *J. Chromatogr. Sci.* **1974**, *12*, 433-437; and In *Introduction to Statistical Thermodynamics*, Hill, T.L. Ed.; Addison-Wesley, Reading, MA, 1960, Chapters 14, 19 and 21.

79. Carr, P.W.; Li, J.; Dallas, A.J.; Eikens, D.I.; Tan, L.C. *J. Chromatogr. A.* **1993**, *656*, 113-133.

80. Dorsey, J.G.; Cooper, W.T. *Anal. Chem.* **1994**, *66*, 857A-867A.

81. Sentell, K.B.; Dorsey, J.G. *Anal. Chem.* **1989**, *61*, 930-934.

82. Sentell, K.B.; Dorsey, J.G. *J. Chromatogr.* **1989**, *461*, 193-207.

83. Wise, S.A.; Sander, L.C. *J. High Resolut. Chromatogr. Chromatogr. Commun.* **1985**, *8*, 248-255.

84. Glavina, L.L. PhD thesis, University of Alberta, 1993.

85. Glavina, L.L.; Cantwell, F.F. *Anal. Chem.* **1993**, *65*, 268-276.

86. Glavina, L.L.; Cantwell, F.F. *Anal. Chem.* **1996**, *68*, 2228-2235.

87. Glavina, L.L.; Cantwell, F.F. *Anal. Chem.* **1993**, *65*, 3299-3307.

88. *1996 Whatman Labsales catalog*, Whatman Labsales, Inc., Hillsboro, OR.

89. May, S.; Hux, R.A.; Cantwell, F.F. *Anal. Chem.* **1982**, *54*, 1279-1282.

90. Karlberg, B.; Thelander, S. *Anal. Chim. Acta* **1978**, *98*, 1-7.

91. Bergamin, F.; Medeiros, J.X.; Ries, B.F.; Zagatto, E.A.G. *Anal. Chim. Acta* **1978**, *101*, 9-16.

92. Kuban, V. *Crit. Rev. Anal. Chem.* **1991**, *22*, 477-557.

93. Liu, H. PhD Thesis, University of Alberta, 1988.

94. Leo, A.; Hansch, C.; Elkins, D. *Chem. Rev.* **1971**, *71*, 525-616.

95. Grunewald, G.L.; Pleiss, M.A.; Gatchell, C.L.; Pazhenchevsky, R.; Rafferty, M. *J. Chromatogr.* **1984**, *292*, 319-331.

96. Cantwell, F.F.; Puon, S. *Anal. Chem.* **1979**, *51*, 623-632.

97. Cantwell, F.F. *J. Pharm. Biomed. Anal.* **1984**, *2*, 153-164.

98. Liu, H.; Cantwell, F.F. *Anal. Chem.* **1991**, *63*, 993-1000.

99. Chen, J-G.; Weber, S.G.; Glavina, L.L.; Cantwell, F.F. *J. Chromatogr. A*, **1993**, *656*, 549-576.

100. Jacobson, J.; Frenz, J.; Horvath, C. *J. Chromatogr.* **1984**, *316*, 53-68.

101. Guiochon, G.; Golshan-Shirazi, S.; Katti, A.M. *Fundamentals of Preparative and Nonlinear Chromatography*, Academic Press: Boston, MA, 1990.

102. Poppe, H. *J. Chromatogr.* **1993**, *656*, 19-36.

103. Jandera, P.; Guiochon, G. *J. Chromatogr.* **1992**, *605*, 1-17.

104. Fornstedt, T.; Zhong, G.; Guiochon, G. *J. Chromatogr.* **1996**, *741*, 1-12; *742*, 55-68.

105. Langmuir, I. *J. Am. Chem. Soc.* **1916**, *38*, 2267; **1918**, *40*, 1361-1403.

106. Brunauer, S. *The Adsorption of Gases and Vapors, vol. I, Physical Adsorption*, Princeton university Press: Princeton, 1943. Chapter IV.

107. Ross, S.; Olivier, J.P. *On Physical Adsorption*, John Wiley & Sons: New York, 1964.

108. Fowler, R.H.; Guggenheim, E.A. *Statistical Thermodynamics*, Cambridge University Press: Cambridge, 1939.

109. Temkin, *J. Physical Chem., Moscou.* **1941**, *15*, 296; *Chem. Abstr.* **1942**, *36*, 6392.

110. Brunauer, S.; Love, K.S.; Keenan, R.G. *J. Am. Chem. Soc.* **1942**, *64*, 751-758.

111. Brunauer, S.; Emmett, P.H.; Teller, E. *J. Am. Chem. Soc.* **1938**, *60*, 309-319.

112. Brunauer, S.; Copeland, L.E.; Kantro, D.L. In *The Solid-Gas Interface*, Vol. 1, Flood, E.A. Ed.; Marcel Dekker: New York, 1967; Chapter 3.

113. Laub, R.J. In *Chromatography and Separation Chemistry, ACS Symp. Ser. No. 297*; Ahuja, S., Ed.; American Chemical Society: Washington, DC, 1986; pp 1-33.

114. Enderby, J.A. *Trans. Faraday Soc.* **1955**, *51*, 106-116.

115. Tilly-Melin, A.; Askemark, Y.; Wahlund, K.G.; Schill, G. *Anal. Chem.* **1979**, *51*, 976-983.

116. Del Ray, M.E.; Vera-Avila, L.E. *J. Liq. Chromatogr.* **1987**, *10*, 2911-2929.

117. Bartha, A.; Vigh, G. *J. Chromatogr.* **1983**, *260*, 337-345.

118. Stahlberg, J.; Hagglund, I. *Anal. Chem.* **1988**, *60*, 1958-1964.

119. Eble, J.E.; Grob, R.L.; Antle, P.E.; Snyder, L.R. *J. Chromatogr.* **1987**, *384*, 45-79.

120. Davies, J.T.; Rideal, E.K. *Interfacial Phenomena*, 2nd ed., Acedamic Press: New York, 1963; chapter 4.

121. Davies, J.T. *Proc. Roy. Soc. London, A*, **1958**, *245*, 417-428; 429-433.

122. Laitinen, H.A.; Harris, W.E. *Chemical Analysis*, 2nd Ed, McGraw-Hill: New York, 1975.

123. Long, F.A.; McDevitt, W.F. *Chem. Rev.* **1952**, *51*, 119-169.

124. Sergeeva, V.F.; *Russ. Chem. Rev.* **1965**, *34*, 309.

125. Harned, H.S.; Owen, B.B. The Physical Chemistry of Electrolyte Solutions, 3rd Ed., Reinhold: New York, 1958.

126. Burns, J.S.; Furter, W.F. In *Thermodynamic Behavior of Electrolytes in Mixed Solvents*, Furter, W.F. Ed.; American Chemical Society: Washington, DC, 1976; pp.99-127.

127. Schantz, M.M.; Martire, D.E. *J. Chromatogr.* **1987**, *391*, 35-51.

128. Li, J.; Carr, P.W. *Anal. Chem.* **1993**, *65*, 1443-1450.

129. Abraham, M.H.; Whiting, G.S.; Fuchs, R.; Chambers, E.J. *J. Chem. Soc. Perkin Trans. 2* 1990, 291-300.

130. Deelder, R.S.; van den Berg, J.H.M.; *J. Chromatogr.* **1981**, *218*, 327-339.

131. Dowling, S.D.; Seitz, W.R. *Anal. Chem.* **1985**, *57*, 602-605.

132. Tchapla, A.; Héron, S. *J. Chromatogr.* **1994**, *684*, 175-188.

133. Hu, W.; Haddad, P.R. *Anal. Commun.* **1998**, *35*, 49-52.

Appendix

This Appendix contains tabulated (x-y) experimental data for the plots shown throughout the thesis.

Data for Figure 2.4:

Time (min)	Apparent K_1 (L/L)
5	1.06
10	1.07
20	1.08
30	1.08
40	1.09

Data for Figure 2.5:

Time (min)	Apparent K_1 (L/L)
10	21.6
20	34.3
30	39.2
40	42.0
50	44.6
70	44.7
90	45.3

Data for Figure 2.8:

Stirring Time (min)	Mephentermine C_{a2} (mol/L)	2-phenylethylamine C_{a2} (mol/L)
3	1.62×10^{-4}	9.04×10^{-5}
5	2.70×10^{-4}	1.60×10^{-4}
10	4.01×10^{-4}	2.78×10^{-4}
15	4.69×10^{-4}	3.63×10^{-4}
20	4.85×10^{-4}	4.07×10^{-4}
25	4.95×10^{-4}	4.41×10^{-4}
30	5.01×10^{-4}	4.61×10^{-4}
40	4.99×10^{-4}	4.83×10^{-4}

Data for Figure 2.9:

Initial Concentration	Peak Area	
$C_{a1,initial}$ (mol/L)	Mephentermine	2-phenylethylamine
1.00×10^{-5}	9.41×10^{5}	5.27×10^{5}
2.00×10^{-5}	1.91×10^{6}	1.08×10^{6}
4.00×10^{-5}	3.76×10^{6}	2.09×10^{6}
6.00×10^{-5}	5.58×10^{6}	3.07×10^{6}
8.00×10^{-5}	7.35×10^{6}	4.13×10^{6}
1.00×10^{-4}	9.06×10^{6}	5.00×10^{6}

Data for Figure 3.2:

Time (min)	EF[a]
2	35
5	156
10	398
15	616
20	798

Data for Figure 3.4:

Time	EF	
(min)	mephentermine	2-phenylethylamine
2	36	16
5	171	53
10	371	111
15	519	164
20	652	221

Data for Figure 3.5:

Time	EF	
(min)	mephentermine	2-phenylethylamine
2	54	24
5	276	77
10	642	165
15	924	246
20	1160	327

Data for Figure 3.6:

Time	EF	
(min)	mephentermine	2-phenylethylamine
2	54	24
5	276	77
10	642	165
15	924	246
20	1160	327
25	1300	394
30	1490	467

Data for Figure 3.7:

Initial Concentration	Peak Area	
$C_{al,initial}$ (mol/L)	Mephentermine	2-phenylethylamine
2.00×10^{-6}	1.62×10^{6}	
4.00×10^{-6}		6.01×10^{5}
1.00×10^{-5}	7.61×10^{6}	1.47×10^{6}
2.00×10^{-5}	1.51×10^{7}	3.02×10^{6}
3.00×10^{-5}	2.13×10^{7}	4.31×10^{6}

Data for Figure 3.9:

Time (min)	EF[a]
2	23
5	122
10	322
15	489
20	605
25	716
30	813

Data for Figure 7.1:

Loading Volume (mL)	Peak Height (mm)			
	IS = 0.050 M		IS = 0.50 M	
	1 mL/min	3 mL/min	1 mL/min	3 mL/min
5	21.4			
10	42.0			
20	82.3			
35	130.4			
50	130.8			
70	127.5			
95	130.9			
7.5		30.2		
15		56.6		
30		114.5		
45		131.6		
60		131.7		
20			81.0	
40			167.2	
60			216.6	
80			217.2	
100			218.4	
15				62.6
30				122.1
45				183.0
60				211.8
90				215.2

Data for Figure 7.2:

Loading Volume	Amount Sorbed ($\times 10^6$ mol)			
(mL)	TBA^+	TBA^{+1}	BuOH	$BuOH^2$
5	21.4			
10		1.02	1.34	1.26
20		2.00	1.37	1.22
30		2.92	1.39	1.21
40	3.88	4.02	1.41	1.17
50		4.90		1.13
60		5.53		1.10
80	5.71	5.76	1.41	1.11
100		5.71		1.10
120	5.81	5.83	1.41	1.09
166		5.81		1.10
180	5.78		1.40	
200		5.86		1.10

1. in the presence of BuOH; 2. in the presence of TBA^+.

Data for Figure 7.3:

Loading Volume	Amount Sorbed ($\times 10^6$ mol)			
(mL)	TBA^+	TBA^+ [1]	BuOH	BuOH [2]
15		1.51	1.58	1.46
30	2.92	2.95	1.60	1.43
45		4.40	1.62	1.37
60	5.82	5.91	1.63	1.31
90	8.50	8.61	1.62	1.19
120	9.56	9.57		1.16
135			1.65	
150		9.47		1.15
166	9.61			
180		9.56		1.16
200	9.66		1.66	
240	9.71	9.71		1.16
270			1.59	
300	9.77	9.55		1.16

1. in the presence of BuOH; 2. in the presence of TBA^+.

Data for Figure 7.7 from ref. 84:

$C_{m,BuOH}$ (mol/L)	$C_{s,BuOH}$ (mol/L)
2.18×10^{-4}	3.22×10^{-3}
5.45×10^{-4}	8.15×10^{-3}
2.18×10^{-3}	3.11×10^{-2}
1.09×10^{-2}	0.131
2.18×10^{-2}	0.237
7.63×10^{-2}	0.582
0.109	0.765
0.218	1.17
0.327	1.52
0.545	2.10
0.654	2.39

Data for Figure 7.8:

IS = 0.50 mol/L		IS = 0.050 mol/L	
$n_{s,BuOH}$ (mol)	$n_{s,TBA}$ (mol)	$n_{s,BuOH}$ (mol)	$n_{s,TBA}$ (mol)
0	9.73×10^{-6}	0	5.62×10^{-6}
1.13×10^{-6}	9.46×10^{-6}	4.05×10^{-7}	5.50×10^{-6}
1.03×10^{-5}	8.58×10^{-6}	1.16×10^{-6}	5.47×10^{-6}
1.95×10^{-5}	7.73×10^{-6}	2.36×10^{-6}	5.47×10^{-6}
3.61×10^{-5}	6.43×10^{-5}	9.47×10^{-6}	5.00×10^{-6}
4.99×10^{-5}	5.31×10^{-6}	1.77×10^{-5}	4.40×10^{-6}
		4.70×10^{-5}	2.93×10^{-6}

Data for Figure 7.9:

IS = 0.50 mol/L		IS = 0.050 mol/L	
$n_{s,TBA}$ (mol)	$n_{s,BuOH}$ (mol)	$n_{s,TBA}$ (mol)	$n_{s,BuOH}$ (mol)
0	3.22×10^{-6}	0	2.52×10^{-6}
8.98×10^{-6}	2.21×10^{-6}	3.93×10^{-6}	2.07×10^{-6}
1.50×10^{-5}	1.91×10^{-6}	5.30×10^{-6}	1.95×10^{-6}
1.77×10^{-5}	1.76×10^{-6}	9.46×10^{-6}	1.75×10^{-6}
2.69×10^{-5}	1.49×10^{-6}	1.16×10^{-5}	1.63×10^{-6}
3.06×10^{-5}	1.42×10^{-6}	1.85×10^{-5}	1.40×10^{-6}
3.47×10^{-5}	1.34×10^{-6}		
3.78×10^{-5}	1.28×10^{-6}	4.88×10^{-6}	1.95×10^{-6}
3.95×10^{-5}	1.24×10^{-6}	7.42×10^{-6}	1.81×10^{-6}
3.96×10^{-5}	1.21×10^{-6}	1.08×10^{-5}	1.62×10^{-6}
		1.49×10^{-5}	1.52×10^{-6}
7.28×10^{-6}	2.29×10^{-6}	2.08×10^{-5}	1.34×10^{-6}
9.11×10^{-6}	2.16×10^{-6}	2.44×10^{-5}	1.23×10^{-6}
1.52×10^{-5}	1.85×10^{-6}	2.69×10^{-5}	1.17×10^{-6}
1.84×10^{-5}	1.71×10^{-6}	2.92×10^{-5}	1.12×10^{-6}
		3.00×10^{-5}	1.09×10^{-6}
0	3.18×10^{-6}		
1.17×10^{-5}	2.03×10^{-6}		
1.78×10^{-5}	1.78×10^{-6}		
2.08×10^{-5}	1.69×10^{-6}		
2.38×10^{-5}	1.59×10^{-6}		
2.50×10^{-5}	1.55×10^{-6}		
2.65×10^{-5}	1.54×10^{-6}		
2.70×10^{-5}	1.52×10^{-6}		
3.75×10^{-5}	1.25×10^{-6}		
4.46×10^{-5}	1.08×10^{-6}		
4.85×10^{-5}	9.43×10^{-7}		
5.10×10^{-5}	8.64×10^{-7}		
5.16×10^{-5}	8.04×10^{-7}		
5.28×10^{-5}	7.84×10^{-7}		

Data for Figure 7.10:

$C_{s,propanol}$ (mol/cm^2)	$C_{s,octane\text{-}1\text{-}sulphonate}$ (mol/cm^2)
0	2.22×10^{-14}
1.10×10^{-15}	2.13×10^{-14}
2.50×10^{-15}	2.00×10^{-14}
3.80×10^{-15}	1.88×10^{-14}
5.00×10^{-15}	1.74×10^{-14}
6.30×10^{-15}	1.63×10^{-14}

Data for Figure 7.11:

$C_{s,propanol}$ (mol/cm^2)	$C_{s,octane\text{-}1\text{-}sulphonate}$ (mol/cm^2)
0	3.41×10^{-14}
7.30×10^{-15}	3.00×10^{-14}
1.22×10^{-14}	2.80×10^{-14}
1.59×10^{-14}	2.65×10^{-14}
1.83×10^{-14}	2.56×10^{-14}
1.91×10^{-14}	2.52×10^{-14}
2.04×10^{-14}	2.46×10^{-14}